Quarterly Reviews of Biophysics **34**, 4 (2001), pp. 473–561. © 2001 Cambridge University Press
DOI: 10.1017/S0033583501003729 Printed in the United Kingdom

Simulation approaches to ion channel structure–function relationships

D. Peter Tieleman*, Phil C. Biggin, Graham R. Smith† and Mark S. P. Sansom‡

Laboratory of Molecular Biophysics, Department of Biochemistry, Rex Richards Building, University of Oxford, South Parks Road, Oxford OX1 3QU, UK

1. Introduction 475
1.1 Ion channels 475
1.1.1 Gramicidin 476
1.1.2 Helix bundle channels 477
1.1.3 K channels 480
1.1.4 Porins 483
1.1.5 Nicotinic acetylcholine receptor 483
1.1.6 Physiological properties 483
1.2 Simulations 484
1.2.1 Atomistic *versus* mean-field simulations 484
2. Atomistic simulations 485
2.1 Modelling of ion-interaction parameters 485
2.1.1 Interatomic distances and the problem of ionic radii 486
2.1.2 Solvation energy 487
2.1.3 Hydration shells and coordination numbers 489
2.1.4 Parameters in common use and transferability 491
2.1.5 Summary 491
2.2 Water in pores *versus* bulk 491
2.2.1 Simple pore models 494
2.2.2 gA 495
2.2.3 Alm 496
2.2.4 $LS3_6$ (and $LS2_4$) 496
2.2.5 Nicotinic receptor M2δ_5 497
2.2.6 Influenza A M2 497
2.2.7 K channels 497
2.2.8 nAChR 498
2.2.9 Porins 498
2.2.10 Relevance 499
2.2.11 Problems with simulations 501
2.3 Dynamics of ions in pores 503
2.3.1 Simple pore models 503
2.3.2 Helix bundles 504

* Present address: Department of Biological Sciences, University of Calgary, 2500 University Drive NW, Calgary, Alberta, T2N 1N4, Canada.

† Present address: Biomolecular Modelling Laboratory, Imperial Cancer Research Fund, 44 Lincoln's Inn Fields, London WC2A 3PX, UK.

‡ Author to whom correspondence should be addressed. Tel.: +44-1865-275371; Fax: +44-1865-275182; E-mail: mark@biop.ox.ac.uk

https://doi.org/10.1017/S0033583501003729 Published online by Cambridge University Press

2.3.3 gA and KcsA 505
2.4 Energetics of permeation and ion selectivity 509
2.4.1 Potential and free energy profiles 509
2.4.2 gA 510
2.4.3 α-Helix bundles 511
2.4.4 KcsA 512
2.4.5 Ion selectivity 514
2.4.6 Problems of estimating energetic profiles 515
2.5 Conformational changes 516
2.5.1 gA 516
2.5.2 Alm and LS3 516
2.5.3 KcsA 517
2.6 Protonation states 523

3. Coarse-grained simulations 524
3.1 Introduction 524
3.1.1 Predicting conductance magnitudes 525
3.2 Electro-diffusion: the Nernst–Planck approach 526
3.2.1 Calculating the potential profile from Poisson and PB theory 528
3.2.2 Calculating the potential profile from BD simulations 530
3.2.3 Combining Nernst–Planck and Poisson: PNP 530
3.3 Beyond PNP 532
3.4 BD simulations 532
3.4.1 Basic theory in ion channels 532
3.4.2 Incorporating the environment 533
3.5 Applications 535
3.5.1 Model systems 535
3.5.1.1 Solving the Poisson and PB equation for channel-like geometries 535
3.5.1.2 Comparing PB, PNP and BD 536
3.5.2 Applications to known structures 537
3.5.2.1 gA 537
3.5.2.2 Porin 539
3.5.2.3 LS3 540
3.5.2.4 Alm 542
3.5.2.5 nAChR 542
3.5.2.6 KcsA 543
3.6 pK_a calculations 543
3.7 Selectivity 544
3.7.1 Anion/cation selectivity 545
3.7.2 Monovalent/divalent ion selectivity 545

4. Problems 546
4.1 Atomistic simulations 546
4.1.1 Problems 546
4.1.2 Parameters 548
4.2 BD 549
4.3 Mean-field simulations 549

5. Conclusions 550
5.1 Progress 550
5.2 The future 550

https://doi.org/10.1017/S0033583501003729 Published online by Cambridge University Press

6. Acknowledgements 551

7. References 551

1. Introduction

1.1 Ion channels

Ion channels are proteins that form 'holes' in membranes through which selected ions move passively down their electrochemical gradients. The ions move quickly, at (nearly) diffusion limited rates (*ca*. 10^7 ions s^{-1} per channel). Ion channels are central to many properties of cell membranes. Traditionally they have been the concern of neuroscientists, as they control the electrical properties of the membranes of excitable cells (neurones, muscle; Hille, 1992). However, it is evident that ion channels are present in many types of cell, not all of which are electrically excitable, from diverse organisms, including plants, bacteria and viruses (where they are involved in functions such as cell homeostasis) in addition to animals. Thus ion channels are of general cell biological importance. They are also of biomedical interest, as several dizeases ('channelopathies') have been described which are caused by changes in properties of a specific ion channel (Ashcroft, 2000). Moreover, passive diffusion channels for substances other than ions are common (porins, aquaporins), as are active membrane transport processes coupled to ion gradients or ATP hydrolysis. An understanding of ion channels may also provide a gateway to understanding these processes.

The structures of a number of ion channels have been determined recently (see below). However, in advance of this a long tradition of membrane biophysical studies (reviewed in Hille, 1992) provided a broad outline of the structure of a 'typical' ion channel (Fig. 1). The key regions of the structure are the transbilayer pore, the selectivity filter and the gate. Although originally postulated on the basis of indirect measurements, these features have subsequently been identified directly by structural studies. One of the challenges facing simulation studies is to relate the molecular structures of channel components to the physiological properties of ion channels.

In attempting to relate the structure of an ion channel to its physiological function, a central problem is that of what is the best level at which to describe the structure of the channel. The simplest model of a channel is a regular cylinder of molecular dimensions, filled with 'solvent' behaving in the same way as bulk electrolyte solution. This approach enables

Abbreviations: Alm, alamethicin; BD, Brownian dynamics; DMPC, dimyristoylphosphatidylcholine; DPPC, dipalmitoyphosphatidylcholine; DPhPC, diphytenoylphosphatidylcholine; fluM2-TM, influenza M2 transmembrane helix peptide; gA, gramicidin A; GMO, glycerol mono oleate; KcsA, K channel from *Streptomyces lividans*; Kir6.2, inward rectifier K channel 6.2 (pore forming subunit of K_{ATP} channel); LS2, synthetic leucine–serine peptide (see Table 1); LS3, synthetic leucine–serine peptide (see Table 1); M2δ, synthetic M2 peptide from nAChR M2 helix of a δ-subunit; MC, Monte Carlo; MD, molecular dynamics; nAChR, nicotinic acetylcholine receptor; PB, Poisson–Boltzmann; PNP, Poisson–Nernst–Planck; PC, phosphatidylcholine; POPC, palmitoyl-oleoylphosphatidylcholine; PS, phosphatidylserine.

https://doi.org/10.1017/S0033583501003729 Published online by Cambridge University Press

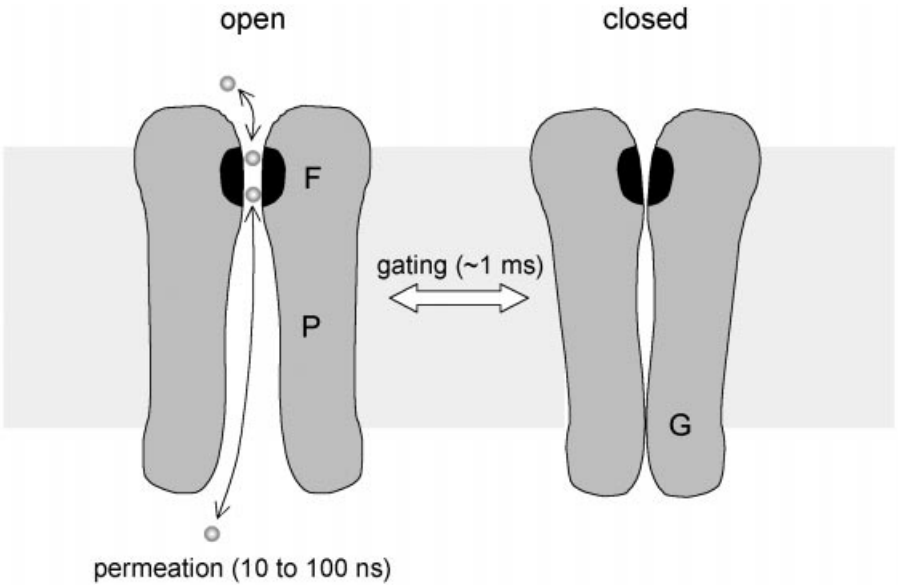


Fig. 1. Diagram of a 'typical' channel structure [as derived from membrane biophysics, after Hille (1992)]. When in the open conformation ions can flow through the channel, the mean time taken for a single ion to pass right through the channel being *ca*. 10–100 ns (i.e. *ca*. 10^{-8} to 10^{-7} s). Gating is the process of switching between an open and a closed state of the channel (the latter impermeable to ions) and typically occurs on a timescale of *ca*. 1 ms. Key regions of the channel are: F, the selectivity filter, which controls which species of ion may pass through the channel; P, the transbilayer pore; G, the gate which prevents ion permeation when the channel is closed.

one to place an upper bound on the conductance of a channel, i.e. on the number of ions per second passing through a transbilayer pore (Hille, 1992). However, to understand the relationship between atomic resolution structure and physiological function, it is evident that a more detailed description of a channel is needed.

Before describing the structures of specific channels, it is useful to consider their classification. Traditionally, channels are classified according to the species of ion for which they are selective (e.g. potassium channels) and/or the process that controls gating of the channel (e.g. ligand-gated ion channels). In addition to complex channel proteins, there are also a number of model ion channels that are formed by relatively simple peptides (Sansom, 1991). Although not as complex in their functional properties as channel proteins, such model systems help us to develop methodologies for relating channel structure to function. In this review we will focus on those channels, both model peptides and 'real' channel proteins, which have been the subject of detailed and extensive simulation studies (see Table 1).

1.1.1 Gramicidin

Gramicidin (gA) is a 15-residue peptide from *Bacillus brevis*. It has long been studied as a simple ion channel. The reader is referred to a number of reviews (Andersen, 1984; Wallace, 1992, 1999b, 2000; Woolley & Wallace, 1992; Roux & Karplus, 1994) and to a conference report (Wallace, 1999a) for further details of these studies. The structure of the principal

https://doi.org/10.1017/S0033583501003729 Published online by Cambridge University Press

Table 1. *Some channels discussed in this review*

Channel	Sequence (details)
	Model peptide channels
gA	f-LVal-Gly-LAla-DLeu-LAla-DVal-LVal-DVal-LTrp-DLeu-LTrp-DLeu-LTrp-DLeu-LTrp-ethanolamine
Alm	Ac-Aib-Pro-Aib-Ala-Aib-Ala-Gln-Aib-Val-Aib-Gly-Leu-Aib-Pro-Val-Aib-Aib-Glu-Gln-Phol
LS2	Leu-Ser-Leu-Leu-Leu-Ser-Leu-Leu-Ser-Leu-Leu-Leu-Ser-Leu-Leu-Ser-Leu-Leu-Leu-Ser-Leu
LS3	Leu-Ser-Ser-Leu-Leu-Ser-Leu-Leu-Ser-Ser-Leu-Leu-Ser-Leu-Leu-Ser-Ser-Leu-Leu-Ser-Leu
M2δ	Glu-Lys-Met-Ser-Thr-Ala-Ile-Ser-Val-Leu-Leu-Ala-Gln-Ala-Val-Phe-Leu-Leu-Leu-Thr-Ser-Gln-Arg
fluM2-TM	Ser-Ser-Asp-Pro-Leu-Val-Ile-Ala-Ala-Ser-Ile-Ile-Gly-Ile-Leu-His-Phe-Ile-Leu-Trp-Ile-Leu-Asp-Arg-Leu-Phe
	Protein channels
KcsA	Bacterial K channel; X-ray structure; selectivity filter sequence: Thr-Val-Gly-Tyr-Gly; K^+ selective
Kir6.2	Inward rectifier K channel; homology model; selectivity filter sequence: Thr-Ile-Gly-Phe-Gly; K^+ selective
NAChR	Nicotinic acetylcholine receptor; electron microscopy structure/model; cation selective

The standard three-letter code for amino-acid sequences is used, with the following additions: Aib = α-aminoisobutyric acid; Phol = phenylalaninol.

channel-forming conformation of this peptide (Fig. 2) has been determined at high resolution by solid-state NMR (Ketchem *et al*. 1993). The channel is formed by a head-to-head dimer of the peptide that adopts a α-helical conformation such that all of the hydrophobic side-chains point out into the surrounding bilayer (Cross *et al*. 1999). Thus the narrow (radius < 2Å; Smart *et al*. 1993) central pore is lined only by atoms of the peptide backbone, namely the carbonyl (C=O) and amide (N–H) groups. gA forms channels permeable to monovalent cations (H^+, Li^+, Na^+, K^+, Rb^+, Cs^+) with conductances of the order of 30 pS (corresponding to *ca*. 2×10^7 ions s^{-1} at 100 mV) depending on, amongst other things, the nature of the membrane lipids and the surrounding ionic concentration.

1.1.2 Helix bundle channels

The majority of membrane proteins (other than those of bacterial outer membranes – Buchanan, 1999; Schulz, 2000) are made up of bundles of α-helices. A simple model of an ion channel based on this architecture is a parallel bundle of amphipathic helices oriented such that their hydrophobic surfaces are exposed to the surrounding lipid and their hydrophilic side-chains line a central water-filled pore through which ions may pass. Although the architectures of 'real' channel proteins are more complex, this simple model has much to commend it and represents at least some aspects of the structure of K channels (Doyle *et al*. 1998), of bacterial mechanosensitive channels (Chang *et al*. 1998) and of the transbilayer domain of the nicotinic acetylcholine receptor (nAChR) (Unwin, 1995; Miyazawa *et al*. 1999).

A number of peptides form ion channels by self-assembly to give bundles of transmembrane

https://doi.org/10.1017/S0033583501003729 Published online by Cambridge University Press

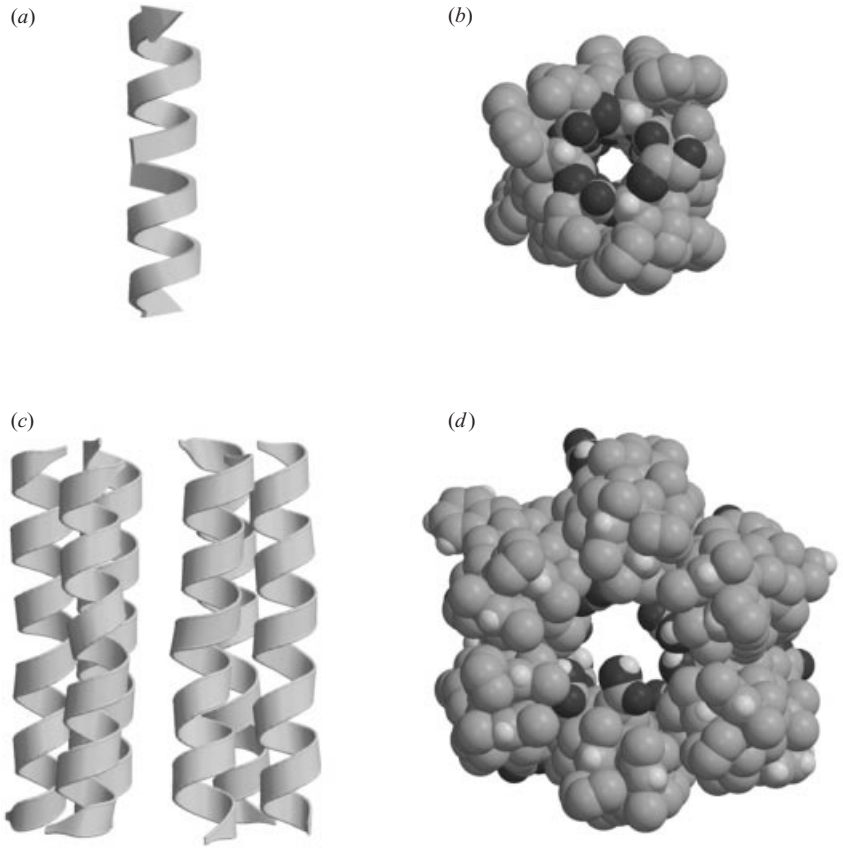


Fig. 2. Peptide model channels. (*a*, *b*) Structure of the gA pore (Ketchem *et al*. 1993). In (*a*) the fold of the channel is given, showing the head-to-head α-helix dimer. (*b*) A view down the channel, in space-filling format. The pore lining carbonyl O and amide N atoms are shown in dark grey. (*c*, *d*) Model of a hexameric Alm pore (Breed & Sansom, 1994). In (*c*) the fold of the channel is given, showing the bundle of 6 parallel α-helices (N-termini at the top). (*d*) A view down the channel, in space-filling format. The pore lining O and N atoms of the Gln and Glu side-chains are shown in dark grey.

(TM) helices. These channels tend to be somewhat short-lived and thus no direct structural studies of an intact channel assembly have (yet) been possible. Instead, there are plausible model structures of such channels based upon experimental structures of their constituent helices, combined with restraints on helix packing derived from their functional properties. Such models have been employed in several simulation studies.

Alamethicin (Alm) is a 20-residue peptide that forms multi-conductance channels in lipid bilayers (Woolley & Wallace, 1992; Sansom 1993; Cafiso, 1994). Alm adopts a largely α-helical conformation in a number of different environments, including in a crystal, in non-aqueous solvents, and in the presence of lipid bilayers. This conformation is stabilized by the presence of a large number of α-aminoisobutyric acid residues in the sequence of Alm (Table 1).

The multi-conductance behaviour of Alm channels is generally explained in terms of the 'barrel stave' model (Baumann & Mueller, 1974; Fox & Richards, 1982; Boheim *et al*. 1983; Mathew & Balaram, 1983) in which multiple Alm molecules form a helix bundle surrounding

https://doi.org/10.1017/S0033583501003729 Published online by Cambridge University Press

a central pore. Different conductance levels correspond to different numbers of helices in the bundle. This model is in accord with a large body of experimental data (reviewed in Sansom, 1993) including neutron-scattering studies from Alm in lipid bilayers (He *et al*. 1995). In particular the work of Woolley and colleagues (You *et al*. 1996; Woolley *et al*. 1997) has demonstrated that channels formed by covalently coupled pairs of Alm helices (which are physically constrained to be parallel to one another) strongly resemble channels formed by unmodified Alm.

Molecular models of channels formed by Alm helix bundles, generated by restrained MD simulations *in vacuo* (Breed *et al*. 1997), have formed the basis of simulation studies (see below). A model of a hexameric Alm pore is shown in Fig. 2. It can be seen that a number of hydrophilic side-chains (Gln and Glu) project into the central pore.

A second intensively studied model of a channel formed by a bundle of amphipathic α-helices is the synthetic leucine–serine peptide LS3 (Table 1), designed and characterized by DeGrado and Lear and their colleagues (Lear *et al*. 1988, 1994; Åkerfeldt *et al*. 1993). From a functional point of view LS3 channels are of interest in that they are cation selective and weakly rectifying (i.e. ions can flow more easily in one direction along the channel than the other; Kienker *et al*. 1994; Lear *et al*. 1997). At a conductance of *ca*. 100 pS inwards and 30 pS outwards in symmetrical 1 M KCl solutions, they have a conductance typical for that of some channel proteins, e.g. nAChR.

From a structural perspective an attractive feature of LS3 as a model is its relative simplicity. There are only two types of side-chain: hydrophobic leucines point outwards into the surrounding lipid whilst hydrophilic serines line the central water-filled pore. There is some debate (Lear *et al*. 1988, 1994, 1997; Åkerfeldt *et al*. 1993; Kienker & Lear, 1995; Mitton & Sansom, 1996; Zhong *et al*. 1998c; Randa *et al*. 1999) as to the most likely number of LS3 helices that self-assemble to form a channel, but a hexameric or heptameric assembly seems most likely. The pore is somewhat narrower than that formed by Alm (minimum radii of *ca*. 2·0 Å for $LS3_6$ and *ca*. 2·5 Å for Alm_6) and is lined solely by hydroxyl groups from the serine residues.

There is also a related synthetic peptide, LS2, which has fewer serines per heptad repeat (Table 1) and forms tetrameric helix bundles (Lear *et al*. 1988; Åkerfeldt *et al*. 1993). These bundles form proton-permeable channels and have received some attention (Mitton & Sansom, 1996; Zhong *et al*. 1998b; Randa *et al*. 1999) as simple models of more complex proton permeable pores (Forrest *et al*. 1998; Sansom *et al*. 1998b; Zhong *et al*. 1998a; Newns *et al*. 2000; Schweighofer & Pohorille, 2000).

In addition to 'simple' peptide models, there have been a number of studies of (synthetic) peptides, derived from more complex channel proteins, and thought to correspond to the main pore-forming element of such proteins. Although this approach has the drawback of uncertainty as to what extent the conformational and functional properties of the peptide mimic those of the parent channel, it has yielded interesting results for two (unrelated) systems.

M2δ (Table 1) is a synthetic peptide corresponding to the pore-lining M2 helix of the nAChR (Oiki *et al*. 1988, 1990; Montal, 1995; Opella *et al*. 1999). It has been shown that the peptide will spontaneously form channels in lipid bilayers. Furthermore, covalently tethered pentameric helix bundles form channels whose properties in several respects (conductance, block) resemble those of the parent nAChR channels (Montal *et al*. 1990, 1993). The peptide helix *in situ* in a lipid bilayer has been studied by solid-state NMR and shown to

https://doi.org/10.1017/S0033583501003729 Published online by Cambridge University Press

be tilted *ca*. 12° relative to the bilayer normal (Opella *et al*. 1999). A model of the pentameric helix bundle, M2δ_5, has been the subject of simulation studies (Law *et al*. 2000). Note that this model is of interest in that the sequence of the peptide is rather more complex than that of Alm or LS3, containing acidic, basic and neutral polar pore-lining side-chains.

Although not the primary concern of this review, H^+ conduction through ion channels is of interest both in terms of channels *per se* and also in relation to proton conductance mechanisms in bioenergetics. M2 protein from influenza A (fluM2) is a small (97 amino-acid) protein that homo-tetramerizes to form a H^+-permeable channel activated by low pH (Holsinger *et al*. 1994). It has been shown that a synthetic peptide corresponding to the single TM helix of fluM2 (fluM2-TM) will form ion channels in lipid bilayers (Duff & Ashley, 1992), and there have been several structural studies of the fluM2-TM peptide in lipid bilayers (Duff *et al*. 1992; Kovacs & Cross, 1997; Kukol *et al*. 1999; Song *et al*. 2000). Combining data from different experimental sources models of the tetramer of fluM2-TM helices have been generated (Forrest *et al*. 1998, 1999, 2000). The pore is quite narrow, containing a number of water molecules, and is constricted towards its C-terminal mouth by the inward-facing His37 residues that are believed to contribute to gating of the channel (Wang *et al*. 1995).

1.1.3 K channels

The X-ray structure of a bacterial K channel (Schrempf *et al*. 1995; Doyle *et al*. 1998; Fig. 3) enables us to develop a detailed physical description of ion permeation and selectivity for a 'real' channel. The overall shape of KcsA resembles a truncated cone with a central pore running down the centre. The wider end of the cone corresponds to the extracellular mouth of the channel. The transbilayer pore is formed by a bundle of eight TM helices (four M1 and four M2 helices) into the extracellular mouth of which is inserted a selectivity filter containing a TVGYG sequence motif characteristic of K channels. In the X-ray structure this adopts an extended conformation, and binds two K^+ ions plus an intervening water molecule. Beneath the selectivity filter is a central water-filled cavity. In the X-ray structure this cavity seems to contain a loosely bound cation. Finally, the pore-lining M2 helices constrict the intracellular mouth to form a putative gate region where the pore radius falls to *ca*. 1·1 Å (i.e. less than the Pauling radius of a K^+ ion, 1·3 Å). From sequence comparisons it appears likely that the architecture of the pore domain is conserved between diverse K channels, and so KcsA provides a framework within which to understand selectivity and permeation of all K channels. Several of the physiological properties of KcsA resemble those of the more intensively characterized mammalian K channels. In particular, KcsA is much more permeable to K^+ than to Na^+ ions (Heginbotham *et al*. 1999; Meuser *et al*. 1999). Furthermore, internal Na^+ ions seem to be able to block the flow of K^+ currents from inside to outside. It has been shown, via mutation and toxin binding to the extracellular channel mouth (MacKinnon *et al*. 1998) that the pore-forming domain of KcsA is closely related to that of mammalian voltage-gate K_v channels. However, it is likely that the resemblance between KcsA and K_v channels may be more distant in terms of channel gating (Camino *et al*. 2000).

KcsA has already been the subject of numerous simulation and theoretical studies. It therefore seems likely to become the *de facto* test system for evaluation of such approaches to understanding channel structure–function relationships.

https://doi.org/10.1017/S0033583501003729 Published online by Cambridge University Press

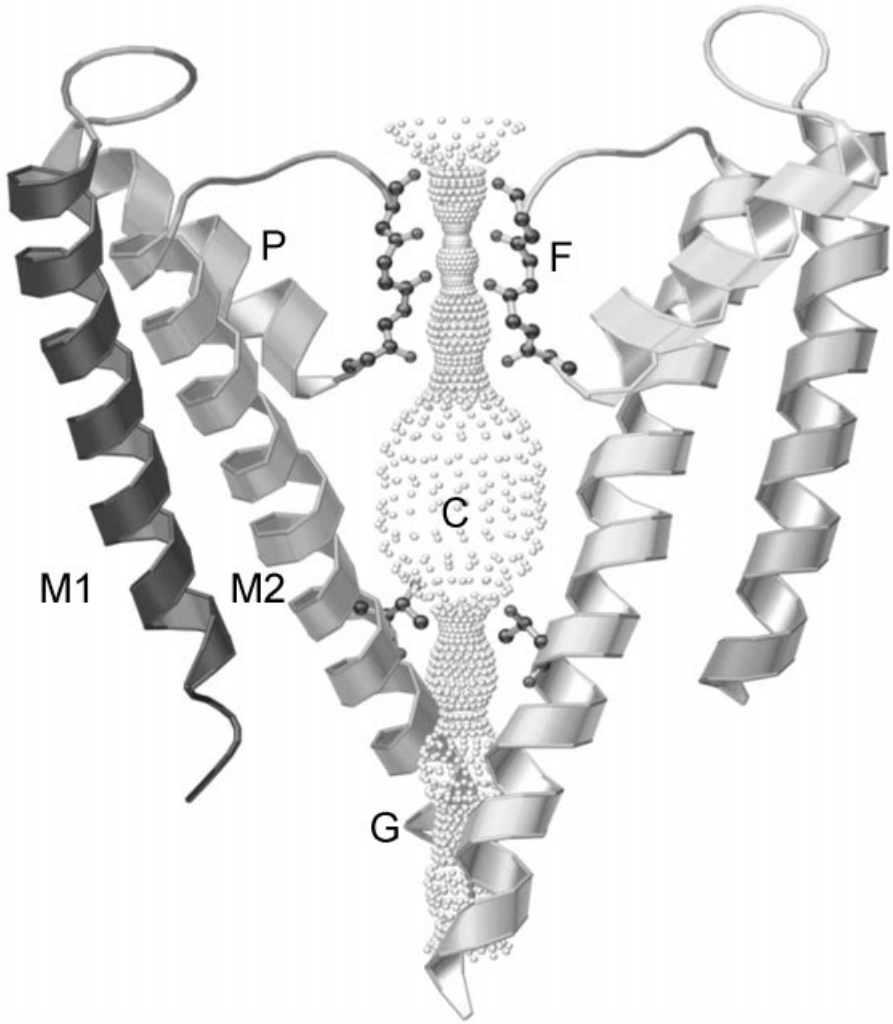


Fig. 3. KcsA – a bacterial K channel. Two of the four subunits are shown, viewed perpendicular to the pore axis, with the selectivity filter at the top of the diagram and the intracellular gate region at the bottom. The lining of the channel (calculated using HOLE; Smart *et al*. 1993) is shown as a dotted surface. The M1, M2, and P helices are labelled, along with the selectivity filter (F), the central cavity (C) and the intracellular gate (G).

The sequences of the P loops of various K channels are homologous, suggesting that they share a similar architecture. Thus, it is possible to generate plausible homology models of mammalian K channels using the bacterial KcsA structure as a template. Such models may provide insights into functional (e.g. permeation) properties of mammalian K channels. For example, a number of groups have generated models of the pore domains of inward rectifier K channels (Kirs; Doupnik *et al*. 1995; Reimann & Ashcroft, 1999) in order to help explain structure–function relationships (Loussouarn *et al*. 1999; Rupunte *et al*. 1999; Capener *et al*. 2000; Thompson *et al*. 2000). In this review we will mention studies of a model of Kir6.2. Kir6.2 is the channel-forming subunit of a K_{ATP} channel (i.e. a K channel gated by the intracellular concentration of ATP; Tucker *et al*. 1997).

https://doi.org/10.1017/S0033583501003729 Published online by Cambridge University Press

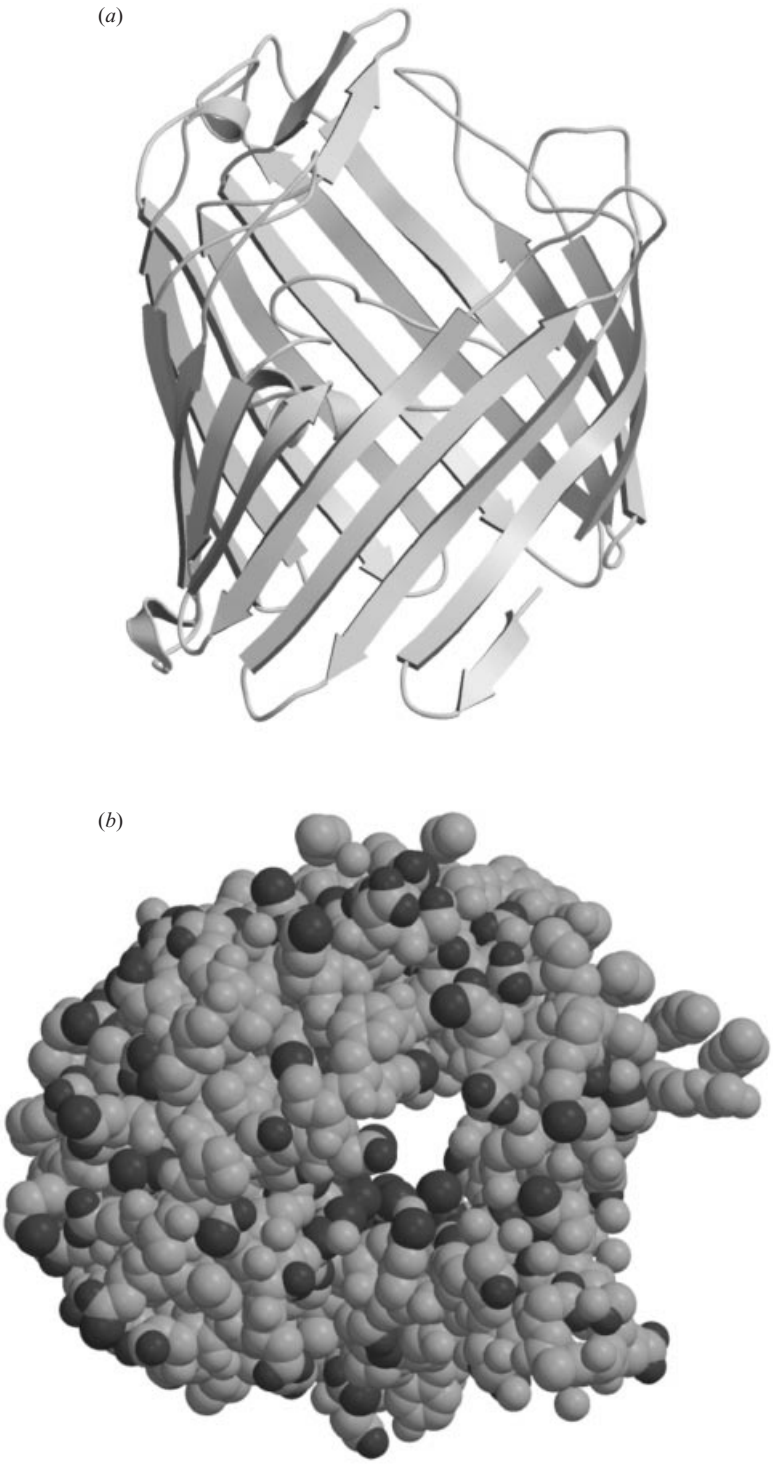


Fig. 4. A porin (OmpF). The structure of a monomer is shown, although the functional porin is a symmetrical trimer. (*a*) Illustrates the secondary structure whereas (*b*) is in space filling format.

https://doi.org/10.1017/S0033583501003729 Published online by Cambridge University Press

1.1.4 Porins

The *outer* membranes of Gram-negative bacteria contain several types of porins (Cowan, 1993; Schirmer, 1998; Dutzler *et al*. 1999). These are passive transporters of low-molecular-weight solutes, including sugars (Schirmer *et al*. 1995; Forst *et al*. 1998), which can also function, at least *in vitro*, as ion channels. High-resolution structures of a number of porins and their mutants are known, and they play a role in helping us to develop methods for simulation of ion channels. For example, the weakly cation-selective porin OmpF (Fig. 4) has been the subject of a number of mutation studies to change its ion selectivity (Schirmer & Phale, 1999). The constriction at the centre of the OmpF pore has acidic and basic side-chains on opposite walls of the pore, creating a strong transverse electrostatic field in this region. The conductances of porins (*ca*. 800 pS) are generally somewhat higher than those of many ion channels (usually in the range 10–100 pS) and their ion selectivities are correspondingly lower. The combination of available electrophysiological, structural and mutational data makes them valuable test systems for theories of ion permeation and selectivity (see below).

1.1.5 Nicotinic acetylcholine receptor

The nicotinic acetylcholine receptor channel (nAChR) is a member of a family of neurotransmitter-gated ion channels that also includes receptors for glycine, GABA, and serotonin (Ortells & Lunt, 1995). It is selective for cations over anions, and has a relatively high single-channel conductance (*ca*. 50 pS). By combining cryoelectron microscopy results (Unwin, 1993, 1995; Miyazawa *et al*. 1999) with mutagenesis and protein chemistry data (Changeux *et al*. 1992; Lester, 1992; Bertrand *et al*. 1993; Galzi & Changeux, 1994; Hucho *et al*. 1996; Corringer *et al*. 2000) one may construct 3D models (Ortells *et al*. 1996; Sankararamakrishnan *et al*. 1996; Adcock *et al*. 1998, 2000; Sansom *et al*. 1998a; Tikhonov & Zhorov, 1998) of the pore formed by the nAChR. In particular, it has been established that the lining of the transbilayer pore is formed principally by a pentameric bundle of M2 helices packed around a central water-filled pore. A 'hybrid' model of the nAChR may be constructed in which the pore-lining M2 helix bundle is treated atomistically and the remainder of the molecule is treated as a 'low-resolution' cylinder. The surface charge on the cylinder is derived from the distribution of charged amino acids in the amino-acid sequence (excluding the M2 segments; Adcock *et al*. 1998, 2000).

1.1.6 Physiological properties

It is evident that there are a number of structures of ion channels that one can attempt to relate to their physiological properties. What are the relevant properties and what are their timescales? The first property is that of conductance. The conductance of a channel (the reciprocal of its electrical resistance) is measured in pS and determines the number of ions per second that flow through a single channel. For example, a channel of conductance $g = 100$ pS ($\equiv 10^{-10}$ S) in a membrane across which there is a voltage difference of $V = 100$ mV ($\equiv 10^{-1}$ V) would allow, by Ohm's law $I = gV$, an electrical current of $I = 10^{-11}$ A $\equiv 6{\cdot}2 \times 10^{7}$ ions s^{-1} to flow. Thus the mean time spent by a *single* ion in passing from one side to the other of the channel is *ca*. $1{\cdot}6 \times 10^{-8}$ s ($\equiv 16$ ns) (assuming that only one ion is passed by the channel at a time, and that the ion is monovalent). This should be contrasted with channel gating which occurs on a timescale of *ca*. 1 ms. Thus, on a molecular scale,

https://doi.org/10.1017/S0033583501003729 Published online by Cambridge University Press

movement of ions through a channel is relatively fast and is not anticipated to involve any substantial (and slow) changes in channel structure, whereas channel gating is believed to require larger and slower changes in channel structure (Fig. 1).

In addition to permeation, the other aspect of channel function we would like to explain is ion selectivity. Different channels exhibit different degrees of selectivity. For example the nAChR and gA allow most monovalent metal ion cations to permeate, whereas K channels will allow K^+ ions (and also Rb^+ ions) through but have a low permeability to Na^+ ions. As well as selectivity *per se*, one would like to explain channel *block*, i.e. how certain ions not only fail to permeate but prevent also other ions from doing so, presumably by binding for long periods of time within the transbilayer pore.

Before embarking on an account of how simulation studies have been based upon known channel structures, a word of caution. Most structures of channels only define the pore domain of the protein. However, it appears that several channels *in vivo* include water-soluble domains or subunits close to one mouth of the pore that may alter the flow of ions (Biggin *et al*. 2000). These include the C-terminal 'tail' of KcsA (missing from the X-ray structure), the T1 domain tetramer of K_v channels (Kreusch *et al*. 1998; Bixby *et al*. 1999), and the cytoplasmic domain of the nAChR (Miyazawa *et al*. 1999). At present these have not been included in simulations. However, it would appear that such domains could alter channel function, and so will need to be included in future calculations.

1.2 Simulations

Ion channels provide an opportunity to address a key aspect of structural biology, namely how to relate an atomic resolution structure of a protein to its biological function, in a more rigorous fashion than is possible for many other systems. In particular, we wish to combine both experimental and theoretical understanding of ion channels in order to describe their physiological properties in terms of underlying physical processes. Simulations enable us to explore dynamic aspects of membranes that cannot be addressed directly by experimental structural biology. For example, X-ray diffraction provides a time- and space-averaged structure of a membrane protein in a specific crystal environment, whereas simulations enable us to explore the structural dynamics of a single-channel protein molecule embedded in a solvated lipid bilayer, in the presence of ions and water molecules. Thus, ion channels enable us to examine structure–function relationships at the level of a single protein molecule. The outcome of such studies may facilitate our understanding of the physiology of other transport proteins such as aquaporin (a passive water transporter) for which structural data are becoming available (Fu *et al*. 2000; Murata *et al*. 2000; Ren *et al*. 2001).

1.2.1 Atomistic *versus* mean-field simulations

A major consideration of any simulation study is that of what is the most appropriate level of detail to include in the description of the system. In principle one could treat the entire system (channel, water, ions, membrane) via quantum mechanics, taking account of the distribution of all electrons in the system. In practice, this is impossible. Even though mixed quantum mechanics and molecular mechanics (QM/MM) simulations have been run for enzymes (in which, e.g., the active site is treated quantum mechanically whilst the surrounding protein and solvent is treated classically; Burton *et al*. 1998), this approach has

https://doi.org/10.1017/S0033583501003729 Published online by Cambridge University Press

not been widely applied to ion channels. The majority of channel simulations fall into one of two categories. In *atomistic* simulations all (or most) of the atoms in a simulation system are treated explicitly (and classically). For a system made up of a channel molecule embedded in a small (*ca*. 100×100 Å) patch of lipid bilayer with water and ions on either side this amounts to *ca*. 50000 atoms or more. Such simulations have become possible in recent years following developments in accurate simulations of pure lipid bilayers (Tieleman *et al*. 1997; Tobias *et al*. 1997; Feller, 2000; Forrest & Sansom, 2000). Systems of *ca*. 50000 atoms are somewhat costly to simulate, even if all atoms and inter-atomic forces are treated classically (as in MD). With current resources this limits simulations to a maximum duration of *ca*. 10 ns. An alternative approach is to use a *mean-field* or *coarse-grained* simulation in which the protein is treated explicitly (the atoms are usually fixed) whereas the surrounding environment is treated as a continuum. Various mean-field approaches allow simulation times to be comparable to experimental times for ion permeation (Roux *et al*. 2000). However, it remains a non-trivial issue to decide on the best mean-field model, and on how to link the results of short timescale atomistic simulations to those of long timescale mean-field simulations.

2. Atomistic simulations

Atomistic simulations enable us to study the motions of ions and water molecules within an ion channel. Central to such simulations are the energetics of interaction of ions with water molecules and with protein. Therefore, before discussing simulation results in detail, it is important to review the current status of theoretical treatments of ion–water and ion–ligand interactions. Clearly this is a large topic, and so our focus is on MD approaches to ionic interactions, as used in most atomistic simulations of channels.

2.1 Modelling of ion-interaction parameters

In current MD force-fields the interaction of charged entities is described by two expressions, one that accounts for the electrostatic interaction and one that accounts for the van der Waals interactions. The electrostatic contribution to the energy is given by:

$$V = \sum_{ij} \frac{q_i q_j}{4\pi\epsilon_0 r_{ij}},$$

where q is the charge, ϵ_0 is the dielectric constant *in vacuo* and r is the separation between those two charges. A molecule will be assigned partial charges, conventionally centred on its nuclei, that best reproduce the electrostatic potential calculated by *ab initio* methods. For an ion the charge will be an integer value. Modelling of the van der Waals interactions is more difficult. The most commonly used expression is a 12-6 potential (the Lennard–Jones potential), that models the sum of the attractive van der Waals interactions (the r^{-6} part below) and the repulsive 'hard core' overlap energy coming ultimately from the Pauli exclusion principle:

$$V = 4\epsilon \left[\left(\frac{\sigma}{r} \right)^{12} - \left(\frac{\sigma}{r} \right)^{6} \right],$$

where ϵ is depth of the energy well that is represented by the potential and σ is the point at which $V = 0$. The separation at which the potential reaches its minimum is often referred to

https://doi.org/10.1017/S0033583501003729 Published online by Cambridge University Press

as $r_{\min}$ and is equal to $2^{1/6}\sigma$. The Lennard–Jones function describes the interaction between two atoms of the same type. In modern simulation programs there are often many different types of atom, representing each chemical species in a variety of different environments. A system with N different atom types would, in principle, require $N(N-1)/2$ parameters to describe all possible pairwize van der Waals interactions. It is common practice to apply mixing rules based on existing non-bonded parameters for homoatomic interactions. The most common of these is the Lorentz–Berthelot mixing rule for two atomic species X and Y:

$$\sigma_{XY} = \tfrac{1}{2}(\sigma_{XX} + \sigma_{YY}),$$

and

$$\epsilon_{XY} = \sqrt{(\epsilon_{XX}\epsilon_{YY})}.$$

Given a way to describe the non-bonded interactions between atoms and ions, what sort of experimental data can we compare such interactions with? There are a few key properties that theorists have concentrated on in recent years. The first we will consider is how well such parameters can reproduce inter-atomic distances, and effective ionic radii. The concept of 'ionic radius' is central to our thinking about ion channels, but such radii are not as easy to define as one might imagine.

2.1.1 Interatomic distances and the problem of ionic radii

An early source of ionic radii was from crystal structures of ionic salts. For example the distance between Na^+ and Cl^- ions in NaCl crystals is simply the sum of their crystal radii. Unfortunately these radii are not transferable; i.e. the same ions will have different radii in different compounds. One of the earliest proposals for ionic radii was by Pauling (1927, 1960), and indeed these radii are often used as a first approximation. When compared to recent crystallographic data, these radii are generally in quite good agreement, with the general trend that Pauling's estimates were too low for cations and too high for anions. Since Pauling there have been several proposals for ionic radii (Waber & Cromer, 1965; Ladd, 1968; Lebedev, 1969) that differ in the manner of their derivation.

However, in the context of ion-channel simulations at least some of the interactions are in aqueous solution and thus it is not obvious that *crystal* radii are applicable. When considering ionic radii in solution, one is particularly interested in ion-oxygen distances. Techniques that have been used to elucidate cation-solvent distances include: X-ray diffraction from ionic solutions; EXAFS (extended X-ray absorption fine structure); and neutron diffraction. EXAFS is limited to short-range interactions but provides very accurate information. Neutron scattering has the advantage that it can also locate hydrogen atoms (or rather deuterium atoms) of water and thus provides important information about the geometry of solvation. As simulations of ion channels will involve both situations that resemble aqueous solution and situations that resemble crystals, it is necessary to consider a variety of data currently available. The inter-atomic distance that is most commonly reported is the $r_{\text{ion-water(O)}}$ distance. In order to define a radius for the ion one needs a constant value for the radius of the water. In liquids, this value can be obtained in both experiment and computer simulation by using the radial distribution function $g(r)$. In order to obtain $r_{\text{water(O)}}$, one method is to take half of the inter-molecular distance in pure water. However, this value is subject to, e.g. temperature and the electrostrictive force that the waters in the first hydration

https://doi.org/10.1017/S0033583501003729 Published online by Cambridge University Press

Table 2. *Cation–oxygen distances and cation radii*

	Cation–oxygen distances (Å)						
	Aqueous solution				Cation radii (Å)		
Ion	X-ray	X-ray[a]	Neutron	Crystals	R(p)	R(m)	R(s/p)
Li^+	–	–	1·90–1·95	1·93–1·98	0·60	0·71 ± 0·07	0·74
Na^+	2·40	2·48	2·50	2·34–2·52	0·95	0·97 ± 0·06	1·02
K^+	2·87–2·92	2·85–2·88	2·70	2·67–3·22	1·33	1·41 ± 0·08	1·38
Rb^+	–	3·00–3·05	–	–	1·48	1·50	1·49
Cs^+	–	4·00–4·25	–	–	1·69	1·73 ± 0·08	1·70
Mg^{2+}	2·10	–	–	2·01–2·14	0·65	0·70 ± 0·04	0·72
Ca^{2+}	2·40	–	2·39–2·46	2·30–2·49	0·99	1·03 ± 0·05	1·00

Data from Burgess (1988), except: [a]X-ray from Krestov *et al.* (1994) (range is dependent upon waters assumed and coordination number).

R(p) = Pauling radii (Pauling, 1960), R(m) = radii assigned by Marcus (1988) and R(s/p) = radii assigned by Shannon & Prewitt (1969).

shell of an ion will experience compared to bulk water. For a detailed explanation of these considerations see Marcus (1988) who proposes a value of $r_{\text{water(O)}} = 1{\cdot}39 \pm 0{\cdot}02$ Å. In the case of crystals it is common to use a value of 1·40 Å, which Pauling assigned as the radius for both oxygen and oxygen anions (Hille, 1992). It is noteworthy that these values agree well with the value in liquid water (1·41 Å; Narten, 1972) and in ice (1·38 Å; Lonsdale, 1958). In Table 2 we show metal–oxygen distances derived from various techniques along with some proposed radii.

2.1.2 Solvation energy

Another property that has received attention in recent years is the solvation-free energy of an ion. Indeed, this is often one of the first tests of parameters for non-bonded interactions (Straatsma & Berendsen, 1988; Aqvist, 1990; Roux & Karplus, 1993; Babu & Lim, 1999). One simple approach to the solvation-free energy is provided by the Born model (Born, 1920; Roux *et al.* 2000), a continuum model in which the hydration energy in a homogeneous dielectric is given by:

$$\Delta G = \frac{q^2 e^2 N}{8\pi\epsilon_0 r}\left(\frac{1}{\epsilon_2} - \frac{1}{\epsilon_2}\right),$$

where q is the valence, ϵ is the dielectric constant of a medium and r is the ionic radius (sometimes called the Born radius). As this equation stands, the predicted hydration-free energies can be rather inaccurate. Rashin & Honig (1985) showed that by assigning a larger radius, this theory can produce much better agreement with experiment. This enlarged radius can be thought of as being at least partly due to the fact that only a certain number of waters can solvate the ion in the first shell, and thus there will be regions around the ion that are empty space. Further improvements to the theory usually stem from the dielectric assignments. In close proximity to the ion the ion will greatly reduce the polarizability of the solvent and a lower dielectric may be more appropriate in this region.

In the context of ion channels, the free energy of ionic hydration is a particularly important consideration, as it is often proposed that ion-channel selectivity is determined by the

https://doi.org/10.1017/S0033583501003729 Published online by Cambridge University Press

Table 3. *Solvation energies for some common cations in biological systems*

Ion	ΔG^{M}	ΔG^{FK}	ΔG^{B}	ΔG^{S}
Li^+	−113·5	−123·5	−122·1	−113·7
Na^+	−87·2	−98·3	−98·2	−88·6
K^+	−70·5	−80·8	−80·6	−71·2
Rb^+	−65·7	−76·6	−75·5	−65·9
Cs^+	−59·8	−71·0	−67·8	−60·4
Mg^{2+}	−437·4	−455·5	−455·5	−434·8
Ca^{2+}	−359·7	−380·8	−380·8	−356·7

ΔG^{M}, from Marcus (1991); ΔG^{FK}, from Friedman & Krishnan (1974) (this is standard molar Gibbs free energy, i.e. 1 atm gas → 1 mol/l^{-1}); ΔG^{B}, from Burgess (1978); ΔG^{S} from Schmid *et al*. (2000) – this corresponds to the FK data but corrected to be the Gibbs free energy of transferring an ion from an empty box into solution. These values are taken directly. No account has been taken of the reference value of $\Delta G^{*}[H^+]$ (for example see the table in Hummer *et al*. 1996). All energies in kcal mol^{-1}.

Table 4. *Some water models commonly used in simulations*

Property	Experimental	SPC	SPC/E	TIP3P	TIP4P	ST2	BF
r(OH) (Å)	0·957	1·0	1·0	0·9572	0·9572	1·0	0·96
θ(HOH) (°)	104·52	109·47	109·47	104·52	104·52	109·47	105·7
q(O)	–	−0·82	−0·82	−0·834	0·0	0·0	0·0
q(H)	–	0·41	0·4238	0·417	0·52	0·2375	0·49
q(M)	–	0·0	0·0	0·0	−1·04	−0·475	−0·98

Data derived from Leach (1996) and Jorgensen *et al*. (1983). The partial charges (in units of e) on the water O and H atoms are given by q(O) and q(H), respectively. For the 4-point charge models q(M) gives the sum of the partial charges associated with the lone pairs of the O atom.

energetic cost of replacing waters with polar atoms that line the channel wall (e.g. oxygen atoms for a cation-selective channel). Thus, to treat channel selectivity quantitatively it is necessary to evaluate a (relatively small) difference between two large numbers: the free energy of hydration of an ion, and the free energy of 'solvation' of the same ion by a channel. Thus, in order to predict selectivity from structure, one must be confident that the calculations are as accurate as possible. A starting point for evaluating such accuracy is to calculate the free energy of hydration of ions or small Lennard–Jones particles. It is perhaps surprising that these calculations remain non-trivial, and that there has been recent debate about how to best perform them (Åqvist & Hansson, 1996, 1998; Ashbaugh & Wood, 1997; Hummer *et al*. 1997, 1998; Ashbaugh *et al*. 1998). In particular, careful consideration of long-range electrostatic interactions seems to be important. There is currently some debate about how these should be calculated, and depending on the method employed different results are obtained (Ashbaugh & Wood, 1997; Hummer *et al*. 1997). The matter is complicated further by the fact that even in commonly cited sources of hydration-free energies (Rossiensky, 1970; Salomon, 1970; Friedman & Krishnan, 1974; Conway, 1978, 1981; Marcus, 1988) the actual values quoted exhibit considerable variation (see Schmid *et al*. 2000, for further discussion). Although detailed discussion of solvation is beyond the scope of this review, Table 3 shows some typical values reported in the literature.

In addition to parameterization of ions *per se* one should remember there are many different models of water that can be used in simulations. Table 4 shows some properties of the more

https://doi.org/10.1017/S0033583501003729 Published online by Cambridge University Press

Table 5. *Ion coordination – first shell solvation numbers*

Ion	NMRa	NMRb	XRND	GM	PCA
Li^+	3·4–5	4	4–6	4	5
Na^+	3–4·6	6	4–6	6	6
K^+	1–4·6	8	6, 8	6	7
Rb^+	1·6–4		6–4, 8	6, 8	8
Cs^+	1–3·9		6–8	8	8
Mg^{2+}	6	6	6	6	6
Ca^{2+}		6	4, 6	6	7

Data are from Krestov (1991), Krestov *et al.* (1994) The numbers shown are for the *first* solvation shell only. Ranges are indicated by a dash and separately reported values are indicated by a comma (see Krestov, 1991; Krestov *et al.* 1994, for more details and references therein). Data sources are indicated by: NMRa = NMR, direct integration of separate signals; NMRb = NMR, chemical shift and spin lattice relaxation; XRND = X-ray and neutron diffraction; GM = gravimetry; PCA = physico-chemical analysis using model solvates.

common water models. For further discussion the reader is referred to Daggett & Levitt, (1993) and Leach (1996). At present the SPC and TIP3P water models are the most commonly employed in ion-channel simulations.

2.1.3 Hydration shells and coordination numbers

When discussing ion permeation and selectivity it is useful to consider how many water molecules form the first hydration shell of an ion, especially as our overall picture of ion permeation is one in which these waters may be replaced by protein ligands. The first hydration shell has been defined as the number of ions within direct contact with the ion. Such data have often been derived from X-ray structures of hydrated complexes. However, a more realistic definition within aqueous solutions is to take the number of water centres that fall within the first minimum of a radial distribution function, i.e. a $g(r)$ *versus* r plot.

There are other ways to obtain an estimate of the coordination number around an ion. Chemically speaking, a coordination number would imply a fixed geometry of ligands (waters) around the ion. However, in solution the shell is dynamic and so the coordination number may be defined as the most probable number of solvent molecules constituting the immediate surroundings of the ion. Sometimes people talk of a solvation number, equal to the coordination number *plus* the number of solvent molecules in the region beyond the immediate vicinity of the ion that show a correlation with the presence of the ion. This solvation number can be as large as 700. Therefore, whilst remembering that waters outside the first shell may be important, it is more common to use the coordination number as this provides a more direct picture of the ion-water complex.

While coordination numbers (Table 5) are a useful aid to our thinking about ion permeation through channels, it must be remembered that the hydration shell is a dynamic entity. That is, waters within this shell have a certain probability of returning into the bulk solution. In the context of ion-channel simulations, it is important to ask whether one can expect to see substitution of hydration shell waters within the timescales of a simulation. In pure water the dielectric relaxation time is of the order of 10 ps (Hille, 1992). Most biologically important ions (other than Mg^{2+}; Diebler *et al.* 1969) have shown that the

https://doi.org/10.1017/S0033583501003729 Published online by Cambridge University Press

https://doi.org/10.1017/S0033583501003729 Published online by Cambridge University Press

Table 6. *Cation parameters for some common force fields*

Parameter sets	Na^+		K^+		Rb^+		Cs^+	
	ϵ	r_{min}	ϵ	r_{min}	ϵ	r_{min}	ϵ	r_{min}
Charmm	−0·0469	1·36375	−0·0870	1·76375	–	–	−0·1900	2·10
Amber	−0·000843	2·0527	−0·000328	2·6577	−0·00017	2·9558	−0·00008	3·3951
Åqvist	−0·000845	2·053	−0·000328	2·660	−0·00017	2·9585	−0·00008	3·3988
Gmx(a)	−0·0148	1·44528	−0·00001353	3·62267	–	–	–	–
Gmx(b)	−0·00084498	2·0638	−0·000328	2·7695	−0·00017051	3·1605	−0·00008	3·7693
MSI	−0·026	1·650	−0·0100	2·350	−0·00653	2·661	−0·00449	2·909

Values are obtained as follows: Charmm values are taken directly from the c27b1 par_all27 parameter files. Amber values are taken directly from the Amber force field. Åqvist are taken from Åqvist (1990). Gmx(a) are values taken from the Gromacs force field (gmx2.0). Gmx(b) are parameters that were originally transfered from Åqvist (1990) into the Gromacs forcefield. MSI parameters are taken directly from the PARM.PRM parameters in the 1998 distribution of Quanta. Units are kcal mol^{-1} (ϵ) and Å (r_{min}).

substitution rate of inner shell waters is greater than 10^8 s^{-1}. Thus one would expect to see to be able to see substitution of protein ligands for water within nanosecond duration simulations.

2.1.4 Parameters in common use and transferability

In the last few years, there have been several attempts to generate parameters for ions, particularly for the monovalent cations, due in part to the availability of structures of gA (Ketchem *et al*. 1993; Cross *et al*. 1999) and more recently KcsA (Doyle *et al*. 1998). Tables 6 and 7 show some simple test calculations for parameters available in commonly used force fields and in the literature. The results indicate that despite variations in the values of ϵ and σ, it is possible to reproduce aspects of *ab initio* gas phase calculations quite closely. More recently (Babu & Lim, 1999) discuss the transferability of Åqvist's parameters to other solvent models (namely TIP3P) and find good agreement between experimental free energies and the calculated ones (Åqvist, 1990).

2.1.5 Summary

The estimation of non-bonded parameters for ions remains problematic. However, it is encouraging that the tests shown in the Table 7 yield results that agree well with at least some of the experimental data. This problem may not be as critical as first envisioned, although there does seem to be some variation between different parameter sets particularly with respect to Na^+ ions. Provided one is consistent in application of these parameters, at least relative calculations may be performed with some degree of certainty. Note that we have limited our discussion to monovalent cations. Clearly parameters for other common biological ions (e.g. Cl^-, Mg^{2+}, Ca^{2+}) are important. Negative ions are interesting in that they induce greater structure in aqueous solvent. This may have important implications for transport through chloride channels (Jentsch *et al*. 1999). Divalent ions are of considerable biological importance, and further work is needed on their parameterization for MD simulations. In particular, the effect of induced polarization is unlikely to be negligible for these ions.

2.2 Water in pores *versus* bulk

In trying to understand the microscopic properties of ion channels it is important first to characterize the properties of water within pores (Fig. 5). In particular, we need to know how the dynamics (e.g. rate of diffusion, rotational correlation times) and structure (e.g. orientation of water molecules) of water within a pore of molecular dimensions differs from that of water in its bulk state. It has been shown that solvents confined in spaces of molecular dimensions possess significantly different properties from those of the same solvents when in the bulk state (Granick, 1991). In particular, a number of MD simulations of water molecules located between two planar hydrophobic surfaces (Jonsson, 1981; Marchesi, 1983; Barabino *et al*. 1984; Lee *et al*. 1984; Rossky & Lee, 1989) or within spherical hydrophobic pockets (Belch & Berkowitz, 1985; Zhang *et al*. 1995) indicate that water thus confined exhibits a greater degree of order than in the bulk solvent, with the formation of distinct 'layers' of molecules parallel to the confining surface. Furthermore, the dynamic properties of the water

https://doi.org/10.1017/S0033583501003729 Published online by Cambridge University Press

https://doi.org/10.1017/S0033583501003729 Published online by Cambridge University Press

Table 7. *Results of simple test simulations of cation–oxygen interactions*

	Na^+				K^+				Rb^+				Cs^+			
	Water		NMA		Water		NMA		Water		NMA		Water		NMA	
Parameter set	*r*	*U*	*r*	*U*	*r*	*U*	*r*	*U*	*r*	*U*	*r*	*U*	*r*	*U*	*r*	*U*
Charmm	2·081	−32·26	2·097	−37·32	2·476	−24·04	2·480	−29·76	–	–	–	–	2·857	−18·95	2·848	−24·89
Amber	2·020	−28·87	2·217	−33·94	2·518	−22·75	2·525	−28·20	2·642	−20·89	2·645	−32·93	2·840	−18·38	2·836	−23·84
Åqvist	2·325	−26·04	2·291	−23·03	2·640	−20·76	2·610	−19·15	2·761	−19·14	2·735	−17·91	2·957	−16·95	2·934	−16·20
Gmx(a)	2·174	−29·60	2·121	−25·93	2·851	−18·04	2·837	−20·26	–	–	–	–	–	–	–	–
Gmx(b)	2·333	−25·88	2·298	−22·92	2·716	−19·74	2·686	−21·72	2·810	−17·56	2·873	−16·72	3·206	−14·70	3·182	−14·45
MSI	2·255	−28·05	2·266	−33·37	2·707	−20·28	2·707	−25·89	2·899	−17·96	2·894	−23·52	3·044	−16·47	3·035	−21·95
Ab initio	2·21	−24·00	2·10	−38·40												

For each cation–water or cation–N-Me-acetamide (NMA) pair, an energy minimization was performed. The table reports the resultant M–O distance (*r*, in Å) and interaction energies (*U*, in kcal mol^{-1}). Ion parameters are as defined in Table 6. The water model used was either TIP3P (for Charmm, Amber, MSI) or SPC [for Åqvist, Gmx(a), Gmx(b)]. The NMA partial charges were from Charmm v.22 (for Charmm, Amber, MSI) or from Gromos [for Åqvist, Gmx(a), Gmx(b)]. All minimizations were performed within Charmm.

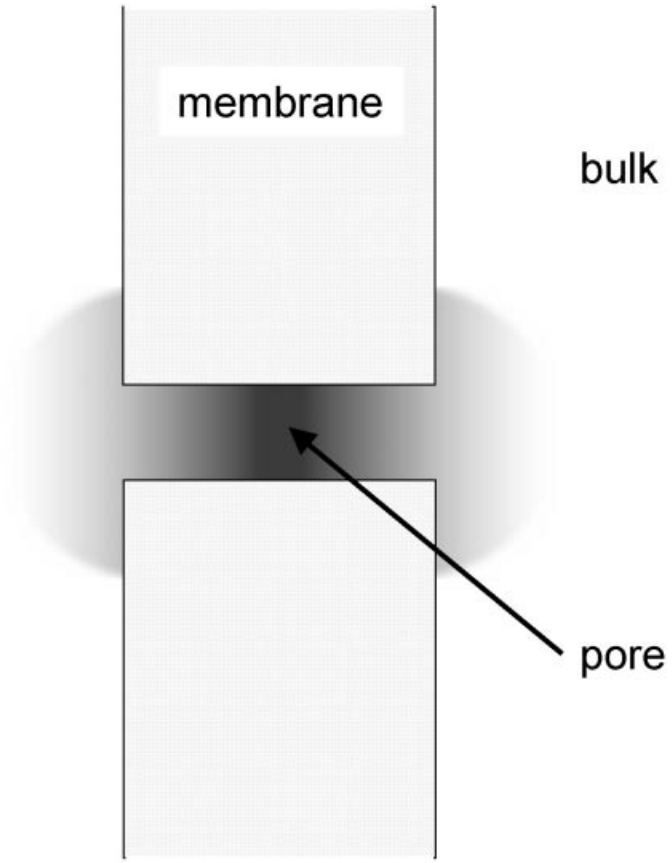


Fig. 5. Schematic diagram of water within a transbilayer pore of molecular dimensions. Within the pore the water properties are perturbed relative to those of bulk water, the degree of perturbation being indicated by the depth of the shading.

molecules close to the surface may be perturbed (Marchesi, 1983; Barabino *et al*. 1984; Zhang *et al*. 1995; Yeh & Berkowitz, 2000).

Translational motion of water is often quantified via a self-diffusion coefficient. This may be estimated from simulations by evaluation of the mean square displacement (MSD) of a water molecule as a function of time:

$$\langle r(t)^2 \rangle = \langle (r(t) - r(0))^2 \rangle.$$

The relationship:

$$\lim_{t \to \infty} \langle r(t)^2 \rangle = 2dDt$$

(where d is the dimensionality of the space in which the displacement is being considered) is then used to fit the MSD data for a suitably long time range. Of course, what is meant by 'suitably long' may be constrained by the practicalities of a simulation, and may in some cases (see below) have a significant impact on estimation of D. Furthermore, it is known that different water models differ in their 'bulk' self diffusion coefficient (Daggett & Levitt, 1993; Levitt *et al*. 1997). Therefore, a convenient measure of the degree of perturbation of water

https://doi.org/10.1017/S0033583501003729 Published online by Cambridge University Press

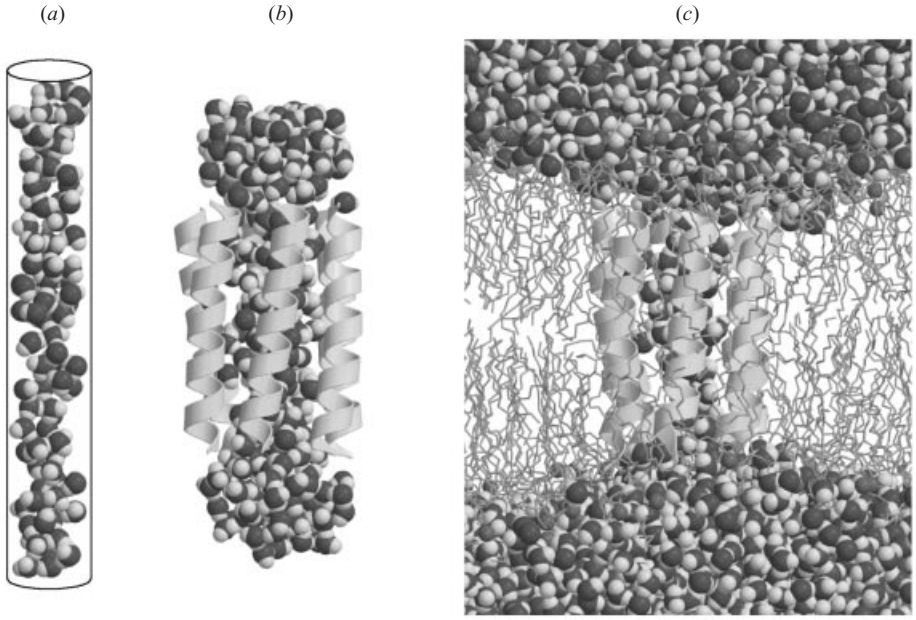


Fig. 6. Water within pores, showing three levels of description of the simulation system. (*a*) Water constrained within a 3 Å radius cylinder; (*b*) water within a helix bundle (a hexameric LS3 pore; Kerr *et al*. 1994; Mitton & Sansom, 1996); (*c*) water within the same helix bundle, but now embedded within a fully solvated phospholipid bilayer (Randa *et al*. 1999).

diffusion rates within a pore can be obtained by calculating the ratio $D_{\mathrm{pore}}/D_{\mathrm{bulk}}$. For very narrow (*ca*. 2 Å or less) channels, diffusion becomes single file (see below) and the relationship used above ($r^2 = 6Dt$) may no longer be appropriate.

2.2.1 Simple pore models

A number of studies have examined water confined within channel-like geometries, i.e. radically simplified models of ion channels with hydrophobic walls and no atomistic structure to the pore (Fig. 6). (Sansom *et al*. 1996) performed MD simulations of water molecules confined within 'channels' modelled as cylindrical cavities with lengths ranging from 15 to 60 Å and radii from 3 to 12 Å. At the end of 50 ps simulations water molecules were observed to be ordered into approximately concentric cylindrical shells. For cavities of radius 3 and 6 Å, water mobility was reduced relative to that of simulated bulk water, whereas for 9 and 12 Å radii waters exhibited mobilities comparable to that in the bulk. If water molecules were confined within an hourglass-shaped cavity (with a central radius of 3 Å increasing to 12 Å at either end) the water mobility was related to the local cavity radius. Lynden-Bell & Rasaiah (1996) simulated water within idealized smooth cylindrical channels of radii between 2·5 and 5·5 Å, and of infinite length. The water molecules formed a cylindrical solvation shell inside the channel walls with some evidence of a second shell in the centre of the largest channel. The diffusion coefficient of water within these channels was somewhat suppressed relative to bulk, this effect being particularly strong for a pore radius of 4 Å. These studies were extended by Allen *et al*. (1999a) who also examined the effects of channel wall structure on water properties. Comparing hydrophobic and hydrophilic cylindrical pores (the latter

https://doi.org/10.1017/S0033583501003729 Published online by Cambridge University Press

constructed from regular cylindrical arrays of oxygen atoms) of 2–6 Å radius revealed different levels of reduction of self-diffusion in hydrophobic and hydrophilic pores due to differences in interactions with the pore lining. These results indicate that in addition to general effects (reduction of translational and rotational mobility) due to confinement, specific effects due to the nature of the pore lining may occur, indicating a need for more realistic pore models. Lu & Green (1997) have examined water in a simple model pore, taking into consideration effects of charges in the pore lining and in the context of possible channel-gating mechanisms.

Simple atomistic models of channels have been examined using two systems: parallel bundles of hydrophobic (Ala_{20}) α-helices; and 8-stranded hydrophobic (Ala_{10}) anti-parallel β barrels. In both systems self-diffusion coefficients of water molecules were reduced significantly relative to bulk water (Breed *et al*. 1996). Water rotational reorientation rates were also reduced within the pores, particularly in those pores formed by α-helix bundles. In the narrowest pore (a pentameric bundle of Ala_{20} helices) self-diffusion coefficients and reorientation rates of intra-pore waters were reduced by approximately an order of magnitude relative to bulk solvent. Furthermore, in Ala_{20} helix bundles the water dipoles oriented anti-parallel to the helix dipoles. No preferential orientation of water dipoles relative to the pore axis was observed in the hydrophobic β-barrel models.

It is known that a simple dipolar liquid confined within a spherical cavity shows a lower dielectric constant than in the bulk phase (Senapati & Chandra, 1999). Zhang *et al*. (1995) estimated a value of 5 based on MD simulations of water in a cavity. The Ala_{20} α-helix bundle and Ala_{10} β-barrel models of ion channels have also been used to explore whether water within channels exhibits a reduced dielectric (Sansom *et al*. 1997). MD simulations in the presence of an electrostatic field along the pore axis were used to estimate the resultant reorientation polarization of water within the pore, and hence to determine local dielectric behaviour. The local dielectric constant of water within a pore *was* reduced for models formed by parallel α-helix bundles, but *not* by those formed by β barrels. Some implications of these studies with respect to continuum electrostatics calculations and other mean-field approaches are discussed below.

More complex behaviour of water is seen in 'real' channel structures. However, the basic observation of perturbation of water properties from those of the bulk phase is preserved. Note that the majority of these results are from simulations of ion channels embedded in a lipid bilayer.

2.2.2 gA

Studies of gA suggest that in this system intra-pore water differs markedly in its dynamic properties from bulk water (Chiu *et al*. 1991, 1993; Sancho *et al*. 1995). Various MD simulations of gA (reviewed by Roux & Karplus, 1994) have revealed a *single-file* column of water molecules that forms a H-bonded chain within the gA channel. The self-diffusion coefficient of these waters is considerably lower than that of bulk water. Using modified TIP3P Roux & Karplus (1994) estimated $D = 0{\cdot}003$ Å^2 ps^{-1}, close to the experimental estimate of $D = 0{\cdot}004$ Å^2 ps^{-1} for gA channel water. Thus, it is evident that substantial translational immobilization of water occurs within the gA pore. Furthermore, studies by Jordan and colleagues (Sancho *et al*. 1995) have emphasized that the presence of a cation within the gA channel will result in further reductions of the rotational mobility of intra-pore

https://doi.org/10.1017/S0033583501003729 Published online by Cambridge University Press

water. Subsequent simulation studies of gA embedded in a large (*ca*. 96 DMPC lipid molecules) patch of bilayer (Chiu *et al*. 1999a, b) have enabled water transport through this channel to be analysed in detail. It was shown that the relative mobility of water in the gA channel, relative to bulk, was *ca*. 0·1, both for simulations of unrestrained gA in a lipid bilayer and for simulations with weak restraints (in the absence of lipid). However, if tight restraints were applied or a rigid channel was employed, water mobility dropped by a further order of magnitude.

2.2.3 Alm

The structural and dynamic properties of water in Alm channels have been explored, using both *in vacuo* simulations of Alm helix bundles containing water within and at each mouth of the pore (Breed *et al*. 1996) and unrestrained simulations of Alm helix bundles in a fully solvated lipid (POPC) bilayer (Tieleman *et al*. 1998, 1999). In both cases the dipole moments of water molecules within the pore were aligned anti-parallel to the helix dipoles (as seen in bundles of simple Ala_{20} α-helices). This may contribute to the stability of the helix bundle, the water dipoles partially counteracting the repulsive interactions of the parallel helix dipoles. However, the exact extent of water dipole alignment may depend on the treatment of long-range electrostatics in the system (Tieleman, unpublished observations; see below). The diffusional motion of water within the pore was also substantially reduced below its bulk value.

2.2.4 $LS3_6$ (and $LS2_4$)

The *de-novo* designed peptides (LS3 and LS2) of Lear *et al*. (1988), which contain only leucine and serine residues, are simple examples of such channels formed by bundles of amphipathic α-helical peptides. Restrained MD simulations of $LS2_4$ and $LS3_6$ peptide helix bundles *in vacuo* but with water molecules within and at the mouths of their pores (Fig. 6*b*) were used to investigate the properties of intra-pore water in these systems (Mitton & Sansom, 1996). As with gA and Alm, the translational and rotational mobility of water molecules within the pores were reduced relative to bulk water. Furthermore, intra-pore waters oriented themselves with their dipoles anti-parallel to the helix dipoles, as did the hydroxyl groups of serine residues. These two systems have since been investigated in longer (ns) unrestrained MD simulations in a bilayer or bilayer-like environment. Simulations of both $LS2_4$ and $LS3_6$ have been performed in a membrane mimetic system consisting of a slab of octane molecules with water on either side (Zhong *et al*. 1998b, c). For $LS2_4$ the tetrameric bundle formed a 'dimer of dimers'; for $LS3_6$ the helix bundle was unstable in the absence of a transbilayer voltage. However, in simulations in a phospholipid bilayer (Randa *et al*. 1999) both $LS2_4$ and $LS3_6$ (Fig. 6*c*) were stable in the absence of an electrostatic field. This may reflect differences in the simulation system (octane slab *versus* phospholipid bilayer), in the initial bundle models used, and/or in the treatment of long-range electrostatics in the simulations (Ewald summation *versus* a simple cut-off). In both the $LS2_4$ and the $LS3_6$ studies the water molecules within the pore were immobilized and aligned anti-parallel to the helix dipoles in the same way as in the Alm simulations and the *in-vacuo* simulations. The water motion in the narrow pore of the 4-helix ($LS2_4$) bundle is highly restricted and may provide suitable conditions for proton transfer via a water wire mechanism (Akeson & Deamer, 1991; Pomes & Roux,

https://doi.org/10.1017/S0033583501003729 Published online by Cambridge University Press

1996). In the wider hexameric ($LS3_6$) pore, water diffuses much more slowly than in bulk but is still mobile.

2.2.5 Nicotinic receptor M2δ_5

This peptide helix bundle, which is believed to mimic some aspects of the channel-forming domain of the nAChR, has been studied by modelling and simulation (Montal, 1995; Law *et al*. 2000) primarily in the context of possible kinking motions of the individual helices and their relevance to models of channel gating (see below). However, a 2 ns simulation of M2δ_5 in a POPC bilayer (Law *et al*. 2000) shows that the motions of water molecules within the pore are reduced relative to the bulk and that the water dipoles are aligned anti-parallel to the helix dipoles, as in the simpler systems discussed above.

2.2.6 Influenza A M2

FluM2 is a relatively simple channel that has been studied in considerable detail (Forrest *et al*. 1998). In a 4-ns MD run of the FluM2-TM tetramer embedded in an octane slab (Zhong *et al*. 1998a), a left-handed coiled coil formed a water-filled funnel-like structure. This funnel was occluded at residue His37, which thus blocked the channel. In a subsequent study it was suggested that the channel could be opened via protonation of His37 (Newns *et al*. 2000), this being related to a possible model of channel gating (see below). Simulations in a POPC bilayer of the FluM2-TM helix bundle using different starting models (Forrest *et al*. 2000) suggest that the results are sensitive to the exact starting structure, at least on a nanosecond timescale, although in general the bundles were occluded at His37. The latter was also true in the simulations of Schweighofer & Pohorille (2000).

It has been suggested that the functional FluM2 protein may act as a proton channel by providing a column of waters through which H_3O^+ transfer may occur, via the proton wire mechanism. The columns of water observed in FluM2-TM simulations could act as 'water wires' for protons. However, in most simulations the pore is occluded around the position of the ring of His37 residues, preventing formation of a continuous column of water along the length of the channel. This suggests that the models are of the 'closed' forms of the channel. Overall, these studies suggest better starting models are needed for future FluM2-TM simulations. This reflects a general problem for peptide helix bundle simulations, where one is never sure how robust the simulation results are to changes in the detail of the starting model.

2.2.7 K channels

There have been a number of studies of water mobility and structure in KcsA and in KcsA-like models. It should be noted that several of these simulations have been on a restrained channel model *in vacuo*, i.e. without explicit inclusion of the bilayer environment. Given the results on gA (see above) one should perhaps exercize a degree of caution with respect to such results. Chung and colleagues have compared two simulations: (i) of a simplified model of KcsA as an appropriately dimensioned, irregular hydrophobic tube into which an atomistic model of the selectivity filter was 'embedded' (Allen *et al*. 1999b); and (ii) of a complete model of the channel, restraining the Cα atoms of the inner and outer helices to maintain the protein

https://doi.org/10.1017/S0033583501003729 Published online by Cambridge University Press

coordinates close to those of the X-ray structure in the absence of a bilayer (Allen *et al*. 2000). Both simulations showed a degree of reduction to the water diffusion coefficient within the cavity (the maximum radius of which is *ca*. 6 Å). In the simplified model $D_{\mathrm{pore}}/D_{\mathrm{bulk}}$ was *ca*. 0·7 for this region, whereas for the more complete model $D_{\mathrm{pore}}/D_{\mathrm{bulk}}$ was *ca*. 0·4. A simulation of a model of KcsA (Ranatunga, 2000; Ranatunga *et al*. 2001a) in which restraints on the protein coordinates were derived from the magnitude of fluctuations in a bilayer-embedded simulation of KcsA (Shrivastava & Sansom, 2000) using the TIP3P water model gave $D_{\mathrm{pore}}/D_{\mathrm{bulk}}$ *ca*. 0·1 for the cavity region. A simulation of KcsA in a POPC bilayer, with SPC water and PME for electrostatics (P. C. Biggin & M. S. P. Sansom, unpublished observations) gave $D_{\mathrm{pore}}/D_{\mathrm{bulk}}$ *ca*. 0·4 for 27 water molecules in the cavity region. Thus it would seem that the exact behaviour of water molecules in the *same* channel model is dependent on the water model used and/or the exact treatment of the environment of the protein (i.e. lipid bilayer *versus* restraints). Clearly if restraints are to be used, some care has to be taken in deciding on their nature and magnitude. To add a further element of complexity, Carloni and colleagues have shown that the presence and location of an ion in the cavity can alter the overall orientation of the water molecules in this region (Guidoni *et al*. 2000). Finally, we note that a careful comparison of the simulations of KcsA (Allen *et al*. 1999b, 2000; Bernèche & Roux, 2000; Guidoni *et al*. 2000; Shrivastava & Sansom, 2000) reveals variation in the number of water molecules placed within the cavity region from *ca*. 15 to *ca*. 40. Clearly this is also an important factor. A measurement of the volume of the cavity based on an internal Connolly surface and a simple assumption of the same density of water in the cavity as in the bulk (which may not be true) yields an estimate of *ca*. 23 water molecules. Using a Monte Carlo (MC) insertion procedure (http://fulcrum.physbio.mssm.edu/~mezei/mmc/) gives *ca*. 27 water molecules in the cavity. However, it remains unclear which is the 'best' approach to solvating complex channel structures in simulation studies, and further work is needed in this area.

We have only considered the behaviour of water molecules in the cavity. As will be seen below, the movement of water molecules within the filter region is strongly coupled to movement of ions in that region, and seems to follow single-filing type motion.

2.2.8 nAChR

The pore of the nAChR is believed to be wider than the pore of KcsA. Of course, at present there is no high-resolution structure of the nAChR and so simulations of water behaviour within its pore have employed models based on the available structural data. A model of the nAChR in which the pore-lining M2 helix bundle is treated atomistically and the remainder of the molecule is treated as a 'low-resolution' cylinder (see above) has been used in MD simulations to estimate the self-diffusion coefficients of water molecules within the channel (Adcock *et al*. 2000). In the narrowest region of the pore, D is reduced *ca*. threefold relative to that of bulk water.

2.2.9 Porins

The bacterial porins are of particular interest in the context of water within transmembrane pores. Firstly, as will be seen below, ion conduction by these relatively high conductance channels (*ca*. 800 pS per monomer) can be approximated by diffusion-based mean-field

https://doi.org/10.1017/S0033583501003729 Published online by Cambridge University Press

simulations and thus it may be possible to develop a quantitative understanding of the importance of water (and ion) diffusion coefficients within the pore. Secondly, porins are one of the few channel systems for which experimental measurements of the dielectric properties of water within the pore have been published. It has been estimated, albeit indirectly, that the dielectric constant for water within the pore of the porin PhoE is *ca*. 20 (Gutman *et al*. 1992). As noted above the arrangement of oppositely charged residues on opposite walls of the narrowest region of the pore creates a strong transverse electrostatic field, which in turn is expected to have a profound effect on the behaviour of water molecules in this region.

MD simulations of the weakly cation-selective porin OmpF in a POPC bilayer (Tieleman & Berendsen, 1998) were the first simulations of a complex protein channel in a full bilayer environment. The simulations (of *ca*. 1 ns duration) revealed complex, non-bulk properties of water within the transbilayer pore. Within the pore, water diffusion coefficients were reduced by tenfold relative to bulk. The transverse electrostatic field in the pore resulted in a high degree of alignment of the water dipoles. This would be expected to reduce the dielectric in this region, in agreement with the experimental studies cited above. The local field within the pore reached a maximum of *ca*. 10^9 V m^{-1}. At such a field strength the water will not behave as a linear dielectric medium. This should be taken into account in more accurate mean-field treatments of such ion channels (see below).

2.2.10 Relevance

What is the relevance of these studies? It is evident that water within channels differs significantly in its properties from water in the bulk state, almost regardless of the microscopic structure of the channel. In particular, most channels result in decreased diffusion of water within the pore relative to bulk, although it is evident that the value of $D_{\mathrm{pore}}/D_{\mathrm{bulk}}$ may be sensitive to the exact nature of the channel model and to the details of the simulation conditions. This is relevant if one is constructing a mean-field model of ion permeation. For example, in a simple approach Smart and colleagues (Smart *et al*. 1997, 1998) have shown that an approximate conductance magnitude can be calculated from the equivalent resistance of a channel-sized cylinder of electrolyte solution (Hille, 1992; Sansom & Kerr, 1995), provided one takes into account reduced diffusion within the pore by correcting ionic mobilities by the ratio $D_{\mathrm{water,pore}}/D_{\mathrm{water,bulk}}$. In principle the latter should be obtained by MD simulations for each channel in question. However, by compiling data from the various sources mentioned above it is possible to demonstrate an overall trend in $D_{\mathrm{pore}}/D_{\mathrm{bulk}}$ *versus* the pore radius (Fig. 7) from values of *ca*. 0·1 (or less) for pore radii *ca*. 2 Å to *ca*. 1 Å for radii of above *ca*. 8 Å. Thus a simple geometrical estimate of the pore radius (e.g. using the program HOLE; Smart *et al*. 1993, 1997) enables one to select an approximate value of $D_{\mathrm{pore}}/D_{\mathrm{bulk}}$ for use in mean-field simulations.

A pore radius of *ca*. 2 Å or below will impose single-file motion on water molecules within such a pore. There is a substantial physical chemistry literature on single-filing motion (Karger *et al*. 1998; Nelson & Auerbach, 1999; Mao & Sinnott, 2000), and it has also been studied in depth for channels formed by gA (Chiu *et al*. 1991, 1999b; Roux & Karplus, 1994). A combined experimental and simulation study (Hahn *et al*. 1996) on single-file diffusion in a zeolite that forms parallel 1D channels showed that, because diffusion must take place by the movement of defects: (i) in contrast to ordinary diffusion (see above) the MSD of the diffusing molecule was proportional to $\sqrt{t}$ (whereas for ordinary diffusion it is proportional

https://doi.org/10.1017/S0033583501003729 Published online by Cambridge University Press

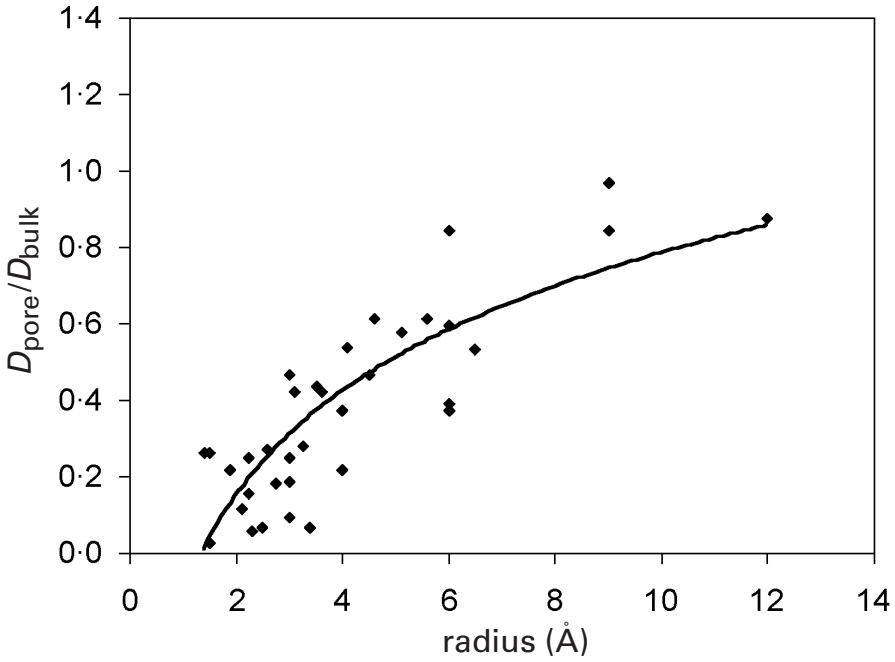


Fig. 7. Water diffusion in pores. The ratio of self-diffusion coefficient of water molecules in pores to water in the bulk state (D_{pore}/D_{bulk}) as a function of pore radius. The data is a compilation for: smooth cylindrical cavities (Sansom *et al*. 1996); simple hydrophilic cylinders (Allen *et al*. 1999a); simple model pores (Breed *et al*. 1996); Alm channels (Breed *et al*. 1996; Tieleman *et al*. 1998); models of the nAChR M2 helix bundle (Smith & Sansom, 1997); and KcsA (Allen *et al*. 2000; Ranatunga & Sansom, unpublished observations). (The fitted line is simply to guide the eye.)

to t); and (ii) this behaviour was only fully revealed in simulations if the MSD was followed for >1 ns. This implies that longer simulations may be advisable if the diffusive motion of water (and by extension, one presumes, ions) in single-file channels (e.g. gA and the KcsA selectivity filter) is to be correctly understood.

The question of dielectric properties of pore water is more complex. Firstly, the degree of alignment of water dipoles within a pore (which determines the extent to which the local dielectric behaviour of intra-pore water will differ from that of bulk) is dependent on the electrostatic field created by the distribution of charges on the surface of the pore. This will vary from channel to channel and, if ionizable side-chains are involved, will require correct treatment of local pK_a (see below). Secondly, the response of the water molecules to this field may be sensitive to the conditions of the simulation (see below). Finally, even if one can demonstrate alignment of water dipoles for a given system, it is difficult to simply convert this to a 'local dielectric constant' which can be used in mean field simulations. As discussed by (Sansom *et al*. 1997; Tieleman & Berendsen, 1998) the basic problem is that as dielectric saturation is approached, the water dipole orientational polarization P_z is a nonlinear function of the local electrostatic field E_z. (Note that $P_z = \mu_z/v_w$, where μ_z is the local average projection of the water dipole moment along the pore axis z and v_w is the volume of a water molecule.) This precludes the use of a simple linear definition of the local dielectric constant based on:

$$P_z(E_z) = \epsilon_0(\epsilon_{local} - 1)E_z.$$

https://doi.org/10.1017/S0033583501003729 Published online by Cambridge University Press

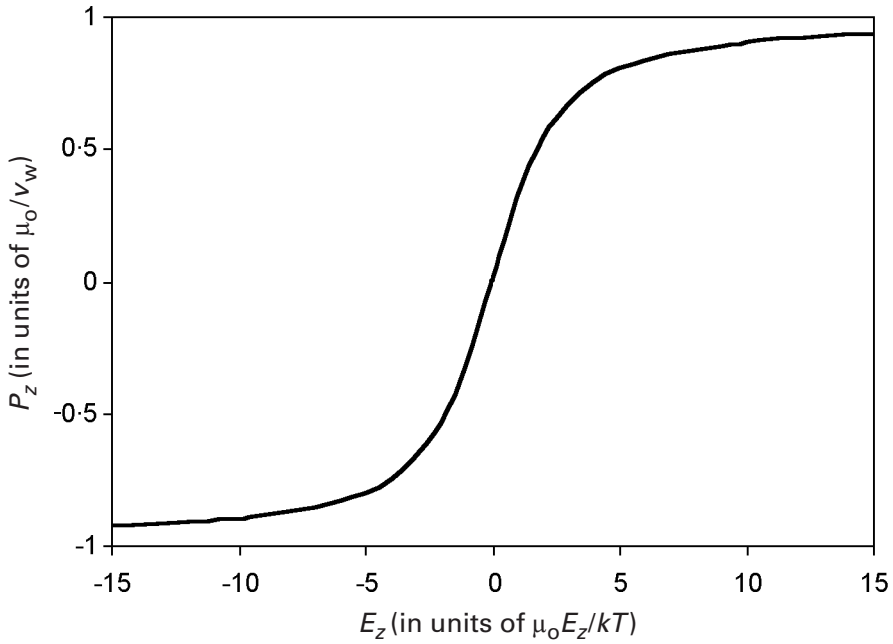


Fig. 8. The relationship between water dipole orientational polarization (P_z, given in units of μ_0/v_w), e.g. within a channel as a function (of the local electrostatic field (E_z, in units of μ_0/kT), as described by the Langevin function (see text and Sansom *et al.* 1977, for details). At high or low values of E_z (i.e. < -5 or $> +5$ μ_0/kT) the water is dielectrically saturated.

Rather, the relationship between P_z and E_z is described by a Langevin function (Fig. 8):

$$P_z = \left(\frac{\mu_0}{v_w}\right)\left[\coth\left(\frac{\mu_0 E_z}{kT}\right) - \left(\frac{kT}{\mu_0 E_z}\right)\right]$$

(where μ_0 is the dipole moment of a water molecule) and the 'local dielectric coefficient' is obtained from the derivative of P_z with respect to E_z (see Sansom *et al.* 1997, for further details). Thus, if a 'local dielectric coefficient' thus defined is to be used in a case where the local electrostatic field is large then an appropriate effective dielectric should be used that captures either the local linear behaviour or the average behaviour of the water dipole orientational polarization as E_z increases from 0. This would be the case if, e.g. one were to consider the electrostatic potential energy of an ion as it passed down a pore. Conversely, if, e.g. the energy of interaction of two ions in the channel was of interest (as in PNP calculations of conductance; see below) then it is the *change* in polarization produced by *extra* charge that is required and then a *differential* definition of the 'local dielectric coefficient' would be appropriate. Clearly this is problematic and further research is needed to effectively incorporate microscopic results on dielectric properties in mean-field theories.

2.2.11 Problems with simulations

There are some problems with the sensitivity of results to the condition of the simulation. This may be exemplified with reference to simulations of water within a hexameric bundle of Alm helices. These simulations have been carried out under three different protocols and the results compared (Fig. 9). The protocols were: (i) a hexameric Alm helix bundle plus pore

https://doi.org/10.1017/S0033583501003729 Published online by Cambridge University Press

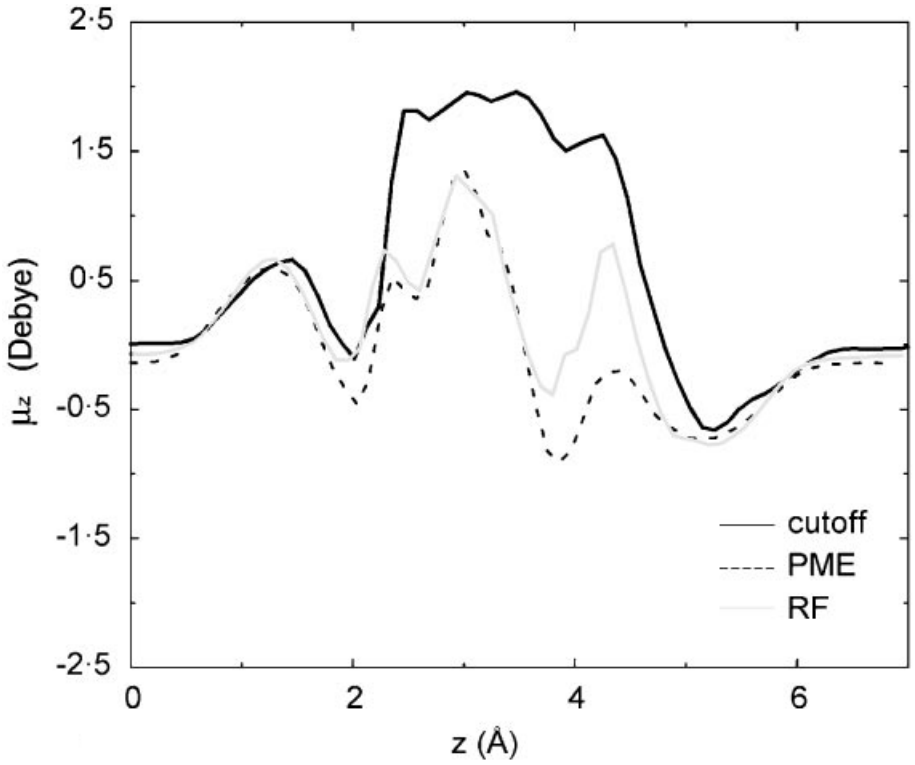


Fig. 9. Water dipole alignment within an Alm pore. A hexameric Alm helix bundle was embedded in a fully solvated POPC bilayer (see Tieleman *et al*. 1999) and multi-nanosecond MD simulations run with long-range electrostatic interactions treated via either a 17 Å cut-off (solid black line), PME (broken black line) or a reaction field (grey line). The average water dipole projected onto the pore (z) axis is shown as a function of the distance along the pore axis.

waters embedded in a POPC bilayer and fully solvated on either face (> 30 waters per lipid molecule), simulated with a cut-off (18 Å) of long-range electrostatic interactions (Tieleman *et al*. 1999); (ii) the same Alm helix bundle in POPC, with long-range electrostatic interactions treated via particle mesh Ewald (PME); and (iii) the same system, but with a cut-off of 14 Å combined with a reaction-field correction that assumes an atom sees a continuum with a dielectric constant of 80 beyond the cut-off distance. All three were run using Gromacs and SPC water. Simulation (i) gave very similar results to a previous simulation of a hexameric Alm helix bundle plus water simulated *in vacuo* using Charmm and TIP3P water with a 13 Å cut-off (Breed *et al*. 1996), suggesting that the diffusional dynamics and water orientation was not over-sensitive to the presence/absence of the bilayer in the simulations and to the water model used. However, comparison of (i) with (ii) and (iii) suggests that the use of PME reduced the extent of alignment of the water molecules within the Alm channel (the maximum value of the water $\mu_z$within the pore fell from *ca*. 2 D to *ca*. 1·3 D). The results from (ii) (PME) and (iii) (reaction field) were similar. Overall, it appears that water ordering is somewhat less with PME or reaction field compared to cut-offs. Water diffusion does not seem to change significantly. It is generally thought that Ewald methods are preferable to cut-off methods in biomolecular simulations (Sagui & Darden, 1999). However, recent studies on peptide folding/unfolding in aqueous solutions (Weber *et al*. 2000) suggest that Ewald methods may

https://doi.org/10.1017/S0033583501003729 Published online by Cambridge University Press

sometimes lead to periodicity artefacts in which dipoles interact with their periodic images. A reaction-field correction works well for isotropic solution, but it is not correct for inhomogeneous systems. In particular, the lipid core has a low dielectric that is badly represented as a dielectric medium with the same dielectric constant as water. Nonetheless, it appears preferable to apply this correction instead of using simple cut-off schemes. Clearly further work is needed in this area if we are to use MD simulations to obtain reliable estimates of pore water dielectric properties for accurate parameterization of mean-field simulations.

2.3 Dynamics of ions in pores

Examining the dynamics of water molecules provides insights into how solvent behaviour changes as a pore becomes narrower. However, to understand channel function it is also important to consider the dynamics of *ions* in pores. This is more complex in that the dynamic properties of ions in a pore are linked to questions of energetics and selectivity. It may be difficult to completely dissect out 'diffusive' motions of ions in pores from hopping of ions between 'sites' within a channel (see Smith & Sansom, 1998, for a more extended discussion). To some extent, one might expect diffusive motion to predominate in wider channels whereas in narrow channels (e.g. gA and the filter of KcsA) single-file motions and strong interactions of ions with 'sites' in the channel will be more important. Thus, we focus first on simple model pores and helix bundle models of channels before progressing to gA and KcsA.

In most simulation studies ion self-diffusion coefficients have been measured from the MSD (as for water – see above). However, in a number of cases the Green–Kubo relation based on the velocity autocorrelation function (Frenkel & Smit, 1996) has been used to extract the diffusion coefficient from the velocity autocorrelation function of an ion. Where these two approaches have been compared for the same simulations the differences do not appear to be substantial (Smith & Sansom, 1999). We should also note that different ion and water parameters give different estimates of the diffusion coefficient in bulk (dilute) solution. Therefore, for the purposes of comparison between different simulations, it is perhaps better to compare the ratio $D_{\mathrm{pore}}/D_{\mathrm{bulk}}$ rather than to compare absolute values of D. One should also remember that, in very narrow channels, both water and ion movements become increasingly spatially and temporally inhomogeneous. Thus, different diffusion coefficients should be defined in different directions (e.g. *xy versus z*; Smith & Sansom, 1998, 1999) and using the equation ($r^2 = 6Dt$) increasingly fails to capture all aspects of the motion because short-time and long-time behaviours are different.

2.3.1 Simple pore models

Ion diffusion coefficients in simple idealized hydrophobic pores have been investigated by Lynden-Bell & Rasaiah (1996), using the SPC/E water model. Na^+ ions in pores ranging in radius from 2 to 5·5 Å, and a number of monovalent anions and cations in a 3 Å radius pore were investigated. For all pore radii the value of $D_{\mathrm{pore}}/D_{\mathrm{bulk}}$ was less than unity, i.e. in all pores the diffusion of ions was slower than in bulk solution. The degree of reduction of ionic mobility in the 3 Å pore was greatest for the smaller ions (Na^+, K^+ and F^-), presumably reflecting the larger size of these ions once their hydration shells are taken into account. These studies were extended (Allen *et al.* 1999a) in a comparison of Lennard–Jones function hydrophobic, atomistic hydrophobic and atomistic hydrophilic (water-lined) idealized pores of various radii. For both classes of hydrophobic pore the (longitudinal) diffusion coefficient

https://doi.org/10.1017/S0033583501003729 Published online by Cambridge University Press

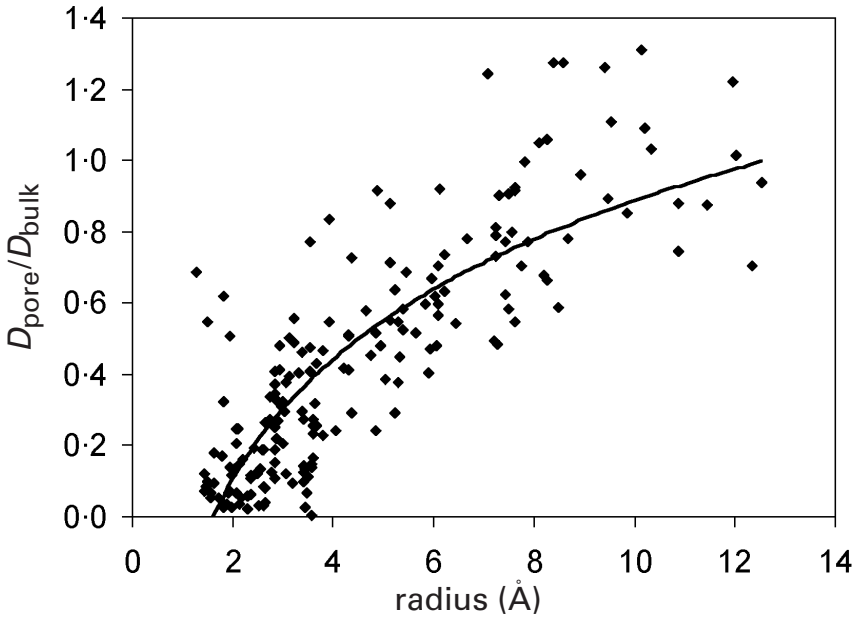


Fig. 10. Ion diffusion in pores. The ratio of coefficients of ions in pores to ions in bulk solution (D_{pore}/D_{bulk}) as a function of pore radius. The data is a compilation for: Na^+ ions in simple model pores (Smith & Sansom, 1997); K^+ and Cl^- in simple model pores (Smith & Sansom, 1999); and K^+ in KcsA (Biggin *et al*. 2001). (The fitted curve is simply to guide the eye.)

of Na^+ rose with increasing radius, although it was still less than its bulk value for pores of radius 5·6 Å. The hydrophilic channel showed a more complex dependence on radius, with on average a smaller diffusion coefficient. This dependency on the nature of the channel wall suggests a need for investigation of a wide range of channel structures.

2.3.2 Helix bundles

α-Helix bundles and related structures (namely: poly-alanine helix bundles and β barrels; $LS3_6$ and Alm6 helix bundles; and a $M2_5$ helix bundle model of the nAChR pore domain) have been used to estimate D_{pore}/D_{bulk} for Na^+ ions (Smith & Sansom, 1998) and for K^+ and Cl^- ions (Smith & Sansom, 1999), using the TIP3P water model. Similar dependencies on pore radius were seen for all three species, suggesting that diffusion *per se* is unlikely to be a significant component of ion selectivity mechanisms in biological ion channels. Combining these data and plotting the 3D diffusion coefficient of an ion *versus* the radius of the pore region it is within (Fig. 10) shows a similar overall pattern to that seen for water (see above and Fig. 7), with effective 'freezing' of the ion at pore radii below *ca*. 2 Å, and near bulk diffusion rates at radii greater than *ca*. 8 Å.

These results suggest that in an intermediate radius range (2–8 Å) it may be possible to treat ion movement as diffusion (see below), provided that a modified local diffusion coefficient is employed. It may be that the 'calibration curve' in Fig. 10 could be used in combination with calculation of a pore radius profile to provide a better estimate of pore conductance than that obtained using the equivalent water diffusion-based 'calibration curve' (Fig. 7). However, further work is needed to see whether this would yield a significant improvement.

https://doi.org/10.1017/S0033583501003729 Published online by Cambridge University Press

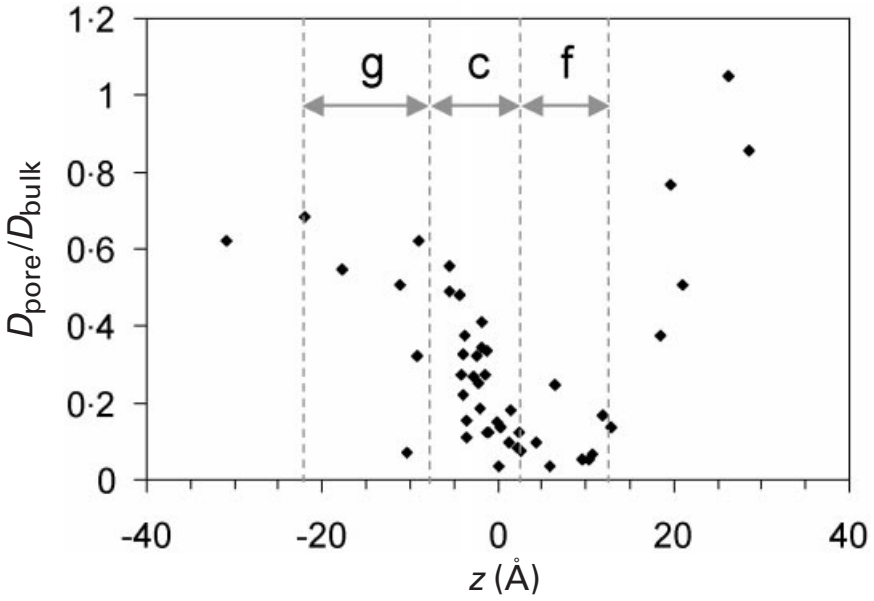


Fig. 11. Relative diffusion coefficient for a single K^+ ion placed at different positions along the pore axis of KcsA (Biggin *et al*. 2001). The gate, cavity and filter regions are labelled g, c and f, respectively.

2.3.3 gA and KcsA

Extensive simulation studies of ion diffusion in gA (Jakobsson & Chiu, 1987; Roux & Karplus, 1991a, b, 1993, 1994; Chiu *et al*. 1993; Roux, 1995) indicate reductions of at least one order of magnitude (and possibly two) for Na^+, and at least one order of magnitude for K^+ [the various estimates are reviewed in Roux & Karplus (1991a, 1994)]. The gA channel differs from the models discussed above because of the close interactions that occur between ion and peptide throughout the length of the channel, which results in single-file motion of ions and water. In this respect, it may more closely resemble the selectivity filter of K channels (see below).

In comparison with simulations on gA, reductions in effective ionic diffusion coefficients for the helix bundle models are smaller. Of course, the effective diffusion coefficient considered in most gA studies is that for crossing a fixed free-energy barrier due to the protein potential, whereas in the idealized pore and helix bundle studies one is concerned more with the effect of the water on ion mobility.

The other channel which has been studied in some detail from the perspective of ion movements is the bacterial potassium channel KcsA. At the outset, it should be emphasized that there are three distinct regions within the KcsA pore: (i) a narrow selectivity filter at the extracellular end of the pore; (ii) a central cavity, which has a maximum radius of *ca*. 6 Å; and (iii) an occluded hydrophobic region at the intracellular end of the pore, which may correspond to the 'gate' of the channel, and is probably in a closed conformation. The gate presents a barrier to ion permeation unless the channel is allowed to change its conformation. Ion motions in the cavity are likely to resemble those in simple channel models. If a single K^+ ion is placed at different positions along the pore axis (Biggin *et al*. 2001) and $D_{\mathrm{pore}}/D_{\mathrm{bulk}}$ evaluated (Fig. 11) it can be seen that for the cavity region (maximum radius *ca*. 6 Å) estimates

https://doi.org/10.1017/S0033583501003729 Published online by Cambridge University Press

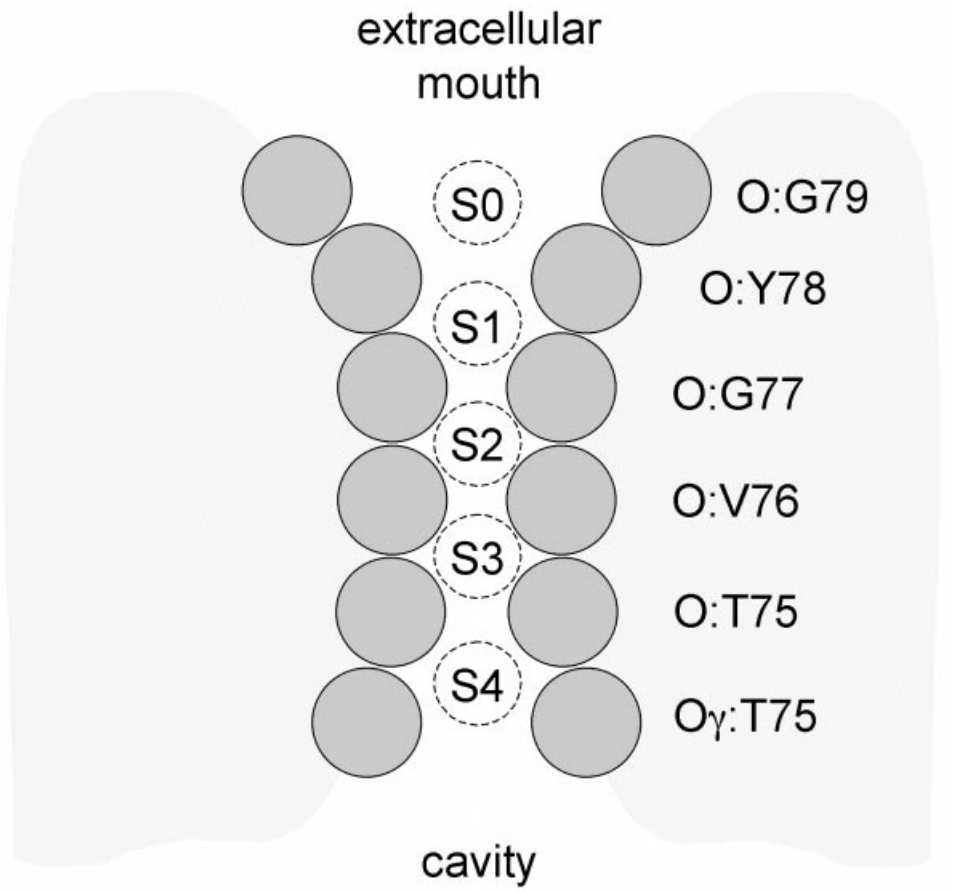


Fig. 12. Schematic diagram of the filter region of KcsA. The grey circles indicate oxygen atoms; the broken line circles indicate the possible 'sites' within the filter.

of $D_{\mathrm{pore}}/D_{\mathrm{bulk}}$ for this region fall close to the curve in Fig. 10. In contrast, diffusion of a single ion within the selectivity filter is very slow. Therefore, we will restrict the subsequent discussion here to motion in the narrow selectivity filter region.

The selectivity filter (Figs. 12, 13) has in places a radius of less than 1·3 Å, i.e. less than the Pauling radius of a K^+ ion. Thus, any motion of water/ions along the filter has to be in single file. The filter is lined by oxygen atoms, from the backbone carbonyls of residues of the $T^{75}VGYG^{79}$ sequence motif and from the side-chain hydroxyl groups of T75 side-chains. This forms 4, possibly 5, 'sites' which are capable of interacting with a cation (or a water molecule; Fig. 12). In the X-ray structure, K^+ (or Rb^+) ions are seen at S1, S3 and S4. It is thought that S3 and S4 are not occupied simultaneously, but rather that sometimes in the crystal there is an ion at S3, sometimes at S4. There is electron density suggested to correspond to a water molecule at S2 (Doyle *et al*. 1998).

There have been a number of MD simulations of KcsA, with varying degrees of approximation of the protein and its environment. A simplified model of KcsA with an atomistic filter and the remainder of the protein treated as a hydrophobic continuum was used by Allen *et al*. (1999b). The whole protein, suitably restrained, with water molecules within

https://doi.org/10.1017/S0033583501003729 Published online by Cambridge University Press

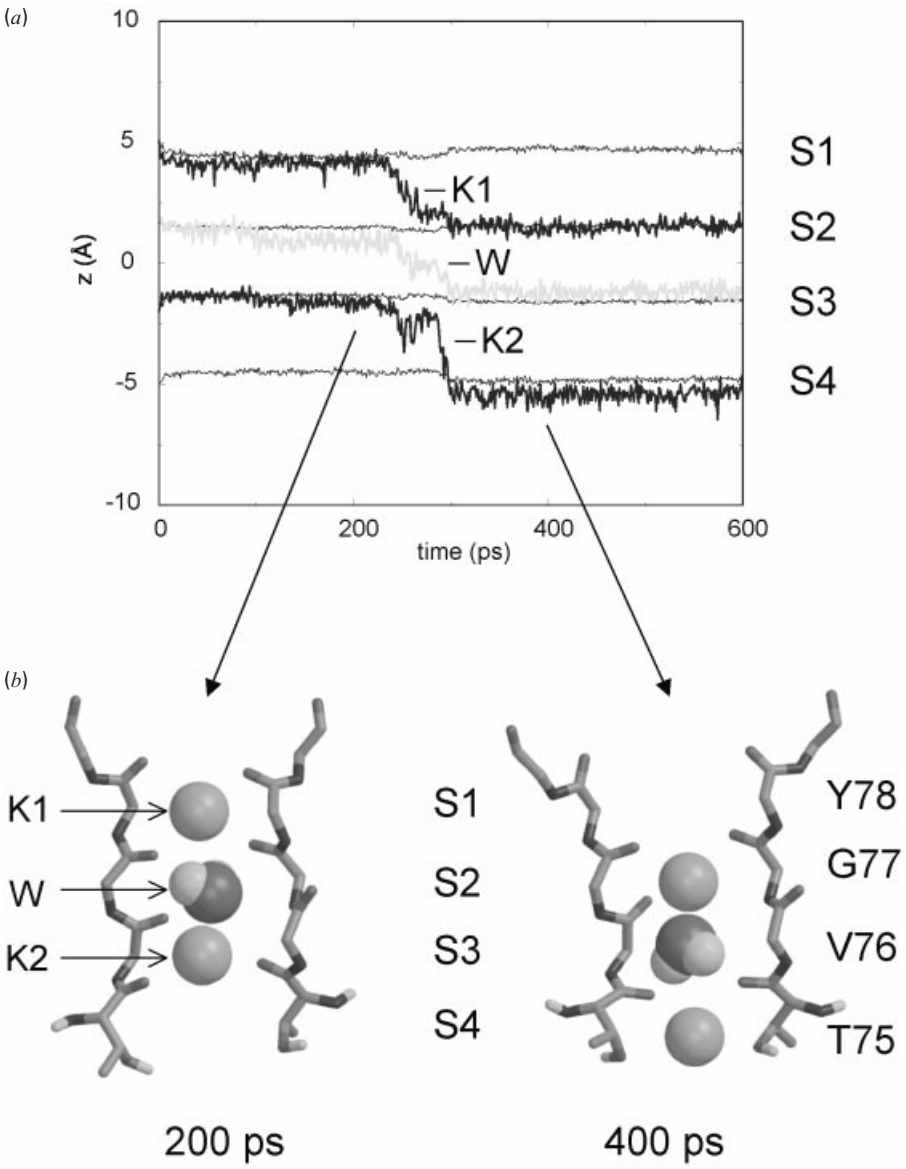


Fig. 13. Concerted single-file motion of two K^+ ions and an intervening water molecule within the selectivity filter of the bacterial K^+ channel KcsA (Shrivastava & Sansom, 2000). (*a*) Shows the positions of the K^+ ions and the water projected onto the pore (z) axis (part of a longer, 2 ns, simulation). (*b*) Shows the selectivity filter of KcsA at 200 and 400 ps showing the concerted motion of two ions and water. At 200 ps there are K^+ ions at sites S1 and S3, and a water molecule at site S2. At 400 ps the K^+ ions are at sites S2 and S4, and the water molecule is at S3. The peptide backbone of the filter and the T75 side-chains are shown (for two subunits only, for clarity).

the pore at either mouth has been simulated (e.g. Allen *et al*. 2000; Biggin *et al*. 2001; Ranatunga *et al*. 2001a). The unrestrained protein has been simulated, embedded in a bilayer-mimetic environment made up of a 'slab' of octane molecules (Guidoni *et al*. 1999, 2000) or of 'hydrocarbon like atoms' (Åqvist & Luzhkov, 2000). Two studies have attempted a more realistic representation of the environment of KcsA, running simulations of the protein

https://doi.org/10.1017/S0033583501003729 Published online by Cambridge University Press

embedded in a fully solvated phospholipid bilayer (Bernèche & Roux, 2000; Shrivastava & Sansom, 2000). Thus, although it remains to be established what level of detail is necessary to get (sufficiently) accurate results, there is a reasonable body of simulation data upon which to draw.

There have been several attempts to estimate $D_{\mathrm{pore}}/D_{\mathrm{bulk}}$ for a K^+ ion in the selectivity filter of KcsA, by placing a single ion (Biggin *et al*. 2001) or multiple (Allen *et al*. 1999b, 2000) ions within this region, running *ca*. 100–200 ps of MD, and then estimating the diffusion coefficient. Estimates of $D_{\mathrm{pore}}/D_{\mathrm{bulk}}$ range from *ca*. 0·1 for simulations (single ion or multiple ions) with the intact KcsA protein to *ca*. 0·3 for the simplified model (Allen *et al*. 1999b). The difference between these two values should alert one to the possible dangers of too radical a simplification of the simulation system. However, it is evident that in this narrow region of the channel ($\ll 2$ Å) the motion of the ion is much slower than in bulk, consistent with the more general analysis presented above.

Given the presence of multiple K^+ ions within the selectivity filter of KcsA (Doyle *et al*. 1998), there have been several simulations to look at the spontaneous motions of different configurations of K^+ ions and water molecules in the filter, ranging in duration from *ca*. 200 ps (Allen *et al*. 1999b, 2000) to $\geqslant 1$ ns (Bernèche & Roux, 2000; Shrivastava & Sansom, 2000; Shrivastava *et al*. In Press). The duration of such simulations is important. Given that the mean time taken for a single K^+ ion to pass through the channel is *ca*. 10 ns, it is likely that simulations of the order 1–10 ns will be needed to sample ion motions within the filter.

It is informative to compare all of the simulations to see which sites within the filter (Figs. 12, 13) are most often occupied by the ions. In the crystal structure the two K^+ ions within the filter occupy S1 and S3 or S1 and S4. Comparing the various simulations, the preferred sites when two ions are present in the filter are: (i) S2 and S4 (Shrivastava & Sansom, 2000); (ii) S2 and S4 (Allen *et al*. 2000; (iii) S1 and S3 (Guidoni *et al*. 2000); (iv) S2 and S4 (Åqvist & Luzhkov, 2000); and (v) S2 and S4 (with a 3rd ion at S0; Bernèche & Roux, 2000). As discussed below, the free-energy calculations of Åqvist & Luzhkov (2000) suggest that the difference in free energy between K^+ ions at S2 and S4, and at S1 and S3 is quite low. Given the differences between the various simulations (bilayer *versus* no bilayer; charge states of side-chains; treatment of long-range electrostatics), it is perhaps not surprising that some differences in preferred configuration are seen.

More significantly, in both of the multi-nanosecond simulations (Bernèche & Roux, 2000; Shrivastava & Sansom, 2000) concerted motions of the K^+ ions in the filter were seen, on a timescale of *ca*. 500 ps. This is illustrated in Fig. 13, from which it can be seen that the K–W–K (i.e. ion–water–ion) triplet moves in a concerted fashion. This is direct evidence for concerted single-file motion within a K-channel selectivity filter. Clearly this complicates attempts to simulate ion flow through K channels as a diffusion process. It is also significant that in both simulations (Bernèche & Roux, 2000; Shrivastava & Sansom, 2000) and also in that of Allen *et al*. (2000) small (generally *ca*. 0·5 Å) changes in conformation of the backbone carbonyls occur. In particular, a 'flipping' of the carbonyl of V76 is observed. This is important, as it indicates that the conformation of the selectivity filter is not static, but can undergo dynamic changes on a timescale comparable to that of passage of the ions through the filter. This may complicate mean field approaches to simulation of ion permeation through KcsA.

It is possible to evaluate to what extent these results are specific to the KcsA channel

https://doi.org/10.1017/S0033583501003729 Published online by Cambridge University Press

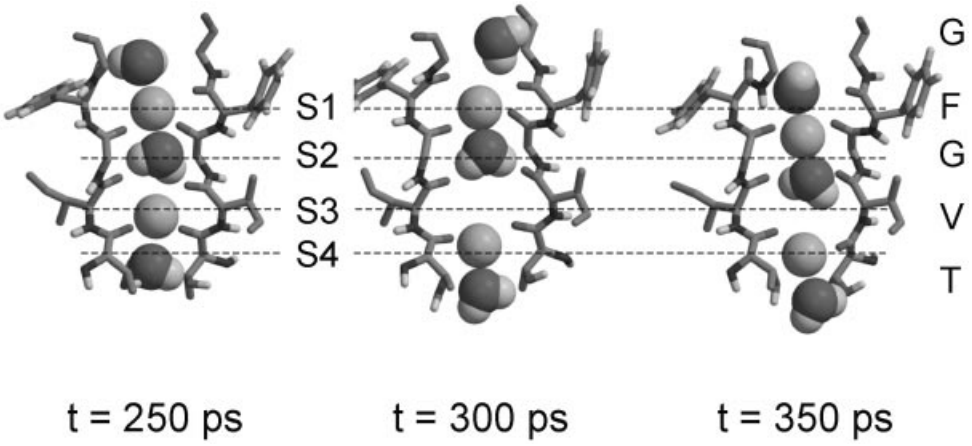


Fig. 14. Concerted single-file motion within the filter of Kir6.2 (Capener *et al*. 2000). Three water molecules and two K^+ ions are shown. The horizontal broken lines indicate the approximate positions of the centres of the sites within the filter.

structure and to what extent they may be shared by a wider range of K channels, given that the selectivity filter sequence motif (and thus, one presumes, conformation) is highly conserved. A homology model of a mammalian K channel (the inward rectifier K channel Kir6.2) has been used as the basis of simulations in a phospholipid bilayer (Capener *et al*. 2000). Such a homology model is, by virtue of the manner in which it was constructed, similar in overall structure to that of KcsA. However, the filter sequence (TVGYG in KcsA) is different (TIGFG in Kir6.2) and the overall distribution of charged side-chains within the molecule differs from that of KcsA. Thus the long-range electrostatic interactions experienced by an ion in the filter will be different from those in KcsA. Despite these differences, single-file motion similar to that in KcsA was observed in the Kir simulations, and the preferred configuration of the filter appeared to be with K^+ ions at S2 and S4, i.e. the same as for KcsA. Again, small conformational changes in the filter were seen during ion–water motions along the filter. Interestingly, one of the transitions in the Kir simulation suggested that single-filing motion may occur via a site becoming transiently 'empty' (Fig. 14). Single-file diffusion models based on movements of vacancies (i.e. empty sites) have been discussed in the context of diffusion in zeolites (Kärger, 1992, 1998; Kukla *et al*. 1996; Nelson & Auerbach, 1999).

It should be noted that in zeolites electrostatic effects are thought to impose single filing of ions even in channels of *ca*. 20 Å radius. It is not clear that this will apply to biological channels where screening is greater and the channel length is much less, but it remains likely that only the widest channels will *not* be confined to single-file transport of ions, even if the water within them is not so constrained.

2.4 Energetics of permeation and ion selectivity

2.4.1 Potential and free-energy profiles

One of the major aims of ion-channel simulations is to understand exactly how the structure of a channel protein provides a low-energy pathway for (selected) ions across a lipid bilayer membrane. Atomistic (or near-atomistic) simulations can be used to estimate the energetic profile along such a pathway. At the simplest level, one may translate an ion along the axis

https://doi.org/10.1017/S0033583501003729 Published online by Cambridge University Press

of a channel and describe the potential energy of interaction of the ion with: (*a*) the protein; and (*b*) the surrounding water molecules. However, this is only a first approximation towards obtaining the free-energy profile. Free energies that are calculated along known coordinate pathways are frequently referred to as providing a *potential of mean force* (PMF). From this statement, the reader will recognize a problem; one does not know the coordinate of ion permeation. However, when a reaction may be described by a single, or at most a few, coordinates, MD or related detailed simulations can be used to calculate a potential of mean force along the reaction coordinate(s). Such an approach is valid when the timescales of motion of the ion along the reaction coordinate and of all other degrees of freedom of the system are sufficiently different to allow the other degrees of freedom to equilibrate at each position of the ion along the reaction coordinate. As will be seen, this is an important consideration.

Ion channels seem to lend themselves naturally to such an approach, as the reaction coordinate in a more or less regular channel can be taken as a straight line (e.g. the z axis) through the channel. The time scale for ion permeation is (probably) long enough to enable other degrees of freedom to approach equilibrium, although this is an important assumption that merits close study from dynamics simulations. Techniques to calculate a PMF are well established and include umbrella sampling, free-energy perturbation and constraint-force calculations (Kollman, 1993; Liu *et al*. 1996). The result of such calculations is a free-energy profile for an ion at different positions along the channel axis. This free-energy profile not only contains the electrostatic and van der Waals components (also in the potential energy profile) but also entropic contributions. In principle, this profile could be used in an approximate way in the Nernst–Planck equation to calculate I–V curves (see Section 3). More frequently, the free-energy profile has been used to study energetic wells and barriers in ion channels, which can be related to rate models (Roux, 1995) and the known permeation characteristics of ion channels.

Another way of calculating the free-energy contributions is to calculate the free energy of transformation of one ion into another, sometimes referred to as 'computer alchemy' (Straatsma & McCammon, 1992). If one performs this transformation for different occupancies of 'sites' within a channel by ions (and water) one can obtain an approximation to the energetics of ion motion along a pore. Of course, this approach pre-supposes knowledge of the location of the sites. Furthermore, this approach can be extended to investigation of the energetics of ion selectivity.

2.4.2 gA

Free-energy profile calculations have been applied to gA by a number of groups (Åqvist & Warshel, 1989; Roux & Karplus, 1991b, 1993; Elber *et al*. 1995; Dorman *et al*. 1996; Hao *et al*. 1997), using different approximations to represent the membrane environment. Several older calculations of reaction coordinates and energy profiles have been reviewed by Roux & Karplus (1994).

Åqvist & Warshel (1989) calculated a free-energy profile for sodium in the gA channel based on the electrostatic Protein Dipoles–Langevin Dipoles (PDLD) model (Warshel & Papazyan, 1998), an semi-microscopic model midway between an all-atom representation and a continuum model, and found reasonable well depths and barriers. They compared the results from this model with free-energy perturbation calculations of the solvation of Na^+ in

https://doi.org/10.1017/S0033583501003729 Published online by Cambridge University Press

bulk water and inside the channel, yielding similar results when the induced dipoles due to the low dielectric membrane environment were taken into account. An interesting aspect of this work is that the membrane low dielectric was taken into account as a lattice of polarizable dipoles. This allows an estimate of the effect of this usually neglected term, which was found to be about 10 kcal mol^{-1}, a significant factor.

Roux & Karplus (1991b, 1993) used free-energy perturbation calculations within a MD framework, with the membrane approximated by uncharged van der Waals spheres; an activated dynamics technique was used to obtain the transmission coefficient of the rare barrier-crossing events. The location of ion-binding sites is reasonably well reproduced, but the energetic barriers were over-estimated. McGill & Schumaker (1996) have used this free-energy profile in an electro-diffusion theory based on work by Levitt (1991) to calculate single-channel conductances. Good agreement with experimental conductance data was obtained if the energetic barriers were lowered by a factor of 3 (McGill & Schumaker, 1996), closer to the barriers found by Åqvist & Warshel (1989).

Elber *et al*. (1995) used reaction path calculations to calculate a free-energy profile for sodium permeation in a system with gA and water but without lipids. They considered the permeation of a quasi-particle (a 'permion') representing the Na^+ as well as a number of water molecules and the protein. This assumes that the timescale of permion motion is separated from all other degrees of freedom. Their calculations suggest that Na^+ does not take a straight path through the channel, and questions the validity of a PMF calculation for a single ion at different locations in the channel. They also showed how the motion of the Na^+ depends critically on motions of the channel and is highly correlated with the motion of water molecules (Elber *et al*. 1995).

Dorman *et al*. (1996) used a microscopic continuum model, representing only part of the gA channel explicitly. They compared free-energy profiles for a series of cations and anions, and showed anions cannot enter the channel due to their different solvation structure and associated cost of desolvation in the channel. One of the most interesting findings from this study is the great importance of the flexibility of the protein for permeation of the ion, in particular the importance of flexible peptide backbone C=O interactions with permeating ions. Such flexibility has also turned out to be crucial in KcsA.

Finally, Hao *et al*. (1997) have compared the free-energy profiles of four organic cations, in a system consisting of the atomic detailed peptide combined with continuum electrostatics corrections to account for the membrane and the solvent. Using umbrella sampling and free-energy perturbation calculations, they showed that there was a large barrier for ethylammonium, whereas methylammonium and formamidinium could permeate. For guanidinium, a well of $-2{\cdot}6$ kcal mol^{-1} was found in the channel, which might explain the blocking properties of this ion.

2.4.3 α-Helix bundles

Because the calculation of free-energy profiles is relatively difficult and time consuming, they have not (yet) been extended to many channels other than gA. Some α-helix bundle channels are currently being studied with simulation methods aimed at calculating a PMF for permeation of a single cation, including $LS3_6$ (Smith & Sansom, In Press) and Alm (D. P. Tieleman *et al*., unpublished observations). One complication of such studies, even though only a single ion is being considered, is that the pores are wider and so one cannot

https://doi.org/10.1017/S0033583501003729 Published online by Cambridge University Press

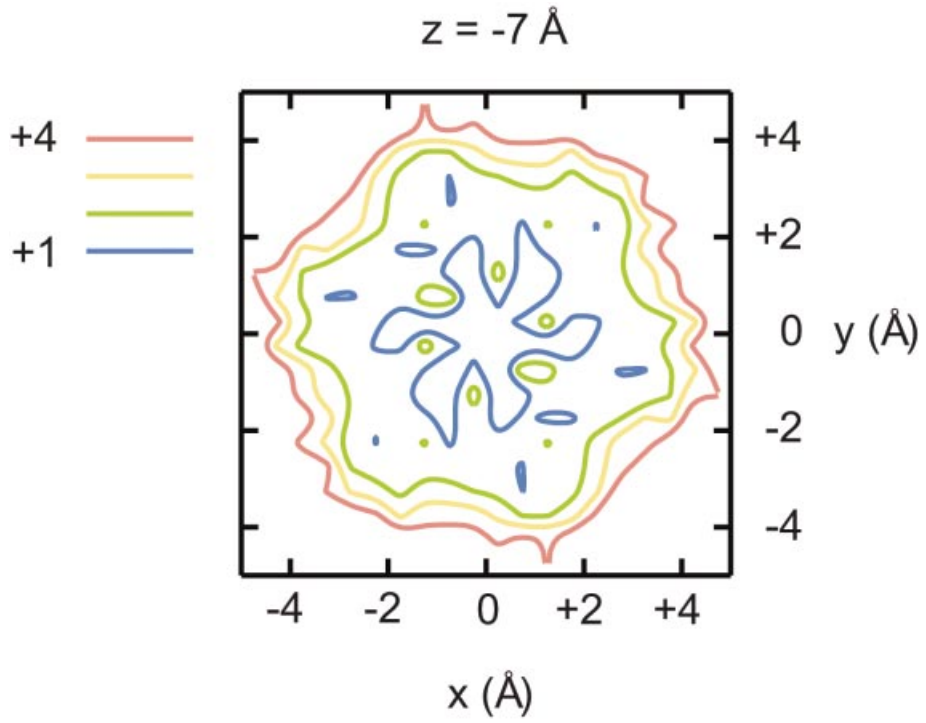


Fig. 15. Cross-section through the free energy (i.e. PMF) surface for a K^+ ion within a model of the $LS3_6$ channel (Smith & Sansom, In Press). The section is taken at about one third of the length of the channel from the N-terminal mouth. The contours show free energies in kcal mol^{-1}. Note that exact sixfold symmetry was assumed in these calculations.

simply assume that the lowest free-energy pathway for an ion corresponds to the axis down the centre of the channel. Indeed, preliminary results for $LS3_6$ shown as a radial section through the channel reveal a complex free-energy surface (see Fig. 15). Furthermore, the presence of potentially mobile side-chains within the pore lining greatly increases the problems of proper sampling during a simulation, as it is possible that such side-chains may move, albeit infrequently, in response to the passage of an ion.

2.4.4 KcsA

A number of groups have used atomistic simulations to explore the energetics of permeation of KcsA. Biggin *et al*. (2001) used MD simulations of a single cation restrained at various points along the pore axis of KcsA to obtain a potential energy profile. The structure of KcsA was restrained to the X-ray coordinates. An energy barrier at the cytoplasmic mouth supported the idea that the crystal structure of KcsA corresponds to a closed conformation of the channel. The potential energy profiles for ion–water and ion–protein interactions (see Fig. 16) are approximate mirror images. This reveals that the overall favourable interaction of the ion with, e.g. the selectivity filter is a relatively small difference between two large numbers. This is one of the main difficulties in estimating accurate energetic profiles from simulations. In terms of ion selectivity (see below) there is a potential energy barrier for a sodium ion in the selectivity filter that is not seen for potassium. Radial distribution functions

https://doi.org/10.1017/S0033583501003729 Published online by Cambridge University Press

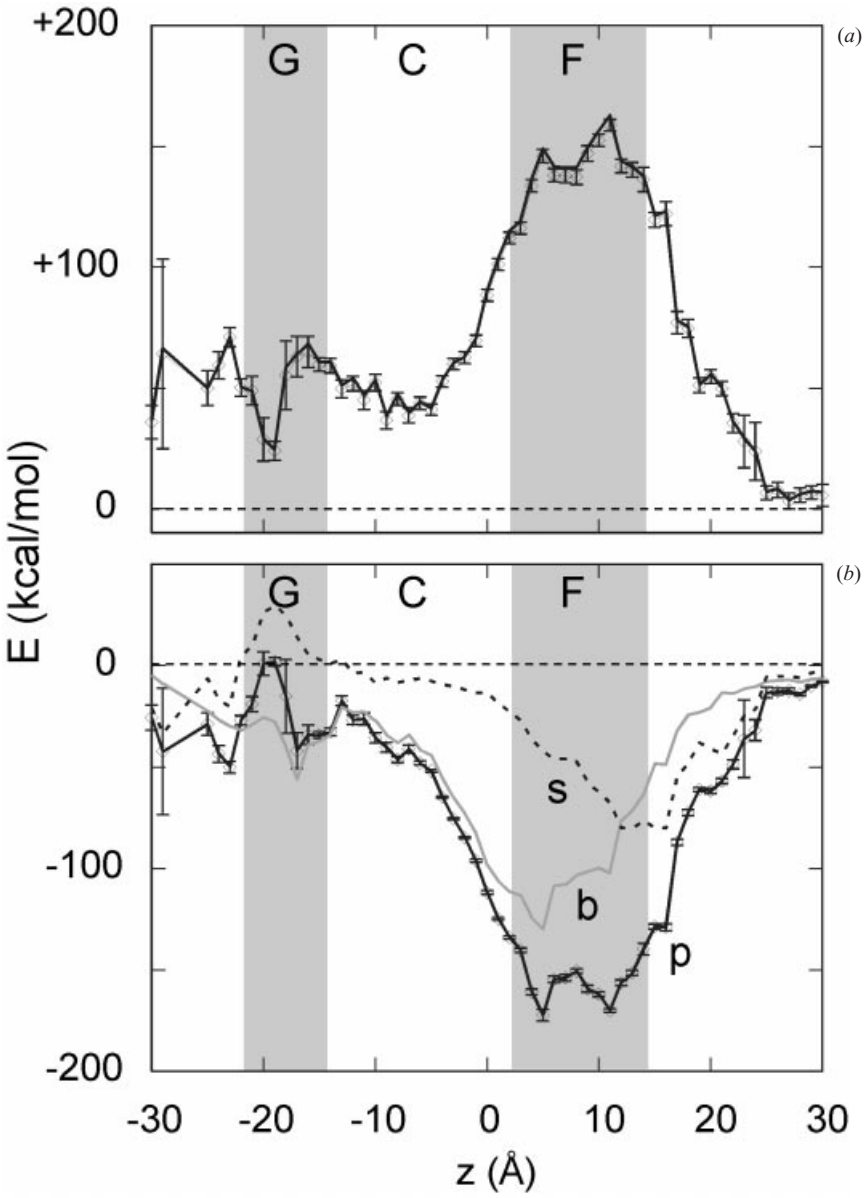


Fig. 16. Potential energy profiles for movement of a single K^+ ion along the pore (z) axis of KcsA (Biggin *et al.* 2001). The intracellular gate (G), central cavity (C) and selectivity filter (F) regions are indicated. (*a*) Ion–water interaction energy profile; (*b*) ion–protein interaction energy profiles indicating the total (p) ion–protein interaction as well as the ion–backbone (b) and ion/side-chain (s) profiles.

for both ions with the carbonyl oxygens of the selectivity filter indicate that sodium may interact more tightly with the filter than does potassium. This suggests that the key to the ion selectivity of KcsA is the greater dehydration energy of Na^+ ions, and may help to explain the block of KcsA by internal Na^+ ions (see below). Allen *et al.* (1999b) have calculated free-energy profiles for K^+ and Na^+ ions in a somewhat simplified model of a K channel, based on a channel-shaped hydrophobic pore onto which a model of the KcsA filter is grafted. Their

https://doi.org/10.1017/S0033583501003729 Published online by Cambridge University Press

results broadly support the 'rigid filter' model of K-channel selectivity (see below). However, the sensitivity of the results to initial assumptions of the rigidity of the filter is a little unclear. In a subsequent paper by the same authors (Allen *et al*. 2000), using a complete model of the protein (but omitting the surrounding bilayer), the free-energy differences between K^+ and Na^+ were about half those with the simplified model. A simulation study based on a mammalian K-channel model (developed before the KcsA structure was determined; Hu *et al*. 2000) suggested that relatively small changes in the filter region of the model resulted in significant changes in the predicted single-channel conductance. This implies that simulation results are sensitive to dynamic structural details. This may cause problems with respect to the use of restrained models (i.e. those omitting a lipid bilayer) to calculate permeation energetics. If such models are to be used, then care must be taken as to the strength and nature of the restraints.

The above calculations refer to *single* ion occupancy of KcsA. However, a variety of experimental evidence (Hille, 1992) indicates that K channels are generally occupied by > 1 ion at a time. Several groups are calculating PMFs for multi-ion occupancy of the filter region of KcsA (Bernèche & Roux, 2001). As such calculations are becoming increasingly feasible on standard computers, it seems likely there will be significant progress in this area in the near future. Preliminary results have been obtained in this area Åqvist & Luzhkov (2000) who showed that occupancy of sites S2 and S4 of the filter (see Fig. 12) by two K^+ ions was more favourable (by *ca*. 2 kcal mol^{-1}) than occupancy of sites S1 and S3. Other configurations were of higher free energy. Thus, a permeation model based on switching of pairs of K^+ ions between these two configurations (0101 and 1010) was proposed.

2.4.5 Ion selectivity

On the basis of the X-ray structure of KcsA it has been suggested that a 'rigid' selectivity filter provides stronger cation–oxygen interactions for K^+ ions than for Na^+ ions (Doyle *et al*. 1998). In this model, the energetic cost of dehydrating K^+ ions is repaid by ion–protein interactions, whilst the latter are too weak to balance the cost of dehydrating Na^+ ions. Whilst this general picture is supported by simulation studies, some results from the latter indicate a more subtle energetic balance may be operating to fully explain selectivity.

The deciding factor for selectivity in channels is that of the free energy of permeation; i.e. how the free energy of the system varies as different species of ion pass through the channel. As a crude approximation though, one may simply observe the differences in potential energies at various points along the central pore axis. Even with this type of calculation a difference between K^+ and Na^+ ions can be observed (Biggin *et al*. 2001). However, for a more quantitative description free-energy calculations are needed. For example Allen *et al*. (2000), show that the free energy (for a $K^+ \rightarrow Na$ transformation) is positive within the filter region. However, the exact figure arrived at was somewhat sensitive to the nature of the restraints applied to the filter during the simulation. Åqvist & Luzhkov (2000) have performed more detailed free-energy perturbation calculations. Their results also supported the 'rigid filter' model of K-channel selectivity. However, it should be noted that in both of these simulation studies it is not clear that the filter had time to fully 'relax' around the different species of cation. Multi-nanosecond MD simulations of KcsA with K^+ ions or with Na^+ ions in the filter suggest that the filter may be able to alter its conformation such that Na^+ ions can bind tightly within (and thus block) the filter. The geometry of interaction of Na^+ ions with the filter

https://doi.org/10.1017/S0033583501003729 Published online by Cambridge University Press

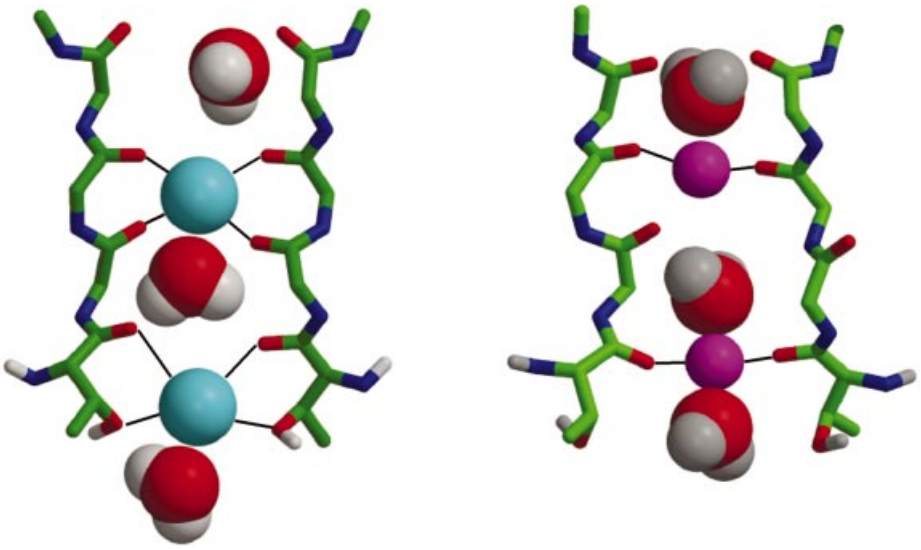


Fig. 17. Illustrations of the filter region from simulations of KcsA with (*a*) K^+ and (*b*) Na^+ ions in the filter (Shrivastava *et al*. In Press). The lines show the close ion–oxygen interactions.

appears to be different from the geometry of interaction of K^+ ions (see Fig. 17). Furthermore, long simulations with either K^+ or Na^+ ions at the extracellular mouth of the filter suggest a degree of selectivity in terms of which ions enter the filter (Guidoni *et al*. 1999; Shrivastava *et al*. In Press). Jordan (2000) has also emphasized the importance of the exact degree of filter rigidity/deformation in determining ion selectivity. This topic is discussed in more detail below (Section 2.5.3). In the context of ion selectivity it is evident that very careful simulations are to be required if the correct balance of ion–water, ion–protein and protein deformation energies is to be obtained.

2.4.6 Problems of estimating energetic profiles

It is evident, both from the studies of gA and of KcsA, that there remain some problems in trying to estimate free-energy profiles of permeating ions, especially if these are to be used to characterize ion selectivity. The various studies of gA yielded reasonable free-energy profiles for ion permeation, but with significant differences between them. Perhaps this is not surprising, given the differences in simulation methods and parameters used, but it demonstrates the importance of further work in this area. It seems that a consistent treatment of all contributions to the electrostatic free energy is a serious issue. Unfortunately, a proper treatment of the short-ranged interactions is equally important. Several papers have shown that protein motion is essential in the transport of ions (Roux & Karplus, 1991b; Elber *et al*. 1995; Dorman *et al*. 1996), which seems an important lesson from gA for the physiologically important ion channels. Clearly, it is also an important lesson for any theoretical treatment of ion channels.

There are several problems with these approaches to calculating the potential of mean force. First of all, in most cases the PMF is a one-ion PMF. Interactions with other ions are not taken into account, even though they might be very strong. This is not a serious problem under specific conditions, such as for gA at low concentrations of salt where the channel is

https://doi.org/10.1017/S0033583501003729 Published online by Cambridge University Press

thought to contain only one ion (Roux & Karplus, 1994). Clearly, it will be a major restriction for larger channels where multiple ions are present inside the channel. Secondly, the simulation results depend on the accuracy of the atomic force-field parameters that are used. Although for many purposes the current force fields seem adequate, the interactions of protein backbone atoms or water with ions are strong and involve large compensating terms. The close contact between channel, solvent and permeating ions might involve significant polarization effects (Woolf, 1997; Duca & Jordan, 1997) that are usually ignored. This has been suggested to be the case for KcsA on the basis of DFT calculations of carbonyl oxygen electronic polarization by permeating K^+ ions (L. Guidoni & P. Carloni, unpublished results). Also, it remains a problem to consistently include long-range electrostatics effects in the finite-sized simulation systems, even although recent progress has been made both for membrane simulations and water-soluble proteins. The PME method (Darden *et al*. 1993) is increasingly popular but has particular problems in membrane systems, as discussed at the end of Section 2.2. However, it remains unclear whether this method is preferable in systems that are not periodic in all dimensions, such as a membrane. In particular its use with a system that involves ionic solvation and ion–ion interactions has raised questions (Hunenberger & McCammon, 1999).

2.5 Conformational changes

MD simulations of ion channels also help us to explore the role of protein conformational changes in channel function. Although we are currently limited to examining relatively small conformational changes on a short (*ca*. 1–10 ns) timescale, it may be possible to extrapolate to longer timescale events.

2.5.1 gA

gA provides an important model for investigating the role of small scale conformational changes in an ion channel. In particular, simulation studies of ion permeation through the gA channel have suggested that there is a 'peristaltic' change in conformation as a cation passes along the channel (Roux & Karplus, 1991b, 1994). It is suggested that the carbonyl oxygens of the peptide backbone are displaced towards the channel axis in the vicinity of the ion, by *ca*. 0·5 Å in order to better solvate the ion. Deformability of the channel seems to play an important role in the dynamics and energetics of permeation of the channel by water and by ions. Indeed, as mentioned above simulations in which the peptide coordinates are restrained *versus* unrestrained simulations in a full bilayer environment yield different estimates of the rate of water diffusion through the channel. Furthermore, as reviewed by Roux & Karplus (1994), estimates of the energetics of cation permeation differ according to whether a rigid or deformable channel model is used.

2.5.2 Alm and LS3

Simulations of the hexameric Alm channel in a lipid bilayer have been extended to 20 ns. This has enabled us to follow the dynamics of the channel in some detail. In particular it has been possible to observe both intra-helix and inter-helix motions within the bundle. Given that these complex motions are almost certainly coupled to the motions of the surrounding lipid bilayer environment, it is evident that some care needs to be taken in correctly treating the

https://doi.org/10.1017/S0033583501003729 Published online by Cambridge University Press

latter in simulations. The possible functional consequences of motions of side-chains in helix bundle models were explored in early (*in vacuo*) simulations of models of channels formed by a peptide closely related to Alm, namely zervamicin-IIB (Sansom *et al*. 1993). It was shown that small changes in the conformations of pore-lining side-chains could result in significant changes in the potential energy profile for a cation translated along the pore axis. If such changes in side-chain conformation in, e.g. Alm, were coupled to bilayer fluctuations, then the *mean* energy profile of an ion moving through the pore might be expected to be sensitive to correct (i.e. properly sampled) treatment of the dynamics of the surrounding bilayer.

Conformational changes have also been observed in simulations of channels formed by the synthetic peptides LS2 and LS3 (Zhong *et al*. 1998b, c; Randa *et al*. 1999). Dynamic changes in the packing of the helices have been observed, both in simulations of the helix bundles within a POPC bilayer and within a bilayer-mimetic octane slab. Furthermore, although on average the serine side-chains adopt a conformation such that they H-bond back to the carbonyl oxygen of the preceding turn of the helix (Gray & Matthews, 1984), both early *in vacuo* simulations (Mitton & Sansom, 1996) and more recent simulations in a POPC bilayer (Randa *et al*. 1999) suggest that dynamic changes in serine side-chain conformation may occur, albeit on a long timescale. In free-energy calculations based on multiple 100-ps trajectories (Smith & Sansom, In Press) the serine side-chains predominantly remained in a $g(+)$ orientation, as was seen by Dieckmann *et al*. (1999), although a few side-chain conformation transitions were observed, especially for serines near the N-terminus of a helix. As the orientation of these side-chains may be anticipated to play a role in, e.g., ion selectivity this merits further study.

2.5.3 KcsA

Simulations of KcsA have provided evidence for conformational changes in different regions of the molecule that may be related to aspects of channel function. At a global level, simulations of KcsA in a bilayer reveal fluctuations that correlate with the estimated disorder/mobility in the X-ray structure (Bernèche & Roux, 2000; Shrivastava & Sansom, 2000). The loops at the extracellular mouth of the pore exhibit a greater degree of mobility than the transbilayer 'core' of the molecule. Perhaps of more significance from a functional perspective, there is a gradient in fluctuations from the intracellular to the extracellular end of the transmembrane domain. This has been seen for simulations of KcsA (Bernèche & Roux, 2000; Sansom & Shrivastava, unpublished observations) and for simulations of a homology model of the pore domain of Kir6.2 (Carpener *et al*. 2000). This trend in backbone fluctuations along the length of the molecule (see Fig. 18) suggests that the intracellular end of the pore, thought to correspond to the 'gate', may be intrinsically more mobile than the opposite end (which contains the selectivity filter).

If one examines small-scale fluctuations of the selectivity filter, three types of conformational transition can be observed: (i) small-scale motions of carbonyl (and threonine side-chain) oxygens in response to movements of ions/water within the filter; (ii) occasional 'flips' of the peptide backbone (especially at V76), involving a larger change in the local backbone conformation of the filter; and (iii) fluctuations in the pattern of H-bonding of the Y78 side-chains with the tryptophan side-chains of the surrounding P-helices. Such conformational fluctuations indicate that the selectivity filter of KcsA is *not* rigid. Thus, models of ion selectivity based upon a completely rigid selectivity filter are at best an

https://doi.org/10.1017/S0033583501003729 Published online by Cambridge University Press

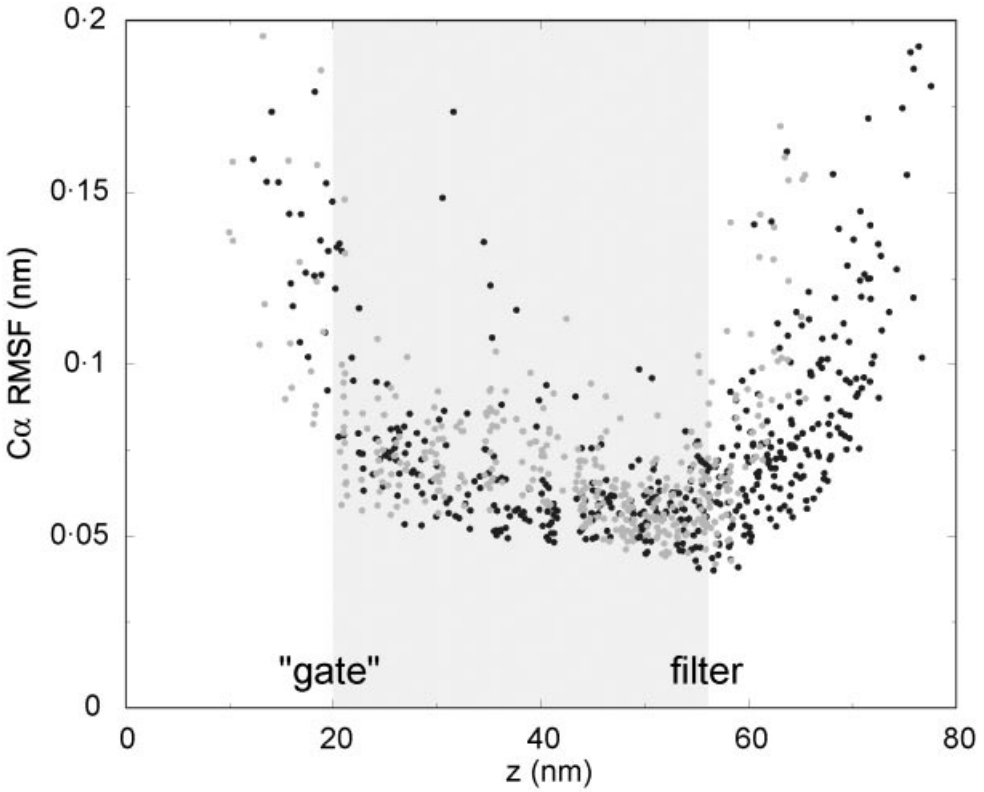


Fig. 18. Fluctuations about their average positions (shown as the root mean square fluctuation, RMSF, of the Cα atom of each residue) as a function of the position along the pore (z) axis. Points are shown for simulations of KcsA (grey points; data from Shrivastava & Sansom, 2000) and of a Kir6.2 pore model (black points; data from Capener *et al*. 2000). The diagonally shaded region indicates the extent along the pore axis of the bilayer.

approximation. Instead, the filter is deformable, especially in response to ions within it. This is reminiscent of the situation for gA (see above). Significantly, more pronounced deformations of the KcsA (and Kir) selectivity filters are seen in simulations *without* any ions in the filter. This may correlate with the experimentally observed loss of function of K channels in the absence of K^+ ions (Melishchuk *et al*. 1998).

At first it may seem strange that a highly selective ion channel has a *flexible* filter. However, there are precedents for conformational changes coupled to the presence/absence of ions within binding sites that nevertheless are highly ion selective. A much studied example is that of the ionophore valinomycin (Duax *et al*. 1996; Forester *et al*. 1997). A more recent simple example is provided by calix[4]tube. This is a small synthetic molecule that forms a tubular 'filter' and exhibits potassium ion selectivity (Schmitt *et al*. 1997). High resolution X-ray structures of this molecule in the absence/presence of K^+ ions reveal a significant conformational transition driven by ion binding (Fig. 19). Interestingly, the 8 ether oxygens of the calix[4]tube interact with the central K^+ ion in much the same fashion as the 8 oxygens of a 'site' in the KcsA selectivity filter [e.g. mean O–K distance = 2·8 Å in calix[4]tube and = 2·9 Å in a KcsA simulation (Shrivastava *et al*. In Press), compared with 3·2 Å in the X-ray structure (Doyle *et al*. 1998)].

https://doi.org/10.1017/S0033583501003729 Published online by Cambridge University Press

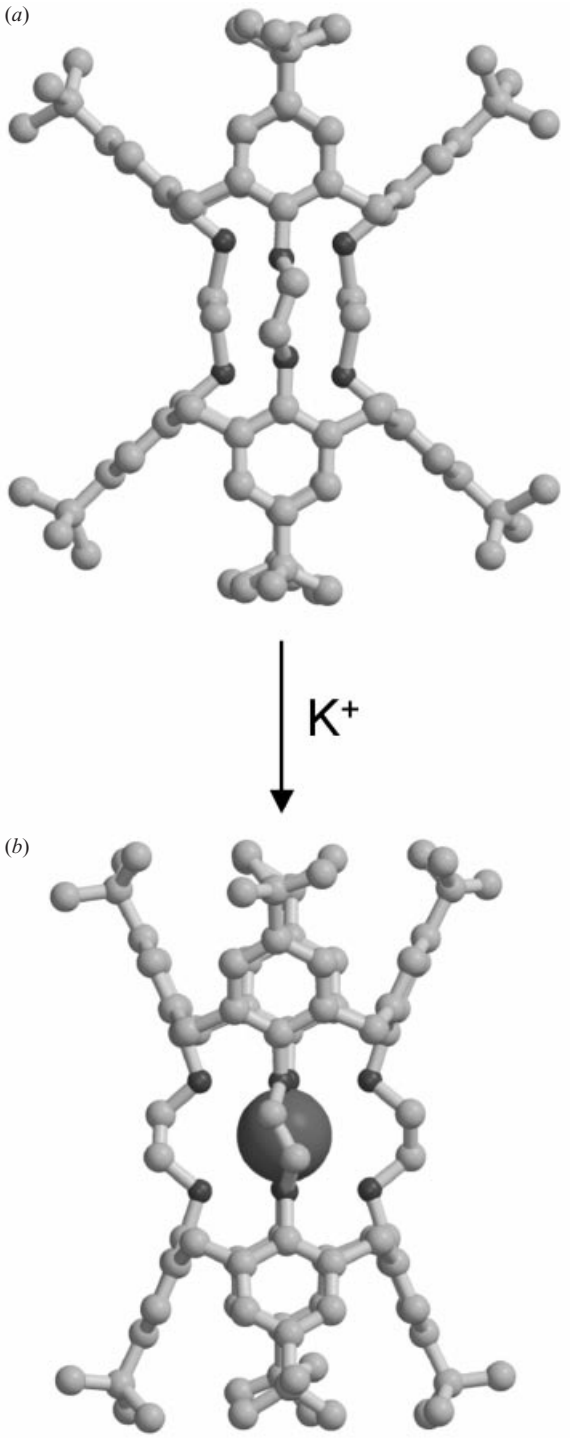


Fig. 19. X-ray structures of a calix[4]tube (Schmitt *et al*. 1997) in the absence (*a*) and presence (*b*) of a K^+ ion. Note the conformational transition to form an 8-oxygen cage around the K^+ ion.

https://doi.org/10.1017/S0033583501003729 Published online by Cambridge University Press

From this brief discussion of conformational flexibility during permeation of ions through gA and through KcsA it is evident that small changes in local conformation are coupled to translocation of ions between 'sites' within the selectivity filter of a channel protein. Thus, altering the local rigidity of a channel protein during a simulation is likely to influence the dynamics and energetics of permeation. This then raises the question of the extent to which the local conformational dynamics of a channel protein are coupled to the global dynamics of the protein and of its bilayer–water environment. In particular, to estimate free-energy profiles of ion permeation (see above) one should allow for small local changes in the conformation of the selectivity filter (which will doubtless influence the energetics of permeation) which in turn may be coupled to larger length and timescale fluctuations in the bilayer environment of the protein. As suggested by, e.g. the pure bilayer simulations of Lindhal & Edholm (2000) large-scale fluctuations in lipid bilayers do occur. If these can be 'transmitted' through a channel protein to its selectivity filter then one should be cautious about approximating the bilayer environment through the use of harmonic restraints (Allen *et al*. 1999b, 2000; Biggin *et al*. 2001; Ranatunga *et al*. 2001), bilayer mimetics (Guidoni *et al*. 1999, 2000; Åqvist & Luzhkov, 2000), or even through the use of relatively small lipid bilayers (Bernèche & Roux, 2000; Shrivastava & Sansom, 2000; Shrivastava *et al*. In Press). Although one might imagine that 'brute force' simulation approaches are unnecessary for studying the local events of ion permeation, it may be rather optimistic to decouple the dynamics of a membrane protein from the dynamics of its immediate environment.

Returning to the intracellular end of the KcsA molecule that, as discussed above, shows somewhat greater average mobility than the selectivity filter, changes in conformation have been seen in simulations (Shrivastava & Sansom, 2000) that may be related to opening of the intracellular 'gate'. In particular, small changes in conformation of the M2 helix have been observed to increase the pore radius in the vicinity of the intracellular mouth of the channel from *ca*. 1 Å (i.e. less than the Pauling radius of a K^+ ion) to *ca*. 2·5 Å (at $t = 6$ ns; see Fig. 20). It is tempting to interpret such conformational changes as being related to KcsA channel gating, but further computational and experimental studies are required to confirm this. It should be remembered that physiological channel gating occurs on a μs to ms timescale, i.e. several orders of magnitude longer than the longest channel simulations. Thus, from current simulation techniques one might hope to glimpse small conformational changes that may be related to channel gating.

Relatively short (up to 10 ns) simulations of KcsA provide some suggestions of a possible mechanism of channel gating, involving movement of the M2 helices to widen the intracellular pore. These are supported, in a broad sense, by experimental studies (see below). Simulation and/or molecular modelling may be used to obtain atomic resolution models of an open state of the KcsA channel. One possibility is to apply some sort of (arbitrary) repulsive force to the ends of the M2 helices, thus forcing them apart and opening the channel. A possible disadvantage of such an approach is that one may 'force' the channel into a conformation it would not otherwise adopt, i.e. the open state may be almost entirely determined by the nature of the restraints used. Of course, if sufficient experimental data are available then such restraints will be an accurate representation of the true gating transition. However, it is not clear that current experimental approaches (see below) are capable of yielding such data. An alternative approach is to employ non-equilibrium ('steered' MD) (Lu *et al*. 1998; Marrink *et al*. 1998; Grubmuller *et al*. 1996). It is known that ions and blockers (such as TEA) access the inner cavity of K channels. Thus by starting from a closed (X-ray)

https://doi.org/10.1017/S0033583501003729 Published online by Cambridge University Press

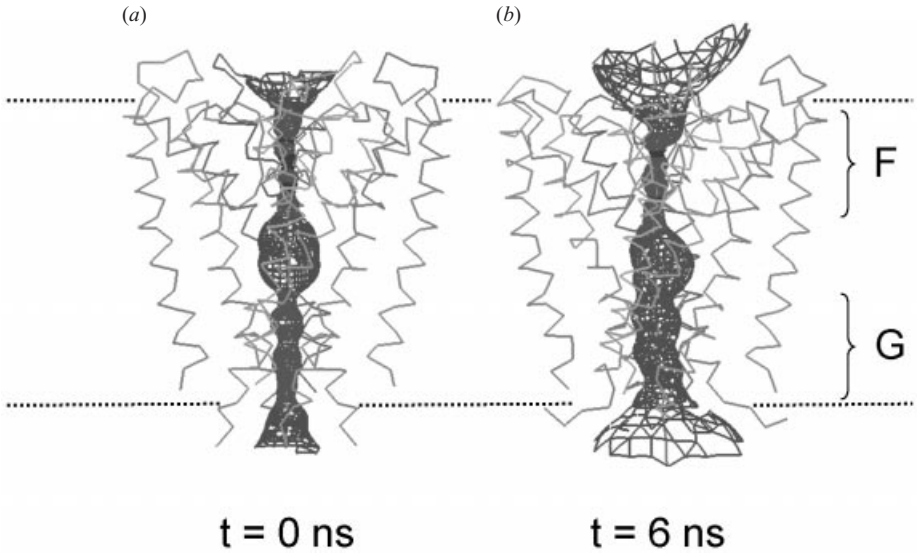


Fig. 20. KcsA in a 'closed' (*a*) and 'open' (*b*) conformation, using two illustrations from the start and end a 6 ns simulation of KcsA in a lipid bilayer (Shrivastava & Sansom, In Press). The channel is shown as a Cα trace and the inner surface of the pore is shown as a mesh, calculated using HOLE (Smart *et al*. 1993). The approximate location of the bilayer is shown by the horizontal dotted lines, and F and G indicate the respective locations of the filter and gate regions of the channel.

conformation of KcsA with such an ion/blocker inside the cavity and slowly 'dragging' the ion/blocker out it may be possible to induce a (transient) channel 'opening' event. Such an approach has been used for exploring the access of substrates to buried active sites in enzymes (Meulenhoff, 1999). Preliminary results (P. C. Biggin & M. S. P. Sansom, unpublished observations) suggest that this approach may be applicable to KcsA. Of course, as with other such 'steered' MD approaches it will be important to establish the extent to which the nature of the induced conformational changes are dependent on, amongst others, the rate of dragging of the ion/blocker (Lu *et al*. 1998; Marrink *et al*. 1998).

It is perhaps useful to briefly examine the nature of experimental data concerning channel gating. Ideally one would determine X-ray structures of a channel in its closed *and* open states. However, given the transient nature of the latter, it may be difficult to isolate by crystallization [although the case of the nAChR (Unwin, 1995) suggests it may be possible to 'freeze' an open channel, at least in a 2D crystal]. Alternative sources of experimental data are spectroscopic experiments, using either fluorescent (Cha *et al*. 1999; Glauner *et al*. 1999) or EPR (Perozo *et al*. 1998, 1999, 2000) probes attached to the channel protein. Leaving aside issues such as the degree of perturbation of channel structure/dynamics by the introduction of bulky spectroscopic probes, such methods are capable of providing estimates of a number of inter-residue distances in the closed *versus* the open state. Such sparse data are on their own insufficient to unambiguously characterize a conformational transition associated with gating. However, by combining such distance restraints with appropriate model building/simulation (Herzyk & Hubbard, 1995; Sansom *et al*. 1995) it may be possible to describe with reasonable accuracy the different conformations of a channel associated with gating.

One way in which simulations may already contribute to an understanding of possible

https://doi.org/10.1017/S0033583501003729 Published online by Cambridge University Press

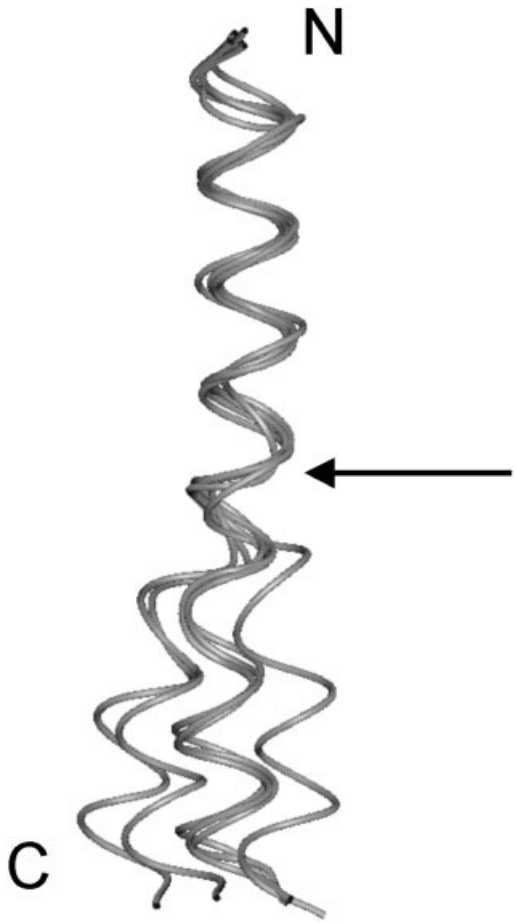


Fig. 21. Hinge-bending in the pore-lining S6 helix of a K_v channel. Superimposed illustrations are shown, taken every 2 ns from a 10 ns simulation of a K_v-S6 helix embedded in a bilayer–mimetic octane slab (Tieleman *et al*. 2001). The arrow indicates the approximate location of the hinge region just N-terminal to the Pro-Val-Pro sequence motif.

channel-gating mechanisms is by enabling us to study the inherent flexibility of the constituent structural elements of a channel protein. For example, a variety of experimental data suggest that 'hinge bending' of pore-lining helices may be associated with channel gating, both in the nAChR and in voltage-gated potassium (K_v) channels (Camino *et al*. 2000). In the latter case the S6 helix of K_v channels (the equivalent of M2 in KcsA) is suggested to be kinked near a highly conserved Pro-Val-Pro sequence motif. *In vacuo* simulations (Kerr *et al*. 1996) and simulations in a bilayer mimetic and in a lipid bilayer (Shrivastava *et al*. 2000; Tieleman *et al*. 2001) have shown that this motif can produce a dynamic swivel in S6 (Fig. 21). One can envisage how such a hinged structural element might be employed in a gating mechanism for K_v channels. Interestingly, possible conformational changes involving proline-induced helix distortions are not limited to K_v channels. Proline-induced hinges have been shown to be present in the channel-forming peptide Alm (Tieleman *et al*. 2001) and in several helices of the G-protein coupled receptor family (Sansom & Weinstein, 2000).

https://doi.org/10.1017/S0033583501003729 Published online by Cambridge University Press

Furthermore, membrane hinges in helices involved in channel gating are not limited to those induced by proline. Simulation studies of the isolated, pore-lining M2δ helix from the nAChR have revealed a central dynamic hinge (Law *et al*. 2000). Long (*ca*. 15 ns) MD simulations of pentameric bundles of the M2 helix (which have been shown experimentally to form ion channels that mimic some of the properties of the parent protein; Montal, 1995) in POPC bilayers reveal fluctuations in helix geometry that may be related to rapid opening/closing transitions of the transbilayer pore (M. S. P. Sansom & R. J. Law, unpublished observations).

2.6 Protonation states

We have discussed how MD simulations reveal dynamic changes in conformation of ion channels. However, this is not the only way in which a channel protein may change. Channel proteins, like all proteins, contain ionizable (i.e. acidic and basic) side-chains. A number of channels, by virtue of their rotational symmetry, contain one or more 'rings' of ionizable side-chains either at the mouth of or within the pore of the channel. Such side-chains can interact with one another and so their pK_a are likely to differ from the 'default' values for the corresponding amino acids. Approximate calculations have shown that this is the case for Alm (Tieleman *et al*. 1998), for models of the nAChR pore (Sankararamakrishnan *et al*. 1996; Adcock *et al*. 1998) and for KcsA (Ranatunga *et al*. 2001a) and other K channels (Capener *et al*. 2000; Ranatunga *et al*. 2001b).

How does this alter simulations on ion channels? This can be best considered with respect to studies of KcsA (Ranatunga *et al*. 2001a). Continuum (PB) calculations on the KcsA protein embedded in a low dielectric slab suggest that side-chains E71 and D80 of each subunit, which lie adjacent to the selectivity filter region of the channel, form a proton-sharing pair in which E71 is neutral (protonated) and D80 negatively-charged at pH 7. This is in agreement with the suggestion of (Bernèche & Roux, 2000) on the basis of careful examination of the X-ray structure of KcsA, and of free-energy perturbation calculations by Luzhkov & Åqvist (2000). When K^+ ions are included in the selectivity filter of KcsA, the pattern of proton sharing predicted by the continuum calculations is subtly altered. In particular, the presence of multiple K^+ ions in the filter increases the probability of E71 being ionized and of D80 remaining neutral (i.e. protonated). The ionization states of the protein side-chains influence the potential energy profile experienced by a K^+ ion as it is translated along the pore axis. In particular, the ionization state of the E71–D80 proton-sharing pair modulates the shape of the potential profile close to the selectivity filter. Such mutual effects of ion occupancy on side-chain ionization states, and of side-chain ionization states on ion potential energy profiles may complicate MD simulations and related studies designed to calculate ion permeation energetics. In fact, the situation is more complicated than this. The calculated pK_a values (and hence ionization states) are sensitive to the detailed conformations of ionizable side-chains in KcsA (not all of which are well determined in the 3·2 Å structure). In turn, the most favourable conformations of these side-chains in a MD simulation is determined by, amongst others, the presumed ionization state. Ideally, one would like to incorporate dynamic protonation/deprotonation of at least some side-chains during an ion channel simulation. However, although there has been some progress in this field, e.g. water (Schmitt & Voth, 1998) such methods have yet to be applied in earnest to ion channel or other membrane proteins.

https://doi.org/10.1017/S0033583501003729 Published online by Cambridge University Press

3. Coarse-grained simulations

3.1 Introduction

Although atomistic simulations have the significant advantage of providing a detailed view of ion, water and protein dynamics, it remains challenging to link such simulations with macroscopic observed properties. In addition to the usual assumptions and approximations inherent in MD simulations, there are a number of additional difficulties in simulating ion channels:

(1) The timescale accessible to MD simulations is currently of the order of tens of nanoseconds. This is too short to observe a sufficiently large number of ions passing through a channel to calculate a macroscopic current.
(2) The non-equilibrium nature of cell membranes is problematic. Specifically, the presence of a transmembrane difference in electrochemical potential is difficult to include consistently in MD simulations. Even uniform low-salt concentrations are not straightforward to represent in a simulation, because it is difficult to sample the motion of the 27 K^+ and 27 Cl^- ions that would make up a 0·15 M KCl solution in a simulation with 10000 water molecules. Such a simulation would also ignore the effect that the lipids have on the local salt concentration near the bilayer (Cavc *et al*. 1990), which can differ significantly from the bulk concentration.
(3) There is a delicate balance between the interactions of ions, water, protein and membrane. Relatively small errors in the energy function, force field, or simulation method may cause significant errors in calculated conductances. It is not yet clear whether current methods are sufficiently accurate for this type of calculation.

Theories based on a continuum or field description of ion channels operate closer to the level of measurements of channel current–voltage (I–V) curves. Over recent years, a number of papers have applied electrostatic and electrodynamic theory to ion channels. Much of this work has been reviewed (Cooper *et al*. 1985; Levitt, 1986; Partenskii & Jordan, 1992; Roux, 1995; Eisenberg, 1996, 1999; Jakobsson, 1998; Roux *et al*. 2000). The relative merits of different approaches, most notably those based on a combination of transport equations and electrostatics *versus* approaches based on BD, have been debated (Jordan, 1999; McCleskey, 1999; Miller, 1999; Nonner *et al*. 1999; Roux, 1999b; Corry *et al*. 2000a, b; Moy *et al*. 2000).

In general, continuum theories for ion channels are based on similar theories developed for macroscopic systems such as electrolyte solutions (McQuarrie, 1976; Vlachy, 1999). In this section we briefly outline the different levels of approximation, and describe each of them in more detail in the next sections.

In the simplest approximation, the ion channel is represented by a hollow cylinder filled with salt solution, with properties similar to properties of bulk salt solution. This approach clearly ignores all specific structural properties of the ion channel and only takes size into account. It is still useful to estimate limiting conductances (Hille, 1992) and the method can be improved by incorporating salt solution properties inside the channel that differ from bulk (Smart *et al*. 1997, 1998). This is discussed below (Section 3.1.1).

A more advanced approach is based on the Nernst–Planck equation, which describes flux of ions driven by an electrochemical potential gradient across the ion channel. One of the input parameters for this calculation is the electrostatic potential at each point inside the channel. As a first approximation, this potential can be assumed to be linear (i.e. the field

https://doi.org/10.1017/S0033583501003729 Published online by Cambridge University Press

everywhere in the channel is the same), leading to the classical Goldman–Hodgkin–Katz solution of the Nernst–Planck equation (Hill, 1992). This is a considerable approximation, but under certain conditions it will be valid (Syganow & von Kitzing, 1999b). In a further refinement of the Nernst–Planck approach, the electrostatic potential in the ion channel can be calculated from the (partial) charges on all atoms of the ion channel protein and from the induced charges due to the different dielectric constants of the protein, membrane and solvent, using the Poisson equation. This approach assumes that permeating ions do not significantly change the local electrostatic potential. By using the PB equation instead of the Poisson equation, the shielding due to the presence of salt can be taken into account. However, the PB theory is a bulk theory, which may not be valid for confined regions of molecular dimensions.

The Nernst–Planck and Poisson equations can be solved simultaneously, with appropriate boundary conditions to take into account the transmembrane difference in electochemical potential. This means that the local electrostatic potential in the channel depends on the fixed charges of the protein, the permeating ions, the induced charges due to the different dielectric constants of the membrane and the solvent, and the boundary conditions. The resulting equations are often referred to as Poisson–Nernst–Planck (PNP), and have the advantage of internal consistency: the electrostatic potential is calculated from *all* the charges in the system. However, there remain several assumptions in PNP-like approaches, and we discuss possible improvements that have been suggested.

A different approach, that maintains some of the benefits of atomistic simulation, is provided by BD. In BD ions are represented explicitly and the ion channel is represented explicitly (or as a simplified geometrical construct) whereas solvent and lipids are represented implicitly. In these simulations, ions move stochastically in a potential that is a combination of ion–ion interactions, ion–protein interactions, and a mean field. All these three components can be treated at different levels of complexity, analogous to the calculation of the electrostatic potential for use in the Nernst–Planck equation.

Finally, we mention another method that has commonly been used to link observed conductance properties to the atomic structure of an ion channel. Rate models, which describe ion permeation in terms of movement across barriers between binding sites, have a long history in ion channels (Hille, 1992; Miller, 1999). They have been the subject of debate in recent years. However, as perhaps they are most useful in helping to infer pore structure from experimental observations, rather than vice versa, we do not consider this important class of models here.

3.1.1 Predicting conductance magnitudes

One can use a simple geometry-based approach to estimate the conductance of a channel based on the pore dimensions. Hille (1992) approximated a channel as a regular cylinder and by calculating the electrical resistance of an equivalent cylinder of electrolyte solution (and taking into account the access resistance at either mouth of the channel) arrived at an upper limit for a channel conductance. Reasonable estimates of the approximate dimensions of a transbilayer pore arrived at an upper limit consistent with the broad range of conductances observed experimentally for a number of channels. Sansom & Kerr (1995) extended this approach to consider the pore radius profile, $r(z)$, of a channel in which case the pore resistance is given by:

https://doi.org/10.1017/S0033583501003729 Published online by Cambridge University Press

$$R_{\text{pore}} = \sum_{i=a}^{b} \left(\frac{\rho}{\pi [r_i(z)]^2} \right) \Delta z_i,$$

where the summation is across sections i from mouth a to mouth b of the pore, is the electrical resistivity of the electrolyte solution, and where the pore radius $r(z)$ is estimated for successive cylindrical sections of thickness Δz. The reciprocal of the pore resistance gives an upper limit to the pore conductance, i.e. $G = R_{\text{pore}}^{-1}$. Applying this to a number of porins gave a conductance prediction that was *ca.* fivefold greater than the experimental value. Smart *et al.* (1997) suggested that an empirical factor could be used to scale the predicted conductance, and further suggested that this scale factor might be related to lower rates of diffusion of water and ions within the confined space of a transbilayer pore (Smart *et al.* 1998). As seen above, rates within pores may be estimated by MD simulations.

Although crude, this approach yields reasonable estimates for ion channel conductances. However, it ignores ion channel electrostatics (other than implicitly by way of the estimated local diffusion coefficients of ions) and so is only a first approximation to describing single channel conductances. It has been used to compare models of the $LS3_6$ (Randa *et al.* 1999) and the nAChR (Adcock *et al.* 2000) channels with experimental data. It is unlikely that this method would work for narrower channels, e.g. KcsA.

3.2 Electro-diffusion: the Nernst–Planck approach

A classical physical chemistry approach towards ion permeation is based on the Nernst–Planck equation (Levitt, 1986; Hille, 1992). The flux $\mathbf{J}_i$ of particles (i.e. ions) of type i is given by:

$$\mathbf{J}_i(\mathbf{r}, t) = -D_i(\mathbf{r}) \left[\nabla n_i(\mathbf{r}, t) + \frac{n_i(\mathbf{r}, t)}{kT} \nabla \mu_i(\mathbf{r}) \right],$$

where $D_i(\mathbf{r})$ is the spatially dependent diffusion coefficient, $n_i(\mathbf{r}, t)$ the number density and $\mu_i(\mathbf{r})$ the external potential acting on the particles. Particles move under the influence of a chemical potential gradient. This general formulation enables incorporation of arbitrary factors that influence ion permeation as long as they can be expressed as a chemical potential. Such factors might include, e.g. interactions between the walls and ions, or interactions between ions at short distances (Levitt, 1991). When applied to ion channels in the steady state limit, the arbitrary chemical potential $\mu_i(\mathbf{r})$ gradient is often replaced by the electrostatic potential gradient, leading to the Nernst–Planck equation for ions of type i:

$$\mathbf{J}_i(z) = -D_i \left(\nabla n_i(z) + \frac{q_i n_i(z)}{kT} \nabla \phi(z) \right),$$

where D_i is the diffusion coefficient of species i, n_i is the position dependent number density, q_i the charge, and ϕ the electrostatic potential. In this form, the driving forces for ion permeation are a concentration gradient and an electrostatic potential gradient. The flux $\mathbf{J}_i$ is related to the current I_i carried by ion type i by:

$$I_i = q_i F S \mathbf{J}_i,$$

where q_i is the charge of ion type i, F is Faraday' constant, S is the channel cross-sectional area (as the flux through ion channels is calculated per area, not per volume element), and $\mathbf{J}_i$ is the flux in the z-direction of ion i, assuming the channel axis is parallel to the z-axis. (Note

https://doi.org/10.1017/S0033583501003729 Published online by Cambridge University Press

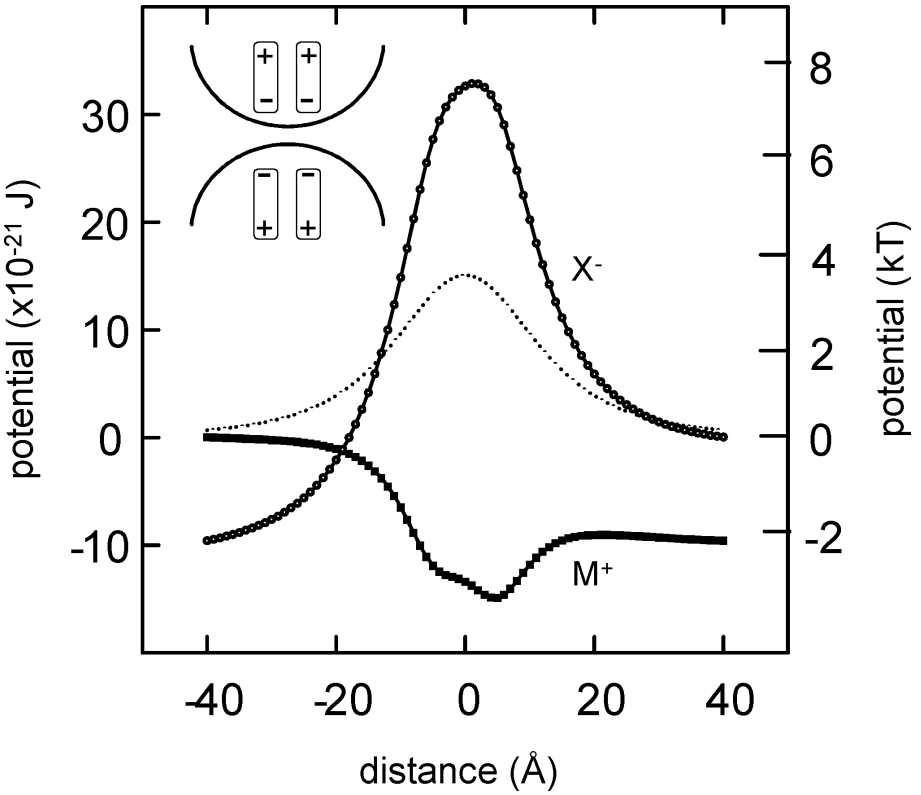


Fig. 22. Effect of dipoles on the potential energy barrier in a simple model channel (figure from Kuyucak *et al*. 1998, with permission), calculated via analytical solution of Poisson's equation. The inset shows the geometry of the channel (minimum radius 4 Å) and the arrangement of the dipoles. The dotted line is the potential energy barrier (to either an anion or cation) in the absence of dipoles or a transchannel electrostatic potential, assuming a solvent dielectric of 80 and a channel dielectric of 2. In the presence of dipoles the potential energy barrier for an anion (X^-) and the potential energy well for cation (M^+) are shown, assuming the right-hand side of the channel is at an electrostatic potential of −60 mV relative to the left-hand side.

that this leaves us with a problem of how to define S for a channel of non-uniform geometry.) The Nernst–Planck equation for current can be rewritten in integral form as:

$$I_i = q_i F \frac{c_{\text{out},i} - c_{\text{in},i} \exp[q_i F \Delta V / RT]}{\int_0^{\delta} \frac{\exp[q_i F \phi(z)/RT]}{D_i} \mathrm{d}z},$$

where $c_{\text{out},i}$ is the extracellular concentration of species i, $c_{\text{in},i}$ is the intracellular concentration of species i, ΔV is the transmembrane potential difference, ϕ is the electrostatic potential, δ is the thickness of the membrane, and the extracellular membrane face is at $z = 0$. In principle, this equation relates the measured current (I) to the transmembrane potential (V), with as input parameters the ion concentrations outside the channel and the electrostatic potential profile $\phi(\mathbf{r})$. It could be generalized to use $\mu(\mathbf{r})$. However, the potential profile $\phi(\mathbf{r})$ or $\mu(\mathbf{r})$ is generally not known and difficult to calculate.

Different approximate solutions of this equation depend on assumptions about the shape of the potential profile and specific boundary conditions. Some severe approximations allow

https://doi.org/10.1017/S0033583501003729 Published online by Cambridge University Press

analytical solution of the Nernst–Planck equation. A common approach is to assume that the field is constant (Hille, 1992). Syganow & von Kitzing (1999b) have studied in detail the consequences and range of validity of this assumption. They have also explored different regimes of the drift due to the external electric field and due to the ion concentration gradient (Syganow & von Kitzing, 1999a). They found that at high external field the analytical solution is possible when concentration gradients can be neglected, and describes the I–V curves of simple channels quite well.

There are several assumptions in the Nernst–Planck approach. A basic assumption is that the ion remains in local equilibrium within the channel, which means the use of a diffusion coefficient to approximate the effect of local forces is justified. Although this is likely to be true in wide channels, it is less obvious that this assumption will hold for very narrow channels with large barriers due to the protein stucture. In such a case, the Nernst–Planck equation might perhaps still describe ion permeation, but D_i is no longer a real diffusion coefficient.

A second important assumption that is made in the Nernst–Planck approach lies in the shape of the potential profile. For analytical solutions very simple shapes have to be assumed, e.g. a constant electric field at any point along the channel (Hille, 1992; von Kitzing & Soumpasis, 1996). For numerical solutions, an arbitrary potential profile can be used. Without structural knowledge of the channel, such a profile could be taken as a simple function with adjustable parameters to fit the known I–V curves (Chen *et al*. 1997). However, when a structure or a model of the structure is available, the electrostatic potential for an ion at any position in the pore can be calculated. In certain cases it also possible to calculate the potential of mean force (free-energy profile) for an ion at different positions in the channel taking also non-electrostatic interactions into account. This latter approach was discussed above (Section 2.4). Here we will focus on more coarse-grained approaches.

3.2.1 Calculating the potential profile from Poisson and PB theory

The basic theory on which nearly all the methods discussed here is based is Gauss's law, or equivalently Poisson's equation relating the charge distribution in a system to the electrostatic potential:

$$\nabla \cdot [\epsilon(\mathbf{r}) \nabla \phi(\mathbf{r})] = -4\pi\rho(\mathbf{r}),$$

where $\epsilon(\mathbf{r})$ is the local dielectric constant, $\phi(\mathbf{r})$ the local electric field, and $\rho(\mathbf{r})$ the local charge density. In its continuum form, Poisson's equation has been used to study the electrostatic potential in simple geometries resembling ion channels (Partenskii & Jordan, 1992; Kuyucak *et al*. 1998). The most striking result of such model calculations is the very high barrier for an ion inside a narrow channel with a high dielectric embedded in an environment of low dielectric (Parsegian, 1969; Partenskii & Jordan, 1992). This by itself already suggests that ion channels need surface (partial) charges in order to allow ions to enter at all. This has been investigated for a simple channel geometry by Kuyucak *et al*. (1998) (see Fig. 22) who showed that a potential energy barrier of *ca*. 4 kT to ion permeation was formed at the narrowest region (radius 4 Å) of a hydrophobic channel, and that this could be removed by embedding dipoles of magnitude 10^{-28} Cm (i.e. *ca*. 30 Debye) in this region of the channel.

PB theory has become an important tool for studying biomolecular systems (Davis & McCammon, 1990; Honig & Nicholls, 1995; Warshel & Åqvist, 1991). It is essentially an

https://doi.org/10.1017/S0033583501003729 Published online by Cambridge University Press

extension and approximation of the Poisson equation that implicitly takes the presence of ions in solution into account. At first sight, it would seem an improvement over using the Poisson equation to study ion channels, and it has been used in several model calculations (Jordan *et al*. 1989; Weetman *et al*. 1997; Moy, 2000). It is assumed that at equilibrium, the distribution of mobile ions in the system can be described by a continuous charge density $\rho_{eq}(\mathbf{r})$, determined by the Boltzmann factor:

$$\rho_{eq}(\mathbf{r}) = \sum_i q_i e n_{0i} \exp[-q_i e\phi(\mathbf{r})/kT],$$

where i is an ionic species, q_i the charge of ion species i, e is the electronic unit of charge, n_{0i} a reference number density for species i, and $\rho(\mathbf{r})$ and $\phi(\mathbf{r})$ are the local equilibrium charge density and the average electrostatic potential, respectively. The electrostatic potential $\phi(\mathbf{r})$ is the solution of Poisson' equation:

$$\epsilon_0 \nabla . [\epsilon(\mathbf{r})\nabla\phi(\mathbf{r})] = -\rho_{eq}(\mathbf{r}) - \rho_{ex}(\mathbf{r}).$$

Assuming a 1:1 electrolyte, these two equations can be combined to give:

$$\epsilon_0 \nabla . [\epsilon(\mathbf{r})\nabla\phi(\mathbf{r})] = 2en_0 \sinh[e\phi(\mathbf{r})/kT] - \rho_{ex}(\mathbf{r}).$$

Here the mobile charges represented by ρ_{eq} are in equilibrium, and the fixed charges on the protein or membrane are represented by ρ_{ex}. This is the full nonlinear PB equation, which can be solved numerically. It can be linearized by expanding sinh and retaining only the leading term. When there are no fixed charges and assuming a spatially homogeneous dielectric, this simplifies to:

$$\nabla^2\phi = \kappa^2\phi,$$

with κ^{-1} its Debye screening length, given by:

$$\kappa^{-1} = \sqrt{\frac{\epsilon_0 \epsilon kT}{2e^2 n_0}}.$$

The Debye screening length $\kappa^{-1} = 8$ Å for 150 mM salt at 298 K in water with a dielectric constant of 80. The screening of a central charge in bulk solution is about 80 % at $r = 3\,\kappa^{-1}$, or *ca*. 25 Å. This distance decreases to about 9 Å for 1 M salt solution. Clearly, compared to the radii of typical channels, these are large distances.

Applying this theory to ion channels seems attractive: the calculations are relatively simple due to the availability of programs that can solve this equation numerically and the PB equation implicitly takes the shielding effect of salt into account. However, it is worth reiterating the assumptions in the PB equation.

(1) The derivation assumes that an ion i is at equilibrium with respect to its surroundings at all times. This assumption is not necessarily true in ion channels. In fact, as has been pointed out repeatedly in the literature (Eisenberg, 1996, 1999), this assumption will hardly ever be true in ion channels.
(2) The Boltzmann factor is not determined by the mean electrostatic potential, but by the potential of mean force between ions. In particular, this means that at short distances from ion i, the potential of mean force does not vary smoothly as $q_j\phi(r_j)$ for all distances larger than the ion diameter, but has a more complicated behaviour.

https://doi.org/10.1017/S0033583501003729 Published online by Cambridge University Press

(3) The PB equation assumes that the potential of mean force between ions can be expressed as a sum of potentials of mean force between pairs of ions. Although this is valid in the limit of very low concentrations, it is not valid at higher concentrations. In fact, in bulk solution the PB theory only accurate up to millimolar concentration at best. The local concentration inside an ion channel is much higher and can be of the order of molar.

Nonetheless, in practice this theory has yielded valuable results on proteins and other systems with a high density of fixed charges and physiological salt concentrations of the order of 0·05–0·5 M. As in theories of bulk electrolytes, it will be important to compare the results from PB and similar theories with the results from direct simulations (MC, MD), from higher level continuum theories [integral equations, density functional theory, and from more advanced theories based on PB (Berry *et al*. 2000; Boda *et al*. 2000; Goulding *et al*. 2000; Graf *et al*. 2000; Hribar *et al*. 2000; Nonner *et al*. 2000)] to establish its range of applicability.

3.2.2 Calculating the potential profile from BD simulations

The Poisson and PB approaches are based on continuum electrostatics descriptions of the channel as a set of fixed partial charges, with the solvent and lipids treated as dielectric media. The most problematic part of this description is the behaviour of the permeating ions. These ions carry a substantial charge that interacts with the rest of the system. MD simulations include these charges but suffer from the problems described in Section 4.1. An attractive intermediate solution would be to use BD. One of the results of such simulations is a concentration profile for ions along a pore, which if expressed as an average charge density could be used to calculate the average electrostatic potential profile. Because BD simulations themselves can be used to calculate conductances directly, this could be an interesting comparison.

3.2.3 Combining Nernst–Planck and Poisson: PNP

Nernst–Planck theory originally was considered a bulk diffusion theory for ion channels. Over the years, the theory has been extended for use with single-occupancy pores (Levitt, 1985), combined with strong electrolyte theory (Debye–Huckel) (Levitt, 1985), and also extended to include multi-ion interactions (Levitt, 1991). Because PB is an equilibrium theory, it cannot in principle be used to describe ion flux. This is because the potential profile $\phi(z)$ is not just a function of the structure of the channel, but also of the average spatially dependent concentration of the ions and the latter are different in non-equilibrium situations from equilibrium situations.

An extension to the non-equilibrium situation is to combine the Nernst–Planck equation with the Poisson equation, to give PNP theory. Originally, this theory was used as a fitting tool in 1D (Chen & Eisenberg, 1993a, b; Eisenberg, 1999). However, as a 3D version is now available, we focus on the 3D applications as these provide a more direct link with atomic resolution structures.

The PNP equations consist of Poisson's equation for the ion channel system:

$$\nabla \cdot [\epsilon(\mathbf{r})\nabla\phi(\mathbf{r})] = -4\pi \left[\rho(\mathbf{r}) + \sum_{i=1}^{N} q_i e n_i(\mathbf{r}) \right],$$

https://doi.org/10.1017/S0033583501003729 Published online by Cambridge University Press

(where the first term on the right-hand side is the charge density of the fixed charges in the channel and the membrane, and the second term is the *average* charge density of the mobile charges) combined with the steady-state equation for drift-diffusion to accommodate the fluxes of the mobile ions:

$$0 = \nabla \cdot \mathbf{J}_i = \nabla \cdot \left[-D_i \left(\nabla n_i(\mathbf{r}) + \frac{n_i(\mathbf{r})}{kT} \nabla \mu_i(\mathbf{r}) \right) \right]; \quad (i = 1, \ldots, n).$$

Here $\mu_i(\mathbf{r})$ is the chemical potential. In its simplest form, this could just be $q_i e \phi(\mathbf{r})$. In this case, ions interact through the average potential $\phi(\mathbf{r})$. However, $\mu_i(\mathbf{r})$ can also include other interactions, providing a way to improve the theory. In these equations, c_i, $\mathbf{J}_i$, q_i, and D_i are respectively the concentrations, fluxes, valences, and diffusion constants of the ion species i.

These two equations are coupled, because the flux changes the potential due to the mobile charges, and the potential changes the flux. In practice, they are solved simultaneously to self-consistency using numerical methods. Several algorithms have been described to do this (Kurnikova *et al*. 1999; Hollerbach *et al*. 2000), including standard finite difference lattice algorithms. When all the fluxes $\mathbf{J}_i$ are zero, and $n_i \sim \exp(-q_i e \phi / kT)$, again with ϕ the average potential, these equations reduce to the normal PB equation. Thus, the PNP equations are an extension of the PB equation, and the same assumptions as in PB theory underly PNP.

This theory is internally consistent in that it includes all charges in the system. It is also mathematically appealing, and presents a clear advance over calculating electrostatic profiles from the PB equation. However, in the form presented here, there remain a number of problems.

(1) Its derivation from PB theory suggests it is likely to be valid for bulk-like situations such as wide channels with many ions, but it is not clear how applicable it is for narrow channels such as, e.g. gA and KcsA.
(2) Ions interact with each other only through the average charge density. This may be problematic, as in ion channels these interactions are discrete: a binding site with an average occupancy of 0·25 will enter the average charge density as a charge of 0·25, but this does not reflect the real situation. It may be argued that this may not be too serious a problem in that the ion channel walls have such a high charge density that ion–ion interactions are less important, and the average charge density is good enough. However, this remains to be determined in specific cases.
(3) In common with almost all other methods except MD, solvent effects that depend on the structure of the solvent cannot be represented. This is a potential problem for phenomena such as single filing (see Section 2.3.3) which depend on the structure of a set of water molecules and ions.
(4) Again in common with most techniques except MD, in the form presented here the theory does not allow for protein mobility. As has been shown for gA and for K channels, changes in protein conformation occur during ion transport, even when a channel is in an open state (see Section 2.5).

Some of these, and other, limitations of PNP theory have been explored in detail (Jordan, 1999; McCleskey, 1999; Miller, 1999; Nonner *et al*. 1999; Roux, 1999b; Corry *et al*. 2000a, b; Moy *et al*. 2000).

https://doi.org/10.1017/S0033583501003729 Published online by Cambridge University Press

3.3 Beyond PNP

Given these reservations concerning the PNP approach, how might it be improved? In principle, one would like to reformulate PNP with a theory that included, e.g. the finite size of ions and single filing of ions and water, using techniques from statistical mechanics of electrolytes. That ion channels are flexible, and that their motion may be coupled to permeation remains a difficult problem. To incorporate this into continuum methods might be possible by making part of the protein 'fuzzy', giving atoms a certain distribution around their mean, derived either from simulations or from crystallographic *B* values.

A number of key papers have started to explore application of newer statistical mechanical approaches to channels and channel-like systems. Graf *et al.* (2000) have used a dynamic lattice MC approach, and compared its performance to PNP for an idealized membrane in which there is a narrow cylindrical pore. These studies suggested that the dielectric self-energy (a substantial energy barrier to ion motion through a narrow channel) is severely underestimated by PNP because of the failure of the latter to treat ions as discrete entities of dimensions comparable to that of the pore. Steric effects have also been explored in an elegant application of density functional theory by Goulding *et al.* (2000). The latter authors showed that considerations of pore width relative to the radii of water molecules, Na^+ ions and K^+ ions may give rise to ion selectivity. Whilst their model pore is clearly highly idealized (and their approach ignores all electrostatic interactions), these studies emphasize the inherent dangers of failing to treat ions as discrete entities when confined within a narrow pore. In an interesting set of papers, Nonner *et al.* (2000) and Boda *et al.* (2000) have shown, using the Mean Spherical Approximation and Density Functional Theory respectively, how much of the behavior of L-type Ca channels can be explained by a simple model based on a small volume that contains 4 glutamate side-chains. Finite volume effects cause a major difference between Na^+ binding and Ca^{2+} binding, as the latter simply have twice as much charge per volume. In summary, attempts to develop theoretical improvements on PNP continue. Results so far suggest that any theory that fails to treat ions discretely will be likely to run into problems for most channels. Although PNP seemed promising, in that it allows fitting of experimental *I–V* curves obtained over a range of concentrations, it is not clear how to interpret the resultant parameter estimates. More subtle continuum theories that take into account steric effects may be more successful. Alternatively, approaches such as BD (next section) that are more coarse-grained than MD simulations but which retain sufficient atomic detail may be more appropriate to the ion channel situation.

3.4 BD simulations

3.4.1 Basic theory in ion channels

In BD simulations the trajectories of individual ions are calculated using the Langevin equation:

$$m_i \frac{\mathrm{d}\boldsymbol{v}_i}{\mathrm{d}t} = -\gamma_i \boldsymbol{v}_i + \mathbf{F}_R + q_i \mathbf{E}_i + \mathbf{F}_s,$$

where m_i, q_i, $\boldsymbol{v}_i$ are the mass, charge and velocity of ion i. Water molecules are not included explicitly, but are present implicitly in the form of a friction coefficient $m_i\gamma = kT/D_i$ and a

https://doi.org/10.1017/S0033583501003729 Published online by Cambridge University Press

stochastic force $\mathbf{F}_R$ arising from random collisions of water molecules with ions, obeying the fluctuation–dissipation theorem. The term $q_i\mathbf{E}_i$ is the force on a particle with charge q_i due to the electric field $\mathbf{E}_i$ at the position of particle i. In a first approximation, this field is due to the partial charges plus an applied external field arising from the transmembrane potential. However, this term could be refined to include effects from multiple ions, reaction field terms and a more accurate treatment of the transmembrane potential (see below). Finally, $\mathbf{F}_s$ is a short-range repulsive force between ions and possibly between ions and protein. This short-range force could be modelled as a hard sphere potential, as the repulsive part of a Lennard–Jones potential, or simply ignored (as a first approximation). When the friction is large and the motions are overdamped, the inertial term $m_i \mathrm{d}\boldsymbol{v}/\mathrm{d}t$ may be neglected, and the simplified form

$$\boldsymbol{v}_i = \frac{D_i}{kT}(q_i\mathbf{E}_i + \mathbf{F}_s) + \mathbf{F}_R$$

may be used. This is the approximation made in BD. This form has been used in several ion-channel simulations, although the high friction limit might not always be appropriate. When the free-energy profile changes rapidly on the scale of the mean free path of an ion, the full Langevin equation including inertial effects must be used. However, it should be possible to verify the assumption of high friction for the specific case to be studied.

BD simulations require only a few input parameters: in its simplest form the diffusion coefficients of the different species of ions and the charge on the ions. However, the model can be refined. The ion channel is present as a set of partial charges, and some form of interaction potential between the mobile ions and the protein must be specified (see above). Several applications to date have studied single ions as they move through a channel (Schirmer & Phale, 1999; Phale *et al*. 2001). In a more realistic scenario multiple ions are present, requiring a term describing interactions between ions to be included, e.g. a short-range repulsive or hard sphere potential.

Regardless of which interactions are included, the result of BD simulations is a large set of trajectories for ions. By averaging over these trajectories and counting crossings of ions from one side of the channel to the other, macroscopic properties such as conductance and ion selectivity may be obtained. In addition, the simulations yield molecular details of the permeation paths for different types of ions. Such simulations have recently been performed for a series of different systems, including simplified ion channel models (Bek & Jakobsson, 1994; Chung *et al*. 1998, 1999; Moy *et al*. 2000) and porins (Schirmer & Phale, 1999; Im *et al*. 2000; Phale *et al*. 2001).

3.4.2 Incorporating the environment

Although BD simulations are conceptually simple, in practice they can give rise to a number of problems for which there may not be an obvious solution:

(1) Representing all solvent effects by a random force and a diffusion coefficient is a drastic simplification, particularly for narrow regions where ions interact very strongly with one or two highly oriented water molecules.
(2) A more technical difficulty is the need to treat the electrochemical gradients across a membrane.

https://doi.org/10.1017/S0033583501003729 Published online by Cambridge University Press

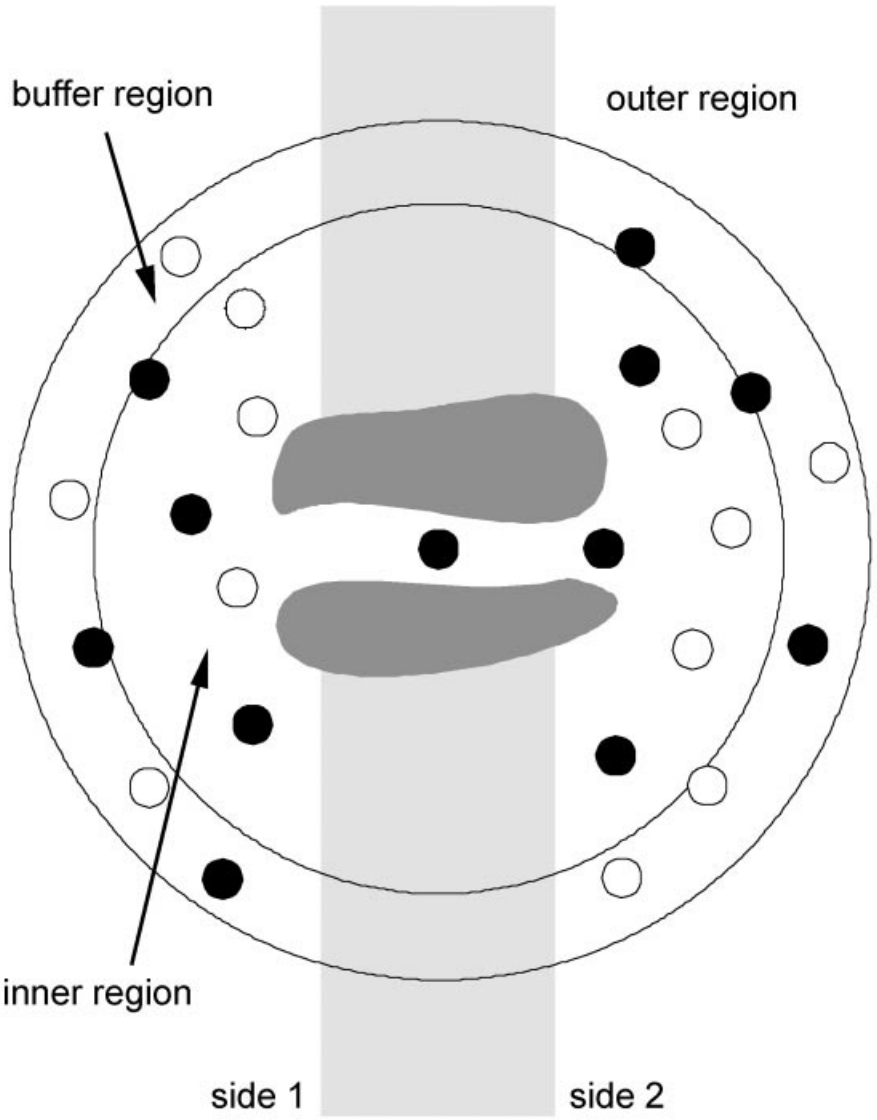


Fig. 23. A system for BD simulations, based on the work of Roux and colleagues (Roux, 1997, 1999a; Im *et al*. 2000). The transmembrane potential is included into a PB based treatment of the membrane. The system is divided in three regions (Fig. 23). The solvent region on side 1 is treated as a continuum, described by the PB equation. The ion channel region itself is described by Poisson's equation, because all ions are explicit in this region. Finally, the solvent region on side 2 is also treated as a continuum, but with a slightly modified version of the PB equation to take into account the different transmembrane potential. (Diagram from Roux, 1999a, with permission.)

Probably the most rigorous method to include the environment of the ion channel in BD simulations of ion channels has been described by Im *et al*. (2000). They build on previous work on incorporating the transmembrane potential into a PB-based treatment of the membrane (Roux, 1997, 1999a). The system, including an ion channel, membrane and solvent, is divided in three regions (Fig. 23). The solvent region on side 1 is treated as a continuum, described by the PB equation. The ion channel region itself is described by

https://doi.org/10.1017/S0033583501003729 Published online by Cambridge University Press

Poisson's equation, because all ions are explicit in this region. Finally, the solvent region on side 2 is also treated as a continuum, but with a slightly modified version of the PB equation to take into account the different transmembrane potential

$$\begin{aligned}
&\nabla \cdot [\epsilon(\mathbf{r})\nabla\phi(\mathbf{r})] = 0 && \text{(pore region)}\\
&\nabla \cdot [\epsilon(\mathbf{r})\nabla\phi(\mathbf{r})] - \kappa^2(\mathbf{r})\phi(\mathbf{r}) = -4\pi\rho_{\mathrm{p}}(\mathbf{r}) && \text{(bulk region, side 1)}\\
&\nabla \cdot [\epsilon(\mathbf{r})\nabla\phi(\mathbf{r})] - \kappa^2(\mathbf{r})[\phi(\mathbf{r}) - V_{\mathrm{mp}}] = -4\pi\rho_{\mathrm{p}}(\mathbf{r}) && \text{(bulk region, side 2),}
\end{aligned}$$

where V_{mp} is the potential on side 2, and the other symbols have the same meaning as before.

The effective force on an ion i is given by the multi-ion potential of mean force $\langle \mathbf{F}_i \rangle$ by

$$\langle \mathbf{F}_i \rangle = -\frac{\partial W(n_1, n_2, \ldots, \mathbf{R}_1, \mathbf{R}_2, \ldots)}{\partial \mathbf{r}_i},$$

where W is the potential of mean force, corresponding to the reversible thermodynamic work function to insert the $(n_1, n_2, \ldots)$ ions at their position $(\mathbf{R}_1, \mathbf{R}_2, \ldots)$ into the system while averaging over all degrees of freedom involving solvent, lipids and ion channel protein. This potential of mean force is essentially the same key quantity that was needed in the generalized Nernst–Planck approach. Interestingly, it is used in the BD integration scheme and also determines the probability of deletion or creation of an ion in the Grand Canonical MC part of the algorithm. In the current treatment, the potential of mean force is calculated from three contributions: the microscopic interactions between ions, modeled as standard Coulomb and Lennard–Jones terms, the interaction of ions with the channel and membrane wall, modelled as a simple repulsive potential, and the interaction of the ion charges with the total electric field, calculated from the modified PB equations.

The authors test their method by calculating ion concentration profiles in a number of simple test systems, with and without net flux, with excellent results. Noteworthy is that in a system of dimensions *ca.* 100 Å, including a membrane slab, edge effects play a minor role when calculating the distribution of salt near a membrane with a transmembrane potential difference of 1 V. These simulations yield a potential difference that is consistent with the different number of cations and anions on either side. This treatment has the advantages of incorporating the transmembrane potential, different salt concentrations on either side of the membrane, and ion–ion interactions. In its current form, it assumes the solution of the PB equation is independent of the presence of ions in the channel, which means the reaction field due to the interactions of the ions with the low dielectric membrane is not taken into account. This reaction field has been included in BD simulations by Chung and co-workers (see below). It will be interesting to see further developments in BD simulations in the near future.

3.5 Applications

3.5.1 Model systems

3.5.1.1 Solving the Poisson and PB equation for channel-like geometries

There have been a number of studies that have involved solving the Poisson and PB equations for channel-like geometries. Partenskii & Jordan (1992) have reviewed earlier calculations. More recently, two papers have used analytical solutions of Poisson's equation to study idealized channels (Hoyles *et al.* 1996; Kuyuck *et al.* 1998). These studies have shown the effect of the low-dielectric environment around the channel on an ion moving through

https://doi.org/10.1017/S0033583501003729 Published online by Cambridge University Press

the channel. They also showed the importance of dipoles and fixed charges inside the channel to allow permeation and modulate charge selectivity. A nice side-effect of the availability of analytical solutions of the Poisson equation in a complex geometry is its usefulness in BD simulations, to speed up the calculation of the potential. Weetman *et al*. (1997) have studied potential profiles in idealized channel geometries using different approaches to the linearized and non-linear PB equation. In this work charges and dipoles were embedded in the channels, with qualitatively similar effects on the electrostatic barriers and wells for cations and anions to those discussed in (Kuyucak *et al*. 1998). Although these studies are somewhat restricted to idealized channel geometries, such studies on model systems are useful, e.g. to compare with MC, BD and other simulations in order to test the applicability of continuum theories to channels. The main result emerging from many such studies is the importance of barriers caused by low dielectric image forces.

3.5.1.2 Comparing PB, PNP and BD

As part of the ongoing discussion between proponents of BD simulations and of continuum methods it is useful to compare the two approaches on the same system. Chung and co-workers have performed a set of calculations on different types of model pores, using a variety of approaches. Although there may be difficulties in setting up an exact comparison, a number of clear differences between BD and continuum methods became apparent.

Moy *et al*. (2000) have compared the results from PB theory with BD in different geometries, including a catenary shape similar to that of the acetylcholine receptor. In these calculations, a spherical, cylindrical or catenary-shaped region of high dielectric is embedded in a region of low dielectric. By placing a test ion at different locations in the models and calculating the force on it with both methods, a direct comparison can be made.

A simple spherical electrolyte-filled cavity provides an instructive example of the difference between BD and PNP. For 0·5 M NaCl (Debye length 4·3 Å) within a cavity of radius 20 Å, the force is nearly 0 for an ion in the centre of the cavity, both in BD and PB. As the ion is moved closer to the wall, the repulsive force from BD persists up to about 2 Debye lengths from the walls, whereas the PB solution shows a force of almost 0. Close to the wall, the BD force increases steeply but the PB force is a factor of 4 less. This is because in the PB case, shielding is provided by counter ions even though there is no physical space for counter ions (Moy *et al*. 2000).

In two more complicated cases (a channel-like cylinder with rounded edges and a catenary shape) similar effects were seen. In particular, in a cylindrical channel of radius 3 Å, PB yielded a maximum force of more than a factor 4 less than BD, again due to overestimation of shielding even in this narrow geometry. In wider channels the difference in maximum force between PB and BD decreased. Thus, when force profiles are integrated, PB underestimates the height of the barriers in the electrostatic potential energy profile. In a second paper, compared PNP theory with BD in the same model cylindrical channels and also in a potassium channel-like geometry. When the channel diameter became less than 2 Debye lengths (note the Debye length is 8 Å in 150 mM KCl), the PNP approach severely overestimated shielding.

Overall, although some aspect of these studies may be criticized on more technical grounds concerning, e.g. the exact treatment of ion concentrations and the transmembrane potential, the results provide clear examples of the dangers of failing to treat ions as discrete entities within confined spaces.

https://doi.org/10.1017/S0033583501003729 Published online by Cambridge University Press

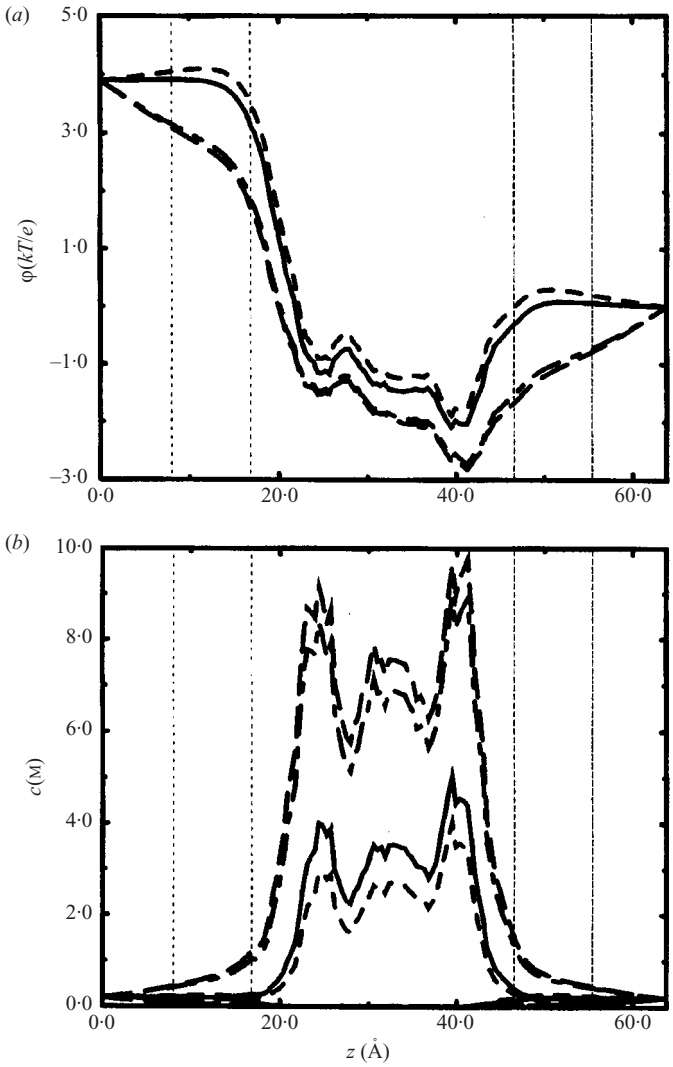


Fig. 24. 3D PNP calculations on the gA channel (Cardenas *et al.* 2000). (*a*) Electrostatic potential energy profile along the pore axis. (*b*) Concentration profiles of cations along the pore axis (the anion concentration is essentially zero within the pore). In both cases, the pore runs from *ca.* 17 to 43 Å (inner vertical lines) with the membrane surfaces shown by the outer vertical lines. Calculations for a neutral membrane (solid line), a dipolar membrane (dashed line), a charged membrane (long dashed line) and a charged and dipolar membrane (dot-dashed line) are shown. The bulk electrolyte concentration is 0·2 M and the voltage difference across the membrane is 100 mV. (Diagrams from Cardenas *et al.* 2000, with permission.)

3.5.2 Applications to known structures

3.5.2.1 gA

gA was the first channel for which BD simulations were used (simplified to 1 dimension because the channel is so narrow; Cooper *et al.* 1985; Jakobsson & Chiu, 1987). There have also been two independent applications of 3D PNP methods to gA. Kurnikova *et al.* (1999) were the first to describe a numerical method based on lattice relaxation to solve the coupled PNP equations for arbitrary 3D geometries, and to apply the theory to gA (Fig. 24). Within

https://doi.org/10.1017/S0033583501003729 Published online by Cambridge University Press

PNP theory the computed steady-state ionic currents scale linearly with the corresponding diffusion constants. The diffusion constants for M^+ and X^- were taken as equal, using a value of 0·013 $Å^2\ ps^{-1}$ for both X^- and M^+. These values can be compared to *ca.* 0·1 $Å^2\ ps^{-1}$ for monovalent ions in bulk. Interestingly, the same *I–V* curves could be obtained by decreasing the dielectric constant of the channel interior and simultaneously increasing the ionic diffusion coefficients (revealing that these parameters are highly correlated if fitting to *I–V* data is attempted). A comparison between the measured and predicted conductance of gA in CsCl solution yielded reasonable results.

Cardenas *et al.* (2000) extended these calculations to study the effects of membrane electrostatics on the conductance properties of gA. Two experimental studies provide data for comparison for these calculations. In the first, Rostovtseva (1998) have measured the gA conductance as a function of membrane surface charge, by titrating a PS bilayer and by gradually adding PS lipids to a PC bilayer. In the second, Busath *et al.* (1999) have compared the conductance of gA in GMO and PC bilayers. The PNP calculations of Cardens *et al.* (2000) build on the methods developed in the earlier study (Kurnikova *et al.* 1999), with a number of important improvements:

(1) The boundary conditions have been improved so that the external potential due to the electrodes in the experiments was fixed sufficiently far away (> 15 Å) from the membrane not to influence the ion distribution near the channel.
(2) Ion concentrations were allowed to vary outside the channel.
(3) Ion diffusion coefficients were allowed to vary spatially, so they can be set to a lower value inside the channel than in bulk, in agreement with most MD simulation (see Section 2.3).
(4) The membrane had surface charges or dipoles that represent the surface charge distribution caused by different lipids, and the membrane thickness was varied

The results of the PNP calculations showed a strong dependence on the lipid surface charge, as would be expected from the experimentally known dependencies. At 0·1 M salt, the current is roughly sixfold larger for a charged PS membrane than for a PC membrane. At 1·0 M, the difference is still about a factor of 2. The experimentally observed reduction in conductance (Busath *et al.* 1998) on going from DPhPC to GMO can be reproduced with this simple model. To a large extent, this is likely to be due to the difference in thickness of the DPhPC bilayer compared to the GMO bilayer. The large changes in conductance properties caused by changing the properties of the membrane, including membrane thickness, lipid charges and lipid dipoles are consistent with experimental measurements. However, they pose the interesting question how 'good agreement' with experimental conductances based on simple PNP models that do not incorporate the effects of a membrane should be interpreted. Of course, it is possible (likely) that gA *I–V* curves may be more sensitive to the nature of the membrane than for larger channel proteins, e.g. porins.

Hollerbach *et al.* (2000) have also used 3D PNP to study sodium current in gA, representing the channel and its environment by a mesh based on spectral elements that allows a high level of detail for the channel structure and a lower level of detail for the environment. Calculated *I–V* curves were in reasonable agreement with experimental data. Occupancies of the gA channel are between 0 and 0·2 for Na^+ ions and about 2 orders of magnitude lower for Cl^- ions at a potential of 60 mV. These occupancies are very low, corresponding to a binding affinity of $< 1\ M^{-1}$, whereas the experimental values range from 1·43 to 100 M^{-1}.

https://doi.org/10.1017/S0033583501003729 Published online by Cambridge University Press

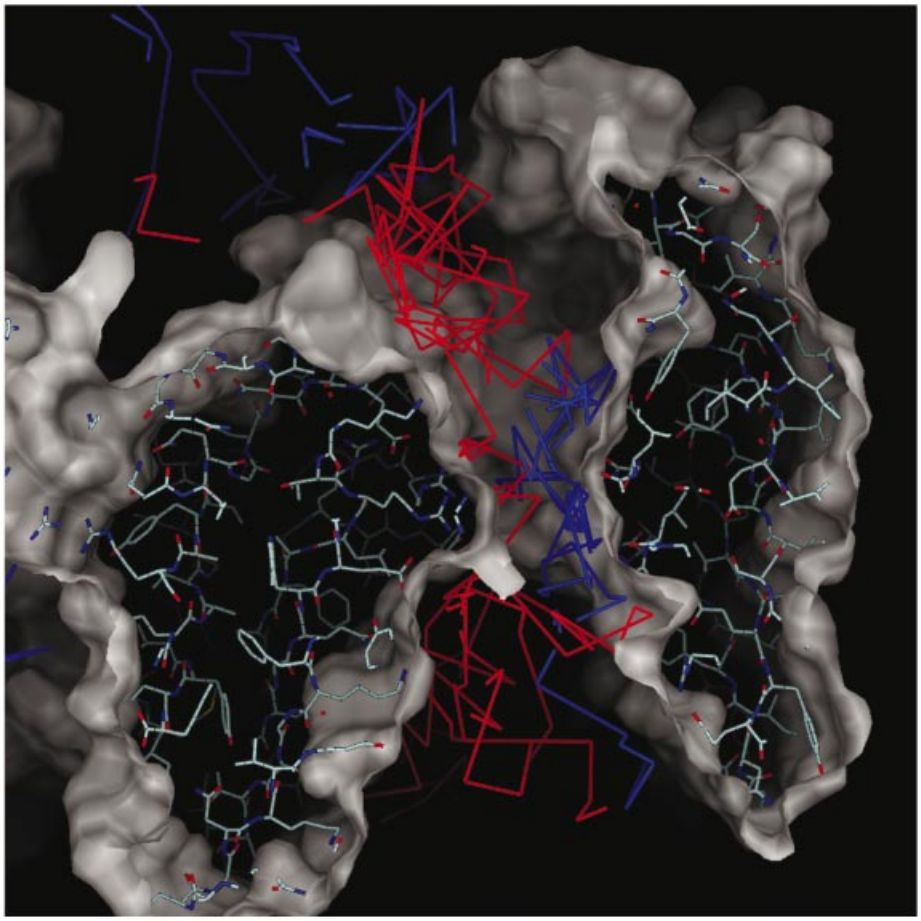


Fig. 25. Diagram (from Schirmer & Phale, 1999, with permission) illustrating the results of BD simulations on the porin OmpF. The molecular surface of the protein is shown in white. The red and blue lines show multiple BD trajectories of anions and cations respectively, indicating that the two types of ions follow different paths through the narrowest region of the pore.

3.5.2.2 Porin

As mentioned above (Section 1.1.4) porins form a nice test case for theoretical methods that describe ion channel properties. However, their conductances are generally very high, and their pores are wide. Consequently, some of the problems with continuum theories arising from the small dimensions of most channels might be less important for porin.

Schirmer & Phale (1999) used most of the calculated charges from Karshikoff *et al*. (1994) for BD simulation of OmpF, osmoporin OmpK36, PhoE and two OmpF charge mutants. These simulations [run using UHBD (Davis *et al*. 1991) with a 10 fs time step] gave single-ion trajectories that revealed how the electrostatic potential at a highly charged channel constriction enhances ion permeability of cations or anions, depending on the type of porin. In contrast to other channels, counter ions were also rapidly translocated. The simulations showed two different pathways, one for cations and one for anions, on opposite sides of the constricted region (Fig. 25). The calculated ion selectivity and relative conductance agree well

https://doi.org/10.1017/S0033583501003729 Published online by Cambridge University Press

with experimental values, and are dependent crucially on the charge constellation at the pore constriction. The experimentally observed decrease in ion selectivity and single channel conductance with increasing ionic strength is well reproduced and can be attributed to electrostatic shielding of the pore lining. In a second paper (Phale *et al*. 2001), the effect of changes in the charge constellation at the pore constriction was explored in more detail. This study provides a paradigm for investigation of structure–function relationships in ion channels, in that a number of new mutants were made, their electrophysiological properties determined, their structures solved to high resolution, and the resulting structures used for BD simulations. Interestingly, the quintuple mutant R42A/R82A/R132A/D113N/E117Q had a *larger* pore cross-section, yet showed a *smaller* conductance. By changing the different charges, the selectivity ratio for cation/anion was varied from 1 to 12. BD simulations as described above on these new mutants yielded qualitative agreement for the conductance of most mutants. The experimental trends in selectivity are reproduced, but the magnitude is overestimated in the simulations by a factor of 2.

It is interesting that the results reported from these simulations are so good. Of course, they could indicate that porin simulations are robust to changes in the level of theory whereas this may not be so for other channels. There are several aspects that could be further developed, most obviously the fact that single ion trajectories were calculated, whereas the channel clearly is large enough to accommodate several ions at any given time. In addition, the transmembrane potential difference was not included in the simulation.

In a recent paper, Im *et al*. (2000) have considered how to include in a general and physically consistent way the transmembrane difference in electrochemical potential (see Section 3.4.2). They calculated the ion distribution in OmpF for 1 M KCl with a transmembrane potential of −100 and +100 mV. Dielectric constants were 80 for water and 2 for protein and membrane, the time step was 25 fs, and the bulk diffusion coefficients for K^+ and Cl^- were used. On average, 6·7 K^+ ions and 1·8 Cl^- ions were present in the pore at +100 mV, 7·1 and 1·6 at −100 mV. This demonstrates the importance of taking into account ion–ion interactions, at least inside channels as wide as porins. Calculated conductances were considerably higher than the experimental values, which may be due to a large extent to the neglect of the reaction field of the ions caused by the dielectric boundaries and to the use of the bulk diffusion coefficients. The reaction field is likely to make it less favourable for ions to move into the channel with its low dielectric environment, which will also have consequences for the importance of ion–ion interactions in the channel.

3.5.2.3 LS3

The leucine–serine peptide LS3 (Lear *et al*. 1988; see Section 1.1.2 above) forms an interesting test case for different methods to calculate *I–V* curves. The LS3 peptide forms cation-selective channels exhibiting intrinsic rectification, i.e. cations flow more easily in one direction along the channel than in the opposite direction (Lear *et al*. 1988; Åkerfeldt *et al*. 1993). Interestingly, several different theories have been applied to LS3 to fit the measured *I–V* curves and explain its selectivity and rectification. Kienker *et al*. (1994) and Kienker & Lear (1995) used a continuum electrodiffusion model based on the Nernst–Planck equation together with a simple geometric model of the pore that included point charges radially arranged around the pore. The experimental data in symmetric KCl solution could be reproduced with a reasonable model and sensible values for the parameters, but in asymmetric solution the agreement was less satisfactory. In addition, the observed charge selectivity could not be explained from these models. Mathematical modelling using rate theory based on a

https://doi.org/10.1017/S0033583501003729 Published online by Cambridge University Press

model for transitions among ion-occupied and empty states allowed fitting of the experimental data, but required 13 adjustable parameters, for which it is difficult to find a physical basis (Kienker & Lear, 1995). Again, this procedure does not make use of the 3D atomic structure.

The 1D version of PNP was used to fit the experimental data (Chen *et al*. 1997). In 1D PNP the potential profile and charge profiles are reduced to 1 dimension, and diffusion coefficients, etc. may be considered empirical fitting parameters. Although this theory gave a reasonable fit of the data, some of the parameters were outside a physically acceptable range. The α-helix end charge was only 5% of the generally accepted value, and the theory predicted that the observed selectivity was based on an eightfold larger diffusion coefficient for K^+ compared to Cl^-. Such a difference in diffusion coefficients was *not* observed in MD simulations of ions within a model of the $LS3_6$ pore (Smith & Sansom, 1999).

Because the true structure of the channel is not known experimentally, Dieckmann *et al*. (1999) used a series of models and structures from a MD simulation (Zhang *et al*. 1998c) as a basis to calculate macroscopic conduction properties based on the 3D structures. Their approach was based on the finite-difference PB methodology combined with the Nernst–Planck equation. The potential profile along the pore axis was calculated from the PB equation. This profile was used as input for the Nernst–Planck equation, which had only the diffusion coefficients of K^+ and Cl^- as adjustable parameters. The main result of these calculations is that the experimental selectivity and rectification can be quantitatively reproduced when the averaged structure of the LS3 channel from a MD simulation is used. Interestingly, because these calculations are based on 3D structures, they make it possible to identify features of the structure that affect the conduction properties.

When the minimum pore radius of the models was less than 3·8 Å, the predicted potential profiles showed large energy barriers. In order to still fit the experimental data, unrealistically high values for the ion diffusion coefficients had to be assumed. At a minimum radius of more than 3·8 Å, ion desolvation energies became quite small, of the order of kT. The PB equation also allows the splitting of contributions to the electrostatic potential. Dieckmann *et al*. (1999) found that the serine side-chains of the helices were a major cause of selectivity. Finally, even in this simple channel, with only serine residues lining the pore, the orientation of the serines is crucial for the calculated conductance. This may explain why the MD structures did well, because they sample a range of orientation of the serines, in a realistic water–channel environment.

The agreement between the experimental data and the structures may still be somewhat fortuitous. Many models were considered, and only a few structures yielded good agreement. However, it is encouraging that models can be made that give good agreement with the experimental data, and that structures from simulations might be used to predict conduction properties, even though the models and the simulations were done at equilibrium. In fact, not only was the transmembrane voltage not taken into account during modelling and the simulations, no ions were present. In addition, the PB equation is meant for equilibrium simulations. However, if the channel is narrow enough to be essentially occupied by 1 ion, the approach of calculating a separate potential profile, independent of permeating ions, might be valid.

MD simulations of a hexameric model of the LS3 channel have also been used to estimate the conductance using the empirical approach of (Smart *et al*. 1998) by using the average radius profile of the pore over the duration of the simulation combined with estimates of the diffusion constants of water along the pore axis (Randa *et al*. 1999). This approach yielded a conductance of 64 pS (in 0·5 M KCl), in reasonable agreement with the experimental values

https://doi.org/10.1017/S0033583501003729 Published online by Cambridge University Press

of 70 pS (Lear *et al*. 1988). Again, this shows the possible advantages of combining atomistic and (albeit crude) coarse-grained treatments of the same system.

3.5.2.4 Alm

Alm is another useful model ion channel formed by the aggregation of α-helical peptides (Sansom, 1993). There is a large body of electrophysiology data for this peptide, as well as a significant number of modelling and simulation studies (see Section 1.1.2). Woolley and co-workers have designed and synthesized covalently linked Alm dimers and characterized their electrophysiological properties (You *et al*. 1996; Woolley *et al*. 1997). Models of this covalently linked Alm dimer were used to predict the conductance properties of the channel, using the Nernst–Planck approach with potential profiles derived from solving the PB equation for a single model structure (Woolley *et al*. 1997). This linked dimer channel is rectifying and cation selective. A simple Nernst–Planck approach was able to reproduce the rectification, which was shown to arise from the aligned helix dipoles, in a similar manner to that for LS3 (see above). Building on this work, Woolley and co-workers also designed a covalently linked dimer of Alm in which the Glu18 has been replaced by a lysine (Starostin *et al*. 1999). This molecule, called Alm-K18, forms channels that are anion selective (by a factor of 4 for Cl^- over K^+) instead of cation selective like the native Alm. Interestingly, the selectivity of these channels can be changed by changing the pH (Borisenko *et al*. 2000). At pH 7 or lower, all lysines are thought to be charged, and the channel is anion selective. When the pH is between 8 and 10, a mixture of non-selective, anion-selective and cation-selective channels is found, and at pH $>$ 11 only cation-selective channels are found. Although PB calculations on an octameric model of the Alm-K18 channel embedded in a low dielectric membrane-mimetic slab could account for the apparent pK_a of the channel, they failed to correctly predict the degree of ion selectivity. In particular, the anion selectivity was severely overestimated. This illustrates some of the strengths and weaknesses of a simple PB approach.

3.5.2.5 nAChR

A model of the nAChR with the pore-lining M2 helix bundle treated atomistically and the remainder of the molecule modelled as a cylinder (with surface charge derived from the distribution of charged amino acids in the amino-acid sequence) has been used to predict single-channel conductance (Adcock *et al*. 2000). A 1D PNP equation calculation of single-channel I–V curves predicted a single-channel conductance (*ca*. 150 pS) threefold higher than that measured experimentally. MD simulations gave self-diffusion coefficients (D) of water molecules within the narrowest region of the pore that were reduced *ca*. threefold relative to that of bulk water. Assuming the diffusion of ions scales with that of water (Sections 2.2 and 2·3) gives a revised prediction of the single-channel conductance of *ca*. 50 pS, i.e. in good agreement with the experiment.

More advanced approaches have been taken to similar simplified models of the nAChR: a toroidal channel (Li *et al*. 1998), for which an analytical solution of the Poisson equation exists (Kuyucak *et al*. 1998), and a simple model channel geometry formed by a cylindrical transmembrane pore linked to a catenary vestibule at each side (Chung *et al*. 1998). These simulations have demonstrated a number of basic features. A channel with a reasonable geometry without charges in the channel protein is impermeable to ions, because of the large repulsive image forces induced by the low dielectric region of the membrane and the protein. By adding dipoles embedded in the channel wall, the channel becomes conducting. When the

https://doi.org/10.1017/S0033583501003729 Published online by Cambridge University Press

dipoles become too large, they create deep wells that trap ions inside the channel, making the ion impermeable again. BD simulations of such simple model channels also allow the placement of arbitrary barriers at arbitrary positions. Several effects that are observed in the nAChR can be reproduced by putting a barrier of 2–3 kT at the narrowest point of the channel. Without barrier, the *I–V* curve in symmetrical solutions is ohmic. With an asymmetric solution, the *I–V* curve approximates the Goldman equation, with the reversal potential close to that predicted by the Nernst equation (Chung *et al*. 1998).

3.5.2.6 KcsA

BD simulations of a multi-ion pore intended to mimic a K channel (Bek & Jakobsson, 1994) have been used to describe how to count ions going in/out of the channel, consistent with the electrolyte concentration. More recently, BD simulations have been performed on a simplified model that aims to reproduce the same features of KcsA (Chung *et al*. 1999). This model included a few residues of the selectivity filter, the general geometrical shape of KcsA (albeit in its closed conformation), and dipoles to represent the effect of the P helices. The overall conductance of KcsA was correctly reproduced.

3.6 pK_a calculations

As discussed above the electrostatic profile along the pore axis of a channel protein is, amongst other things, dependent upon the ionization state of acidic and basic side-chains within that protein. Although the majority of such side-chains will have their expected ionization state (-1 for acidic side-chains, $+1$ for basic) within a protein at neutral pH, in some cases p$K_a$values of side-chains *in situ* may differ significantly from those of the individual amino acid in solution. The main reason for such shifts in pK_a is proximity of ionizable side-chains to one another (e.g. 'rings' of acidic side-chains at the mouth of a cation-selective ion channel), which leads to mutual electrostatic interactions that suppress complete ionization. However, in α-helix bundle channels helix (backbone) dipoles can also have an effect.

The ionization states of side-chains in channel models can be estimated via pK_a calculations, using the linearized PB equation to estimate solvation energies as described in detail in, e.g. Adcock *et al*. (1998) and Ranatunga *et al*. (2001a). This procedure has two stages. Firstly, intrinsic pK_a values are calculated using:

$$\mathrm{p}K_{\mathrm{a,\,intrinsic}} = \mathrm{p}K_{\mathrm{a,\,model}} - \frac{1}{2{\cdot}303}[\Delta\Delta G_{\mathrm{born}} + \Delta\Delta G_{\mathrm{back}}],$$

where p$K_{\mathrm{a,\,model}}$ is the pK_a of an isolated amino acid, $\Delta\Delta G_{\mathrm{born}}$ is the solvation contribution to the pK_a shift and $\Delta\Delta G_{\mathrm{back}}$ is the contribution due to the interaction of a residue with non-titrating charges in a protein (Bashford & Karplus, 1991; Karshkoff *et al*. 1994). Absolute pK_a values may be obtained via calculation of titration curves obtained via calculation of:

$$p(\mathbf{x}) \propto \exp\left[-\ln 10 \sum_i \gamma_i (pK_{\mathrm{a,\,intrinsic},i} - \mathrm{pH}) - \beta \sum_i \sum_{k<i} \Delta\Delta G_{i,k} \right],$$

where $p(\mathbf{x})$ is the probability of a residue existing in its ionized state and $\mathbf{x}$ is an N-element state vector (i.e. a vector whose elements are 0 or 1 depending on whether the residue is un-ionized or ionized respectively), where $\gamma = -1$ for a basic residue, $\gamma = +1$ for an acidic residue, and $\Delta\Delta G_{i,k}$ is the screened Coulombic interaction energy between pairs of ionizable residues i and k (Bashford & Karplus, 1991; Lim *et al*. 1991).

https://doi.org/10.1017/S0033583501003729 Published online by Cambridge University Press

This method has been applied to a number of model channels made up (at least in part) of bundles of parallel α-helices. These systems include the pore domain (M2 helix bundle) of the nAChR (Adcock *et al*. 1998), and Alm channels (Tieleman *et al*. 1998) and their derivatives (Borisenko *et al*. 2000). In all of these cases two effects influence side-chain ionization: (*a*) the dipole of a parallel bundle of α-helices, which will favour ionization of, e.g. an acidic side-chain at the N-terminus of a helix, whilst suppressing ionization at the C-terminus; (*b*) 'rings' of similar/identical side-chains in close proximity to one another within the channel.

This approach has also been applied to KcsA (Ranatunga *et al*. 2001a) and to a homology model of the core pore-forming domain of a voltage-gated K channel (Ranatunga *et al*. 2001b). PB calculations on the crystal structure of the KcsA channel protein embedded in a low dielectric slab suggest that side-chains E71 and D80 of each subunit, which lie adjacent to the selectivity filter region of the channel, form a proton-sharing pair in which E71 is neutral (protonated) and D80 negatively charged at pH 7. When (multiple) K^+ ions are introduced within the filter the pattern of proton sharing is altered such that the probability of E71 being ionized and of D80 remaining neutral (i.e. protonated) is enhanced. The ionization states of the protein side-chains influence the potential energy profile experienced by a K^+ ion as it is translated along the pore axis. In particular, the ionization state of the E71–D80 proton-sharing pair modulates the shape of the potential profile in the vicinity of the selectivity filter. Such reciprocal effects of ion occupancy on side-chain ionization states, and of side-chain ionization states on ion potential energy profiles will complicate, e.g. MD simulations intended to explore ion permeation energetics. Similar calculations on a homology model of the *Shaker* K_v channel reveal a ring of four Asp447 side-chains at the mouth of the pore that are predicted to be incompletely ionized at neutral pH. The potential energy profile for a K^+ ion moved along the central axis of the *Shaker* pore domain model selectivity filter reveals a shallow well, the depth of which is modulated by the ionization state of the Asp447 ring.

There are some worries about using the PB equation to calculate electrostatic interactions to get pK_a estimates. In particular, especially in narrower channels, it may be more appropriate to use just Poisson's equation to calculate pK_a. The main worry with using the PB approach is again of unphysical screening. To some extent this can be overcome by including a Stern radius over the surface of the protein from which ions are excluded. Further work is required to optimize general methods for pK_a calculations to ion channels.

3.7 Selectivity

Ion selectivity can be studied both via full atomistic simulations (see Section 2.4) and via more coarse-grained simulations. To some extent, which method is more appropriate depends on the nature of the channel. Porins, gA and Alm provide model systems for studying broad selectivity (e.g. anions *versus* cations), and so may be addressable via coarse-grained simulations. Porin and Alm are useful model systems because their anion/cation selectivity can be changed by mutations (Jaikaran *et al*. 1997; Starostin *et al*. 1999; Borisenko *et al*. 2000; Phale *et al*. 2001). gA is interesting because it shows some degree of discrimination between monovalent cations. However, understanding the more subtle aspects of selectivity in, e.g. K channels based on their atomic structure will probably require more fine-grained (i.e. atomistic) simulations. In addition to studies of 'real' channels, a number of recent studies

https://doi.org/10.1017/S0033583501003729 Published online by Cambridge University Press

on simple models of channels have addressed the factors that might give rise to selectivity in ion channels, without directly linking these factors to known channel structures.

3.7.1 Anion/cation selectivity

Selectivity between anion/cations is dominated by electrostatics, as might be expected. This is clear from combined BD and mutation studies in porin and in Alm (see above). The cation selectivity of gA remains a little more contentious. Cation selectivity of gA has been explored by MC simulations using a semi-microscopic model of the channel (Dorman *et al*. 1996). Ion, water and peptide COs were treated explicitly, whereas the remainder of the system was modelled in a continuum fashion. Cation selectivity resulted from differences in ion transfer free energies from bulk water to the channel interior, i.e. because anions bind hydration water more strongly. Indeed, the *anion* stabilization free energy within the channel was actually somewhat greater than the cation stabilization energy. A somewhat different origin of cation selectivity was suggested by MD simulations (Roux, 1996) using 'alchemical' transformation of a K^+ ion to a Cl^- ion whilst inside the channel. The latter studies suggested a difference in interactions of cations *versus* anions with the gA channel due to the asymmetry of the permanent charge distribution of the channel backbone (in the Charmm force field, $q(O) = -0{\cdot}51e$ for the carbonyl oxygen *versus* $q(H) = +0{\cdot}31e$ for the amide hydrogen). This difference emphasizes the difficulties arising from problem in parameterization of ion–ligand interactions (see Section 2.1).

3.7.2 Monovalent/divalent ion selectivity

There have been several attempts to use electrostatic-based approaches to explain selectivity between monovalent and divalent cations. For example, electrostatic effects of the central cavity and the P-helices in the KcsA channel have been analysed via the Poisson equation (Roux & MacKinnon, 1999). The cavity and P helices overcome the destabilizing influence of the low dielectric environment provided by the membrane and thus stabilize a cation within the cavity. The combined contributions of the ion self-energy and the P-helix electrostatic field are suggested to provide selectivity for monovalent (over divalent) cations in the water-filled cavity. However, it is likely that such calculations will be somewhat sensitive to the dielectric properties of the solvent in the cavity and to the long-range effects of ionizable side-chains and their protonation states.

There have also been attempts, using somewhat idealized models, to explain the selectivity of Ca channels for Ca^{2+} over Na^+ ions. It has been established by site-directed mutagenesis (Ashcroft, 2000) that such selectivity resides in a region comparable to the P loop of K channels. In Ca channels this region contains four glutamate residues and so is presumed (in the absence of any structure on which to base pK_a calculations) to have a net charge of *ca*. -4. In the Na channel the comparable region contains the residues Asp, Glu, Lys, Ala, given an expected net charge of *ca*. -1. Various statistical mechanical approaches have been used to explore the behaviour of a net charge of *ca*. -4 in a confined volume typical of a channel to explain the observed selectivity.

Ca^{2+} selectivity over Na^+ can be modelled by a simple PNP model when it is assumed that the divalent ion binds selectively in the 4-glutamate residue region of Ca channels (Nonner & Eisenberg, 1998). More recent calculations use the mean spherical approximation

https://doi.org/10.1017/S0033583501003729 Published online by Cambridge University Press

(MSA – which ions are represented as a solid sphere instead of a point) to model the Ca channel selectivity filter as a small volume (*ca*. 375 Å^3, i.e. equivalent in volume to *ca*. 12 water molecules) containing 8 O anions, each with charge −0·5. The results from the combined PNP/MSA calculations are in plausible agreement with the experimental data (Nonner *et al*. 2000). Of course, it remains to be seen whether this model of the filter resembles that present in the Ca-channel structure.

A related approach has been used by Boda *et al*. (2000) who modelled a Ca channel as an infinite cylinder with 8 $O^{-0.5}$ ions within a restricted region, and then used MC simulations to explore the densities of Ca^{2+} *versus* Na^+ ions within the channel. Again, the 'channel' was Ca^{2+} selective. This work was extended in a density functional theory approach, yielding similar results to the MC simulations. The overall conclusion agrees with that of Nonner *et al*. (2000) on the same system, suggesting that excluded volume effects and more effective screening by the divalent Ca^{2+} ions are determining factors of selectivity in this type of Ca channel. Both of these studies extend those of (Goulding *et al*. 2000), who saw K^+ *versus* Na^+ selectivity based on steric factors alone, in that they show that competition between steric (volume exclusion) and electrostatic effects can lead to quite subtle ion selectivity problems. They demonstrate the virtues of extending purely continuum theories, e.g. PNP by considering ions as discrete entities.

4. Problems

4.1 Atomistic simulations

4.1.1 Problem

There are a number of problems in using atomistic simulations to study ion permeation. Two of these are related to the maximum practical cpu times of such simulations, given current computer resources. Available cpu time limits both the size (in terms of total numbers of atoms) of the simulation system and the maximum simulation time. With current resources an upper limit of *ca*. 10 ns for *ca*. 100000 atoms would be realistic. The relatively small number of atoms (for example *ca*. 100000 atoms would correspond to a bilayer of *ca*. 700 lipid molecules plus 30 water molecules per lipid in a box of dimensions *ca*. $210 \times 210 \times 80$ Å^3 and yet would contain only *ca*. 38 K^+ and 38 Cl^- for 100 mM KCl) may make it difficult to 'scale' the microscopic results to macroscopic properties. In particular, the relatively small number of ions is likely to introduce substantial 'noise' (i.e. stochastic fluctuations) into the electrostatics of the system, which fluctuations may have a relatively long correlation time. The timescale of most simulations (*ca*. 10 ns) is short, of comparable duration to that of permeation of a single ion. Thus, simply averaging across atomistic simulations is *not* going to provide a picture of ion permeation. However, as we have seen such simulations do provide clues as to what features (e.g. filter mobility) it may be necessary to accommodate in more coarse-grained simulations. Also, atomistic simulations may provide sufficient sampling to allow us to estimate parameters (e.g. diffusion coefficients) that are required as input to more approximate descriptions of permeation.

There is another fundamental problem with atomistic simulations (related to the relatively small system size). This is the difficulty of how to include macroscopic boundary conditions such as a transbilayer electrochemical potential difference. Returning to our 100000 atoms

https://doi.org/10.1017/S0033583501003729 Published online by Cambridge University Press

simulation system, e.g. a transbilayer voltage difference of 100 mV would correspond to a difference of *ca*. 19 K^+ ions on the two sides of the bilayer (assuming for this example that the membrane is selectively permeable to K^+ ions). Thus, movement of just one K^+ ion across the membrane during a simulation would have a significant effect on membrane potential.

One way around some of these problems is to use novel methods for searching more efficiently for *paths* followed by ions through a channel (Elber *et al*. 1995). Such methods to date have mainly been used, e.g. looking at conformational transitions of proteins (Smart, 1994; Smart & Goodfellow, 1995) but recently have also been used to explore oligosaccharide passage through a maltoporin pore (Fischer, 2000).

There are a number of more technical problems that need to be addressed with respect to MD (and other atomistic) simulations of ion channels and of membrane proteins in general. The first of these is that of how to treat long-range electrostatics. The origin of the problem is the prohibitive computational cost of calculating *all* pairwise atom–atom electrostatic interactions according to Coulomb's equation. The majority of such interactions, over a relatively long distance, make only a small contribution to the overall electrostatic energy. This is the basis of the first approximation to deal with this problem, namely using a cut-off whereby electrostatic interactions over a distance greater than, e.g. 15 Å are simply ignored. This is simple to implement, but has been shown to lead to artefacts, especially in highly charged systems, e.g. DNA. A popular alternative is to treat long-range interactions via Ewald summation in reciprocal space. This has the advantage of including all long-range interactions, but does mean that one is treating the simulation system as a 'crystal' made up of units cells corresponding to the simulation box. Also, a serious problem is that there is no exact statistical mechanical theory of non-equilibrium steady states with long-range interactions, as reviewed by Sarman *et al*. (1998).

There is a considerable literature comparing the cut-off *versus* Ewald summation approaches for simulation of pure lipids bilayers (e.g. Tobias *et al*. 1997; Tieleman *et al*. 1997), in which case it appears that, with suitable parameterization, either approach can reproduce experimental data. However, which approach is better for ion channels and membrane proteins remains unclear, as few systematic comparisons have been performed. What is clear from those cases where comparisons have been made (e.g. Alm and $LS3_6$) is that changing from, e.g. cut-offs to Ewald summation (e.g. PME) can have an effect, especially in terms of fluctuations in helix bundle structure and/or dynamics of intra-pore water. One might simply assume that Ewald summation is preferable. However, it should be remembered that parallel helix bundles have a significant macrodipole parallel to the bilayer normal. In an infinite periodic system (such as is generated by PME) such dipoles will be able to interact and so may induce artefactual cooperative effects. In this context it is of interest to note that Weber *et al*. (2000) have shown such cooperative electrostatic effects can lead to stabilization of an Ala_8 peptide in water unless the simulation box is sufficiently large to prevent artefactual interactions of helix dipoles. Further work is needed to explore this problem in the context of membrane proteins. It may be limited to those ion channels formed by parallel bundles of α-helices. However, a macrodipole could also result from an asymmetric distribution of charged side-chains along the bilayer normal. The latter might be anticipated to arise, especially for bacterial membrane proteins, as a consequence of the 'positive inside rule' that governs membrane protein topology (von Heijne, 1992).

A second problem is that of the correct treatment of side-chain ionization states in ion channel simulations. As seen above, there are approaches, albeit approximate, that allow

https://doi.org/10.1017/S0033583501003729 Published online by Cambridge University Press

estimation of the ionization states of acidic and basic side-chains within a (membrane) protein. However, a major difficulty with using such calculations in conjunction with MD is their sensitivity to side-chain conformation. Thus, if one runs a (static) pK_a calculation at the outset of a simulation this may yield reasonable ionization states for the side-chains in their initial conformations, but if these conformations change during the simulation then the predicted pK_a should also be allowed to change. What is needed is dynamic protonation–deprotonation during a simulation. This may be especially important for ion channels with rings of side-chains at the mouths of the channel as the ionization state of these may be sensitive to the presence/absence of an ion, and likewise the energetics of ion permeation may be sensitive to the ionization state of the ring of side-chains. There have been some attempts to include dynamic (de)protonation during a simulation (Sandberg & Edholm, 1997) but evidently further work is needed in this area. For example, dynamic protonation is likely to be much easier to implement in MC than in MD simulations.

A serious problem for atomistic approaches (e.g. calculation of potentials of mean force) is that of *multiple* ions present within a pore, as is the case with, e.g. K channels. This is problematic because it requires the calculations (which are already computationally expensive) to be repeated for every possible configuration of ions within the channel. Of course, single filing somewhat simplifies this situation. Multiple ions in a pore also present problems for mean- field approaches such as PNP because discrete ions are not treated correctly.

A further problem that can, in principle, be addressed but will prove somewhat taxing in practice, is that of atomic polarizability. In most current MD simulations of channels atoms are treated as point partial charges, i.e. dynamic redistribution of electronic charge (atomic polarizability) is not allowed. This is clearly an approximation that one might expect to influence energetics of ion–water and ion–protein interactions. Indeed, there have been some attempts to include, e.g. carbonyl oxygen polarizability in MD simulations of gA (Roux & Karplus, 1991b). Furthermore, Duca & Jordan (1997) showed that including electronic polarizability in models of gA changed ion–water and ion–protein interactions. A polarizable peptide tended to raise internal translocation barriers, whereas polarizable water tended to lower barriers by enhancing ion–water and water–water interactions. Guidoni & Carloni (2001) have shown, using DFT calculations of electron redistribution for snapshots taken from a (non-polarizable) MD simulation, that when K^+ ions are in the filter of KcsA, polarization of the carbonyl oxygens is significant. Such effects are likely to be of importance in accurate treatment of ion selectivity. In principle it should be possible to include atomic polarizability in MD simulations, albeit at some computational cost. However, there is a difficulty in that its inclusion is not consistent with current force fields. This is another area in which basic development work is needed.

4.1.2 Parameters

We have described above the current state, both experimental and theoretical, of treating ion–water and ion–oxygen interactions. It is perhaps surprising that a definitive set of parameters has yet to emerge. What is clear is that any treatment of the energetics of permeation (and selectivity) will be sensitive to the choice of parameters. This is because the energetics of selectivity involve a difference between two large energy terms, namely ion/water and ion/protein.

https://doi.org/10.1017/S0033583501003729 Published online by Cambridge University Press

4.2 BD

BD simulations of ion channels are attractive in that the simulation timescale seems more appropriate to events of ion permeation. For example, simulations of a porin (Im *et al*. 2000) have used a time step of 25 fs and total simulation time of 10×500 ns $= 5$ μs. This allowed *ca*. 150 permeation events per 100 ns to be simulated. However, there remain a number of difficulties with BD simulations. The main one is to treat the continuum electrostatics of the system correctly, which is computationally expensive and has all the problems of mean-field approaches (see next section). It is also difficult to get good parameters, e.g. ion diffusion coefficients for use in BD simulations, although here a hierarchical approach combining MD simulations to yield short timescale properties with BD simulations to explore longer timescale events is likely to be productive (Mashl *et al*. In Press). A more difficult problem is that of how to include protein flexibility. MD simulations of, e.g. gA and KcsA clearly demonstrate the importance of such flexibility if ion–protein interactions are to be treated properly. As a consequence of this it may be that BD will perform better for large radius (high conductance, rigid) channels, e.g. porins, than for smaller radius channels (low conductance, flexible) channels, e.g. KcsA. More systematic studies are needed of this alongside detailed comparison with experimental electrophysiological data.

In the context of combining MD and BD simulations, it is perhaps important to remember that the idea of a 'random walk' (characterized by a diffusion coefficient) over a potential surface may not always be quite good enough because it ignores inertial effects in the barrier crossings. Roux (1995) has approached this via activated dynamics. The pioneering work of Kramers on diffusion over barriers may be of relevance here (Rubi & Perez-Madrid, 1999), whose equations do treat the high-inertia (low-friction) case although low inertia is usually assumed. In a BD/Langevin dynamics simulation, going beyond the low-inertia case would imply the use of the full Langevin equation possibly with the 'random force' term using coloured (time-correlated) noise rather than white noise.

4.3 Mean-field simulations

To some extent mean-field simulations have yet to prove themselves for more complex ion channels, but look promising based on simulations of highly simplified systems and of gA. They do, however, have a number of inherent problems. Firstly, a number of mean-field simulations ignore the short (i.e. molecular) length/scale of channels, which means that the molecular nature of water and ions within the channel becomes important. We have seen how, e.g. ignoring ions as discrete entities can result in overestimation of electrostatic screening in PNP. However, this situation can be improved upon by more sophisticated theoretical approaches.

One serious problem with mean-field theories is that solvent dielectric constants are macroscopic properties, and thus are (probably) not appropriate for descriptions of electrostatic interactions in, e.g. the selectivity filter of an ion channel, which almost by definition is likely to be narrow and to have a strong electric field. Furthermore, filters/channels appear to contain multiple ions that give complicated correlations that are not easily put into a mean-field description.

There are other problems related to trying to capture correctly the dynamics of ion transport in such theories. As discussed above, proteins are flexible and can move on the

https://doi.org/10.1017/S0033583501003729 Published online by Cambridge University Press

timescale of ion permeation. Also, we need to consider carefully what exactly we mean by ion diffusion within a channel (this is also a problem with BD), especially in the narrowest regions of channels. Related to both of these problems is that of how to describe transport of ions across a fluctuating barrier (i.e. stochastic resonance; Doering & Gadoua, 1992). It is evident that there are interesting and important problems in the physical chemistry of ion transport through channels that remain to be addressed in detail.

5. Conclusions

5.1 Progress

It is timely to review compuational and theoretical approaches to ion-channel function. In particular, the simultaneous emergence of high-resolution structural data, significant theoretical developments and sufficiently powerful computers has resulted in significant progress in this field, which looks set to continue. Already we have a first draft of how channels work at an atomistic level. However, much work is required in order to refine this first draft, and to extend the description to a wider range of channel molecules.

5.2 The future

There are two key areas to be developed in the future. One is related to experimental studies, and will be driven by the emergence of new structural data on channels and related transport proteins. For example, whilst writing this review we have witnessed the determination of an atomic resolution structure for a glyceroaquaporin (Fu *et al*. 2000) and of near-atomic resolution structures for aquaporin (Murata *et al*. 2000; Ren *et al*. 2000, 2001). Both of these molecules contain transbilayer pores, permeable to glycerol and to water, respectively, but impermeable to ions. Simulation studies to reveal the exact nature of this impermeability may provide new insights into possible mechanisms of channel gating. So, the parallel pursuit of new structures and simulation studies of channel and transport proteins should uncover general principles underlying structure–function relationships at atomic resolution.

A second key area of development will be to integrate properly atomistic and coarse-grained approaches to channel simulation. This will require the technical issues explored in more detail above to be addressed at a fundamental level. This may require more frequent dialogue between, e.g. the chemical physics and biophysics communities.

In order to make progress, we undoubtedly need better reality checks for simulation results. For example, most attempts to simulate ion permeation are, at best, tested against single channel I–V data. It is not self-evident that such data are sufficiently varied ('rich') to enable discrimination between competing plausible models. Progress in this area may require closer working together of the experimental and simulation communities.

However, we should not let these qualifications blind us as to the progress that has been made. Our understanding of ion-channel function at a fundamental physical level is perhaps better than that for many other classes of protein molecule. Thus, computational approaches to ion channels may be considered to provide a paradigm for structure–function of more complex membrane transport proteins.

https://doi.org/10.1017/S0033583501003729 Published online by Cambridge University Press

6. Acknowledgements

Research in M. S. P. S.'s laboratory is supported by the Wellcome Trust. P. C. B. is supported by the Wellcome Trust. D. P. T. is an AHFMR Scholar. The authors thank many colleagues for copies of papers and preprints, and for their interest in this work.

7. References

Adcock, C., Smith, G. R. & Sansom, M. S. P. (1998). Electrostatics and the selectivity of ligand-gated ion channels. *Biophys. J.* **75**, 1211–1222.

Adcock, C., Smith, G. R. & Sansom, M. S. P. (2000). The nicotinic acetylcholine receptor: from molecular model to single channel conductance. *Eur. Biophys. J.* **29**, 29–37.

Åkerfeldt, K. S., Lear, J. D., Wasserman, Z. R., Chung, L. A. & DeGrado, W. F. (1993). Synthetic peptides as models for ion channel proteins. *Acc. chem. Res.* **26**, 191–197.

Akeson, M. & Deamer, D. W. (1991). Proton conductance by the gramicidin water wire. *Biophys. J.* **60**, 101–109.

Allen, T. W., Bliznyuk, A., Rendell, A. P., Kuyucak, S. & Chung, S. H. (2000). The potassium channel: structure, selectivity and diffusion. *J. chem. Phys.* **112**, 8191–8204.

Allen, T. W., Kuyucak, S. & Chung, S. H. (1999a). The effect of hydrophobic and hydrophilic channel walls on the structure and diffusion of water and ions. *J. chem. Phys.* **111**, 7985–7999.

Allen, T. W., Kuyucak, S. & Chung, S. H. (1999b). Molecular dynamics study of the KcsA potassium channel. *Biophys. J.* **77**, 2502–2516.

Andersen, O. S. (1984). Gramicidin channels. *Annu. Rev. Physiol.* **46**, 531–548.

Åqvist, J. (1990). Ion water interaction potentials derived from free-energy perturbation simulations. *J. phys. Chem.* **94**, 8021–8024.

Åqvist, J. & Hansson, T. (1996). On the validity of electrostatic linear response in polar solvents. *J. phys. Chem.* **100**, 9512–9521.

Åqvist, J. & Hansson, T. (1998). Analysis of electrostatic potential truncation schemes in simulations of polar solvents. *J. phys. Chem* (*B*) **102**, 3837–3840.

Åqvist, J. & Luzhkov, V. (2000). Ion permeation mechanism of the potassium channel. *Nature* **404**, 881–884.

Åqvist, J. & Warshel, A. (1989). Energetics of ion permeation through membrane channels: solvation of Na^+ by gramicidin A. *Biophys. J.* **56**, 171–182.

Ashbaugh, H. S., Sakane, S. & Wood, R. H. (1998). Reply to comment on 'Electrostatic potentials and free energies of solvation of polar and charged molecules'. *J. phys. Chem.* (*B*) **102**, 3844–3845.

Ashbaugh, H. S. & Wood, R. H. (1997). Effects of long-range electrostatic potential truncation on the free energy of ionic hydration. *J. chem. Phys.* **106**, 8135–8139.

Ashcroft, F. M. (2000). *Ion Channels and Disease*. San Diego: Academic Press.

Babu, C. S. & Lim, C. (1999). Theory of ionic hydration: Insights from molecular dynamics simulations and experiment. *J. phys. Chem.* (*B*) **103**, 7958–7968.

Barabino, G., Gavotti, C. & Marchesi, M. (1984). Molecular dynamics simulation of water near walls using an improved wall–water interaction potential. *Chem. Phys. Lett.* **104**, 478–484.

Bashford, D. & Karplus, M. (1991). Multiple-site titration curves of proteins: an analysis of exact and approximate methods for their calculation. *J. phys. Chem.* **95**, 9556–9561.

Baumann, G. & Mueller, P. (1974). A molecular model of membrane excitability. *J. supramol. Struct.* **2**, 538–557.

Bek, S. & Jakobsson, E. (1994). Brownian dynamics study of a multiply-occupied cation channel – application to understanding permeation in potassium channels. *Biophys. J.* **66**, 1028–1038.

Belch, A. C. & Berkowitz, M. (1985). Molecular dynamics simulations of TIPS2 water restricted by a spherical hydrophobic boundary. *Chem. Phys. Lett.* **113**, 278–282.

Bernèche, S. & Roux, B. (2000). Molecular dynamics of the KcsA K^+ channel in a bilayer membrane. *Biophys. J.* **78**, 2900–2917.

Bernèche, S. & Roux, B. (2001). Mechanism of ions permeation in the KcsA potassium channel. *Biophys. J.* **80**, 175a.

Berry, R. S., Rice, S. A. & Ross, J. (2000). *Physical Chemistry* (*Topics in Physical Chemistry*). Oxford: Oxford University Press.

Bertrand, D., Galzi, J. L., Devillers-Thiéry, A., Bertrand, S. & Changeux, J. P. (1993). Stratification of the channel domain in neurotransmitter receptors. *Curr. Opin. Cell Biol.* **5**, 688–693.

Biggin, P. C., Roosild, T. & Choe, S. (2000). Potassium channel structure: domain by domain. *Curr. Opin. struct. Biol.* **10**, 456–461.

Biggin, P. C., Smith, G. R., Shrivastava, I. H., Choe, S. & Sansom, M. S. P. (2001). Potassium and sodium ions in a potassium channel studied by molecular dynamics simulations. *Biochim. Biophys. Acta* **1510**, 1–9.

Bixby, K. A., Nanao, M. H., Shen, N. V., Kreusch,

https://doi.org/10.1017/S0033583501003729 Published online by Cambridge University Press

A., Bellamy, H., Pfaffinger, P. J. & Choe, S. (1999). Zn^{2+}-binding and molecular determinants of tetramerization in voltage-gated K^+ channels. *Nature struct. Biol.* **6**, 38–43.

Boda, D., Busath, D. D., Henderson, D. & Sokolowski, S. (2000). Monte Carlo simulations of the mechanism for channel selectivity: the competition between volume exclusion and charge neutrality. *J. phys. Chem (B)* **104**, 8903–8910.

Boheim, G., Hanke, W. & Jung, G. (1983). Alamethicin pore formation: voltage-dependent flip-flop of α-helix dipoles. *Biophys. Struct. Mech.* **9**, 181–191.

Borisenko, V., Sansom, M. S. P. & Woolley, G. A. (2000). Protonation of lysine residues inverts cation/anion selectivity in a model channel. *Biophys. J.* **78**, 1335–1348.

Born, M. (1920). Volumen und hydratationswarme der ionen. *Z. Physik.* **1**, 45–48.

Breed, J., Biggin, P. C., Kerr, I. D., Smart, O. S. & Sansom, M. S. P. (1997). Alamethicin channels – molecular modelling via restrained molecular dynamics simulations. *Biochim. Biophys. Acta* **1325**, 235–249.

Breed, J., Sankararamakrishnan, R., Kerr, I. D. & Sansom, M. S. P. (1996). Molecular dynamics simulations of water within models of transbilayer pores. *Biophys. J.* **70**, 1643–1661.

Breed, J. & Sansom, M. S. P. (1994). Alamethicin channels modelled by simulated annealing and molecular dynamics. *Biochem. Soc. Trans.* **22**, 157S.

Buchanan, S. K. (1999). β-Barrel proteins from bacterial outer membranes: structure, function and refolding. *Curr. Opin. struc. Biol.* **9**, 455–461.

Burgess, J. (1988). *Ions in Solution – Basic Principles of Chemical Interactions*. Chichester: Ellis Horwood Ltd.

Burgess, M. A. (1978). *Metal ions in Solution*. Chichester: Ellis Horwood.

Burton, N. A., Harrison, M. J., Hart, J. C., Hillier, I. H. & Sheppard, D. W. (1998). Prediction of the mechanisms of enzyme-catalysed reactions using hybrid quantum mechanical molecular mechanical methods. *Faraday Disc.* **110**, 463–475.

Busath, D. D., Thulin, C. D., Hendershot, R. W., Phillips, L. R., Maughan, P., Cole, C. D., Bingham, N. C., Morrison, S., Baird, L. C., Hendershot, R. J., Cotten, M. & Cross, T. A. (1998). Noncontact dipole effects on channel permeation. I. Experiments with (5F-indole) Trp13 gramicidin A channels. *Biophys. J.* **75**, 2830–2844.

Cafiso, D. S. (1994). Alamethicin – a peptide model for voltage gating and protein membrane interactions. *Annu. Rev. Biophys. biomol. Struct.* **23**, 141–165.

Camino, D. D., Holmgren, M., Liu, Y. & Yellen, G. (2000). Blocker protection in the pore of a voltage-gated K^+ channel and its structural implications. *Nature* **403**, 321–325.

Capener, C. E., Shrivastava, I. H., Ranatunga, K. M., Forrest, L. R., Smith, G. R. & Sansom, M. S. P. (2000). Homology modelling and molecular dynamics simulation studies of an inward rectifier potassium channel. *Biophys. J.* **78**, 2929–2942.

Cardenas, A. E., Coalson, R. D. & Kurnikova, M. G. (2000). Three-dimensional Poisson–Nernst–Planck theory studies: influence of membrane electrostatics on gramicidin A channel conductance. *Biophys. J.* **79**, 80–93.

Cevc, G., Strohmaier, L., Berkholz, J. & Blume, G. (1990). Molecular mechanism of protein interactions with the lipid bilayer membrane. *Studia Biophysica* **138**, 57–70.

Cha, A., Snyder, G. E., Selvin, P. R. & Bezanilla, F. (1999). Atomic scale movement of the voltage-sensing region in a potassium channel measured via spectroscopy. *Nature* **402**, 809–813.

Chang, G., Spencer, R. H., Lee, A. T., Barclay, M. T. & Rees, D. C. (1998). Structure of the MscL homolog from *Mycobacterium tuberculosis*: a gated mechanosensitive ion channel. *Science* **282**, 2220–2226.

Changeux, J. P., Galzi, J. I., Devillers-Thiéry, A. & Bertrand, D. (1992). The functional architecture of the acetylcholine nicotinic receptor explored by affinity labelling and site-directed mutagenesis. *Quart. Rev. Biophys.* **25**, 395–432.

Chen, D. & Eisenberg, R. (1993a). Charges, currents, and potentials in ionic channel of one conformation. *Biophys. J.* **64**, 1405–1421.

Chen, D. & Eisenberg, R. (1993b). Flux, coupling, and selectivity in ionic channels of one conformation. *Biophys. J.* **65**, 727–746.

Chen, D., Lear, J. & Eisenberg, B. (1997). Permeation through an open channel: Poisson–Nernst–Planck theory of a synthetic ionic channel. *Biophys. J.* **72**, 97–116.

Chiu, S. W., Jakobsson, E., Subramanian, S. & McCammon, J. A. (1991). Time-correlation analysis of simulated water motion in flexible and rigid gramicidin channels. *Biophys. J.* **60**, 273–285.

Chiu, S. W., Novotny, J. A. & Jakobsson, E. (1993). The nature of ion and water barrier crossings in a simulated ion channel. *Biophys. J.* **64**, 98–109.

Chiu, S. W., Subramaniam, S. & Jakobsson, E. (1999a). Simulation study of a gramicidin/lipid bilayer system in excess water and lipid. I. Structure of the molecular complex. *Biophys. J.* **76**, 1929–1938.

Chiu, S. W., Subramaniam, S. & Jakobsson, E. (1999b). Simulation study of a gramicidin/lipid bilayer system in excess water and lipid. II. Rates and mechanisms of water transport. *Biophys. J.* **76**, 1939–1950.

Chung, S. H., Allen, T. W., Hoyles, M. & Kuyucak,

https://doi.org/10.1017/S0033583501003729 Published online by Cambridge University Press

S. (1999). Permeation of ions across the potassium channel: Brownian dynamics studies. *Biophys. J.* **77**, 2517–2533.

Chung, S. H., Hoyles, M., Allen, T. & Kuyucak, S. (1998). Study of ionic currents across a model membrane channel using Brownian dynamics. *Biophys. J.* **75**, 793–809.

Conway, B. E. (1978). The evaluation of and use of properties of individual ions in solution. *J. Sol. Chem.* **7**, 721–770.

Conway, B. E. (1981). *Ionic Hydration in Chemistry and Biophysics*. Amsterdam: Elsevier.

Cooper, K., Jakobsson, E. & Wolynes, P. (1985). The theory of ion transport through membrane channels. *Prog. Biophys. molec. Biol.* **46**, 51–96.

Corringer, P. J., Le Novere, N. & Changeux, J. P. (2000). Nicotinic receptors at the amino acid level. *Annu. Rev. Pharmacol. Toxicol.* **40**, 431–458.

Corry, B., Kuyucak, S. & Chung, S. H. (2000a). Invalidity of continuum theories of electrolytes in nanopores. *Chem. Phys. Lett.* **320**, 35–41.

Corry, B., Kuyucak, S. & Chung, S. H. (2000b). Tests of continuum theories as models of ion channels. II. Poisson–Nernst Planck theory versus brownian dynamics. *Biophys. J.* **78**, 2364–2381.

Cowan, S. W. (1993). Bacterial porins – lessons from 3 high-resolution structures. *Curr. Opin. struct. Biol.* **3**, 501–507.

Cross, T. A., Arseniev, A., Cornell, B. A., Davis, J. H., Killian, J. A., Koeppe, R., Nicholson, L. K., Separovic, F. & Wallace, B. A. (1999). Gramicidin channel controversy – revisited. *Nature struct. Biol.* **6**, 610–611.

Daggett, V. & Levitt, M. (1993). Realistic simulations of native-protein dynamics in solution and beyond. *Annu. Rev. Biophys. biomol. Struct.* **22**, 353–380.

Darden, T., York, D. & Pedersen, L. (1993). Particle mesh Ewald – an N.log(N) method for Ewald sums in large systems. *J. chem. Phys.* **98**, 10089–10092.

Davis, M. E., Madura, J. D., Luty, B. A. & McCammon, J. A. (1991). Electrostatics and diffusion of molecules in solution: simulations with the University of Houston Brownian dynamics program. *Comput. Phys. Comm.* **62**, 187–197.

Davis, M. E. & McCammon, J. A. (1990). Electrostatics in biomolecular structure and dynamics. *Chem. Rev.* **90**, 509–521.

Diebler, H., Eigen, M., Ilgenfritz, G., Maas, G. & Winkler, R. (1969). Kinetics and mechanism of reactions of main group metal ions with biological carriers. *Pure Appl. Chem.* **20**, 93–115.

Dieckmann, G. R., Lear, J. D., Zhong, Q., Klein, M. L., DeGrado, W. F. & Sharp, K. A. (1999). Exploration of the structural features defining the conduction properties of a synthetic ion channel. *Biophys. J.* **76**, 618–630.

Doering, C. R. & Gadoua, J. C. (1992). Resonant activation over a fluctuating barrier. *Phys. Rev. Lett.* **69**, 2318–2321.

Dorman, V., Partenskii, M. B. & Jordan, P. C. (1996). A semi-microscopic Monte Carlo study of permeation energetics in a gramicidin-like channel: the origin of cation selectivity. *Biophys. J.* **70**, 121–134.

Doupnik, C. A., Davidson, N. & Lester, H. A. (1995). The inward rectifier potassium channel family. *Curr. Opin. Neurobiol.* **5**, 268–277.

Doyle, D. A., Cabral, J. M., Pfuetzner, R. A., Kuo, A., Gulbis, J. M., Cohen, S. L., Cahit, B. T. & MacKinnon, R. (1998). The structure of the potassium channel: molecular basis of K^+ conduction and selectivity. *Science* **280**, 69–77.

Duax, W. L., Griffin, J. F., Langs, D. A., Smith, G. D., Grochulski, P., Pletnev, V. & Ivanov, V. (1996). Molecular structure and mechanisms of action of cyclic and linear ion transport antibiotics. *Biopolymers* **40**, 141–155.

Duca, K. A. & Jordan, P. C. (1997). Ion–water and water–water interactions in a gramicidinlike channel: effects due to group polarization and backbone flexibility. *Biophys. Chem.* **65**, 123–141.

Duff, K. C. & Ashley, R. H. (1992). The transmembrane domain of influenza A M2 protein forms amantadine-sensitive proton channels in planar lipid bilayers. *Virology* **190**, 485–489.

Duff, K. C., Kelly, S. M., Price, N. C. & Bradshaw, J. P. (1992). The secondary structure of influenza A M2 transmembrane domain. *FEBS Lett.* **311**, 256–258.

Dutzler, R., Rummel, G., Albertí, S., Hernández-Allés, S., Phale, P. S., Rosenbusch, J. P., Benedí, V. J. & Schirmer, T. (1999). Crystal structure and functional characterization of OmpK36, the osmoporin of *Klebsiella pneumoniae*. *Structure* **7**, 425–434.

Eisenberg, R. S. (1996). Computing the field in proteins and channels. *J. Membr. Biol.* **150**, 1–25.

Eisenberg, R. S. (1999). From structure to function in open ionic channels. *J. Membr. Biol.* **171**, 1–24.

Elber, R., Chen, D. P., Rojewska, D. & Eisenberg, R. (1995). Sodium in gramicidin: an example of a permion. *Biophys. J.* **68**, 906–924.

Feller, S. E. (2000). Molecular dynamics simulations of lipid bilayers. *Curr. Opin. Coll. Interface Sci.* **5**, 217–223.

Fischer, S. (2000). Molecular kinematics: essential motion and energetics of slow processes in proteins. *J. molec. Graphics Mod.* **18**, 186.

Forester, T. R., Smith, W. & Clarke, J. H. R. (1997). Antibiotic activity of valinomycin – Molecular dynamics simulations involving the water/membrane interface. *J. Chem. Soc. Faraday Trans.* **93**, 613–619.

Forrest, L. R., DeGrado, W. F., Dieckmann, G. R. & Sansom, M. S. P. (1998). Two models of the

https://doi.org/10.1017/S0033583501003729 Published online by Cambridge University Press

influenza A M2 channel domain: verification by comparison. *Folding & Design* **3**, 443–448.

Forrest, L. R., Kukol, A., Arkin, I. T., Tieleman, D. P. & Sansom, M. S. P. (2000). Exploring models of the Influenza A M2 channel: MD simulations in a lipid bilayer. *Biophys. J.* **78**, 55–69.

Forrest, L. R. & Sansom, M. S. P. (2000). Membrane simulations: bigger and better? *Curr. Opin. struct. Biol.* **10**, 174–181.

Forrest, L. R., Tieleman, D. P. & Sansom, M. S. P. (1999). Defining the transmembrane helix of M2 protein from influenza A by molecular dynamics simulations in a lipid bilayer. *Biophys. J.* **76**, 1886–1896.

Forst, D., Welte, W., Wacker, T. & Diederichs, K. (1998). Structure of the sucrose-specific porin ScrY from *Salmonella typhimurium* and its complex with sucrose. *Nature struct. Biol.* **5**, 37–46.

Fox, R. O. & Richards, F. M. (1982). A voltage-gated ion channel model inferred from the crystal structure of alamethicin at 1.5 Å resolution. *Nature* **300**, 325–330.

Frenkel, D. & Smit, B. (1996). *Understanding Molecular Simulation*. San Diego: Academic Press.

Friedman, H. L., Krishnan, C. V. (1974) *Water: A Comprehensive Treatise* (ed. F. Franks), pp. 1–118. New York: Plenum Press.

Fu, D., Libson, A., Miercke, L. J. W., Weitzman, C., Nollert, P., Krucinski, J. & Stroud, R. M. (2000). Structure of a glycerol-conducting channel and the basis of its selectivity. *Science* **290**, 481–486.

Galzi, J. L. & Changeux, J. P. (1994). Neurotransmitter-gated ion channels as unconventional allosteric proteins. *Curr. Opin. struct. Biol.* **4**, 554–565.

Glauner, K. S., Mannuzzau, L. M., Gandhi, C. S. & Isacoff, E. Y. (1999). Spectroscopic mapping of voltage sensor movement in the *Shaker* potassium channel. *Nature* **402**, 813–817.

Goulding, D., Hansen, J.-P. & Melchionna, S. (2000). Size selectivity of narrow pores. *Phys. Rev. Lett.* **85**, 1132–1135.

Graf, P., Nitzan, A., Kurnikova, M. G. & Coalson, R. D. (2000). A dynamic lattice Monte Carlo model of ion transport in inhomogeneous dielectric environments: method and implementation. *J. phys. Chem.* (*B*) **104**, 12324–12338.

Granick, S. (1991). Motions and relaxations of confined liquids. *Science* **253**, 1374–1379.

Gray, T. M. & Matthews, B. M. (1984). Intrahelical hydrogen bonding of serine, threonine and cysteine residues within α-helices and its relevance to membrane-bound proteins. *J. molec. Biol.* **175**, 75–81.

Grubmuller, H., Heymann, B. & Tavan, P. (1996). Ligand binding: molecular mechanics calculation of the Streptavidin-Biotin rupture force. *Science* **271**, 997–999.

Guidoni, L., Torre, V. & Carloni, P. (1999). Potassium and sodium binding in the outer mouth of the K^+ channel. *Biochem.* **38**, 8599–8604.

Guidoni, L., Torre, V. & Carloni, P. (2000). Water and potassium dynamics in the KcsA K^+ channel. *FEBS Lett.* **477**, 37–42.

Gutman, M., Tsfadia, Y., Masad, A. & Nachiel, E. (1992). Quantitation of physical-chemical properties of the aqueous phase inside the phoE ionic channel. *Biochim. Biophys. Acta* **1109**, 141–148.

Hahn, K., Kärger, J. & Kukla, V. (1996). Single-file diffusion observation. *Phys. Rev. Lett.* **76**, 2762–2765.

Hao, Y., Pear, M. R. & Busath, D. D. (1997). Molecular dynamics study of free energy profiles for organic cations in gramicidin A channels. *Biophys. J.* **73**, 1699–1716.

He, K., Ludtke, S. J., Huang, H. W. & Worcester, D. L. (1995). Antimicrobial peptide pores in membranes detected by neutron in plane scattering. *Biochem.* **34**, 15614–15618.

Heginbotham, L., LeMasurier, M., Kolmakova-Partensky, L. & Miller, C. (1999). Single *Streptomyces lividans* K^+ channels: functional asymmetries and sidedness of proton activation. *J. gen. Physiol.* **114**, 551–559.

Herzyk, P. & Hubbard, R. E. (1995). Automated-method for modeling 7-helix transmembrane receptors from experimental-data. *Biophys. J.* **69**, 2419–2442.

Hille, B. (1992). *Ionic Channels of Excitable Membranes*. Sunderland, MA: Sinauer Associates Inc.

Hollerbach, U., Chen, D. P., Busath, D. D. & Eisenberg, B. (2000). Predicting function from structure using the Poisson–Nernst–Planck equations: sodium current in the gramicidin A Channel. *Langmuir* **16**, 5509–5514.

Holsinger, L. J., Nichani, D., Pinto, L. H. & Lamb, R. A. (1994). Influenza A virus M_2 ion channel protein: a structure–function analysis. *J. Virol.* **68**, 1551–1563.

Honig, B. & Nicholls, A. (1995). Classical electrostatics in biology and chemistry. *Science* **268**, 1144–1149.

Hoyles, M., Kuyucak, S. & Chung, S. H. (1996). Energy barrier presented to ions by the vestibule of the biological membrane channel. *Biophys. J.* **70**, 1628–1642.

Hribar, B., Vlachy, V., Bhuiyan, L. B. & Outhwaite, C. W. (2000). Ion distributions in a cylindrical capillary as seen by the modified Poisson–Boltzmann theory and Monte Carlo simulations. *J. phys. Chem.* (*B*) **104**, 11522–11527.

Hu, J., Goldman, S., Gray, C. G. & Guy, H. R. (2000). Calculation of the conductance and selectivity of an ion-selective potassium channel (IRK1) from simulation of atomic scale models. *Molec. Phys.* **98**, 535–547.

https://doi.org/10.1017/S0033583501003729 Published online by Cambridge University Press

Hucho, F., Tsetlin, V. I. & Machold, J. (1996). The emerging three-dimensional structure of a receptor: the nicotinic acetylcholine receptor. *Eur. J. Biochem.* **239**, 539–557.

Hummer, G., Pratt, L. R. & Garcia, A. E. (1996). Free energy of ionic hydration. *J. phys. Chem.* **100**, 1206–1215.

Hummer, G., Pratt, L. R., Garcia, A. E., Berne, B. J. & Rick, S. W. (1997). Electrostatic potentials and free energies of solvation of polar and charged molecules. *J. phys. Chem.* (*B*) **101**, 3017–3020.

Hummer, G., Pratt, L. R., Garcia, A. E., Garde, S., Berne, B. J. & Rick, S. W. (1998). Reply to comment on 'Electrostatic potentials and free energies of solvation of polar and charged molecules'. *J. phys. Chem.* (*B*) **102**, 3841–3843.

Hunenberger, P. H. & McCammon, J. A. (1999). Ewald artifacts in computer simulations of ionic solvation of ion–ion interaction. *J. chem. Phys.* **110**, 1856–1872.

Im, W., Seefeld, S. & Roux, B. (2000). Grand canonical Monte Carlo–Brownian dynamics algorithm for simulating ion channels. *Biophys. J.* **79**, 788–801.

Jaikaran, D. C. J., Biggin, P. C., Wenschuh, H., Sansom, M. S. P. & Woolley, G. A. (1997). Structure–function relationships in helix-bundle channels probed via total chemical synthesis of alamethicin dimers: effects of a Gln7 to Asn7 mutation. *Biochem.* **36**, 13873–13881.

Jakobsson, E. (1998). Using theory and simulation to understand permeation and selectivity in ion channels. *Methods: A Companion to Methods in Enzymology*. **14**, 342–351.

Jakobsson, E. & Chiu, S. W. (1987). Stochastic-theory of ion movement in channels with single-ion occupancy – application to sodium permeation of gramicidin channels. *Biophys. J.* **52**, 33–45.

Jentsch, T. J., Friedrich, T., Schriever, A. & Yamada, H. (1999). The CLC chloride channel family. *Pflug. Archiv. Eur. J. Physiol.* **437**, 783–795.

Jonsson, B. (1981). Monte Carlo simulations of liquid water between two rigid walls. *Chem. Phys. Lett.* **82**, 520–525.

Jordan, P. (2000). Ionic energetics in narrow channels. In *Proceedings of the IMA Workshop on Membrane Transport and Renal Physiology* (ed. H. Layton). Berlin: Springer-Verlag.

Jordan, P. C. (1999). Ion permeation and chemical kinetics. *J. gen. Physiol.* **114**, 601–603.

Jordan, P. C., Bacquet, R. J., McCammon, J. A. & Tran, P. (1989). How electrolyte shielding influences the electrical potential in transmembrane ion channels. *Biophys. J.* **55**, 1041–1052.

Jorgensen, W. L., Chandrasekhar, J., Madura, J. D., Impey, R. W. & Klein, M. L. (1983). Comparison of simple potential functions for simulating liquid water. *J. chem. Phys.* **79**, 926–935.

Kärger, J. (1992). Straightforward derivation of the long-time limit of the mean-square displacement in one-dimensional diffusion. *Phys. Rev.* (*A*) **45**, 4173–4174.

Kärger, J., Hahn, K., Kukla, V. & Rödenbeck, C. (1998). Moleküle im gänsemarsch. *Physikalische Blätter*. **54**, 811–815.

Karshikoff, A., Spassov, V., Cowan, S. W., Ladenstein, R. & Schirmer, T. (1994). Electrostatic properties of two porin channels from *Escherichia coli*. *J. molec. Biol.* **240**, 372–384.

Kerr, I. D., Sankararamakrishnan, R., Smart, O. S. & Sansom, M. S. P. (1994). Parallel helix bundles and ion channels: molecular modelling via simulated annealing and restrained molecular dynamics. *Biophys. J.* **67**, 1501–1515.

Kerr, I. D., Son, H. S., Sankararamakrishnan, R. & Sansom, M. S. P. (1996). Molecular dynamics simulations of isolated transmembrane helices of potassium channels. *Biopolymers* **39**, 503–515.

Ketchem, R. R., Hu, W. & Cross, T. A. (1993). High-resolution conformation of gramicidin A in a lipid bilayers by solid-state NMR. *Science* **261**, 1457–1460.

Kienker, P. K., DeGrado, W. F. & Lear, J. D. (1994). A helical-dipole model describes the single-channel current rectification of an uncharged peptide ion channel. *Proc. natn. Acad. Sci. USA* **91**, 4859–4863.

Kienker, P. K. & Lear, J. D. (1995). Charge selectivity of the designed uncharged peptide ion channel. Ac-(LSSLLSL)3-CONH2. *Biophys. J.* **68**, 1347–1358.

Kollman, P. (1993). Free-energy calculations – applications to chemical and biochemical phenomena. *Chem. Rev.* **93**, 2395–2417.

Kovacs, F. A. & Cross, T. A. (1997). Transmembrane four-helix bundle of influenza A M2 protein channel: structural implications from helix tilt and orientation. *Biophys. J.* **73**, 2511–2517.

Krestov, G. A. (1991). *Thermodynamics of Solvation. Solution and Dissolution, Ions and Solvents, Structure and Energetics*. Chichester: Ellis Horwood.

Krestov, G. A., Novosyolov, N. P., Perelygin, I. S., Kolker, A. M., Safonova, L. P., Ovchinnikova, V. D. & Trostin, V. N. (1994). *Ionic solvation*. Harlow: Pearson Higher Education.

Kreusch, A., Pfaffinger, P. J., Stevens, C. F. & Choe, S. (1998). Crystal structure of the tetramerization domain of the *Shaker* potassium channel. *Nature* **392**, 945–948.

Kukla, V., Kornatowski, J., Demuth, D., Girnus, I., Pfeifer, H., Rees, L. V. C., Schunk, S., Unger, K. K. & Kärger, J. (1996). NMR studies of single-file diffusion in unidimensional channels zeolites. *Science* **272**, 702–704.

Kukol, A., Adams, P. D., Rice, L. M., Brunger, A. T. & Arkin, I. T. (1999). Experimentally based orientational refinement of membrane protein models: a

https://doi.org/10.1017/S0033583501003729 Published online by Cambridge University Press

structure for the influenza A M2 H^+ channel. *J. molec. Biol.* **286**, 951–962.

Kurnikova, M. G., Coalson, R. D., Graf, P. & Nitzan, A. (1999). A lattice relaxation algorithm for three-dimensional Poisson–Nernst–Planck theory with application to ion transport through the gramicidin A channel. *Biophys. J.* **76**, 642–656.

Kuyucak, S., Hoyles, M. & Chung, S.-H. (1998). Analytical solutions of Poisson's equation for realistic geometrical shapes of membrane ion channels. *Biophys. J.* **74**, 22–36.

Ladd, M. F. C. (1968). The radii of spherical ions. *Theoret. Chim. Acta* **12**, 333–336.

Law, R. J., Forrest, L. R., Ranatunga, K. M., La Rocca, P., Tieleman, D. P. & Sansom, M. S. P. (2000). Structure and dynamics of the pore-linking helix of the nicotinic receptor: MD simulations in water, lipid bilayers and transbilayer bundles. *Proteins: Struct. Funct. Genet.* **39**, 47–55.

Leach, A. R. (1996). *Molecular Modelling: Principles and Applications*. Harlow: Longman.

Lear, J. D., Schneider, J. P., Kienker, P. K. & DeGrado, W. F. (1997). Electrostatic effects on ion selectivity and rectification in designed ion channel peptides. *J. Am. chem. Soc.* **119**, 3212–3217.

Lear, J. D., Wasserman, Z. R. & DeGrado, W. F. (1988). Synthetic amphiphilic peptide models for protein ion channels. *Science* **240**, 1177–1181.

Lear, J. D., Wasserman, Z. R. & DeGrado, W. F. (1994). Use of synthetic peptides for the study of membrane protein structure. In: *Membrane Protein Structure: Experimental Approaches* (ed. S. H. White). Oxford: Oxford University Press.

Lebedev, V. I. (1969). *Ionic Atomic Radii and Their Role in Geochemistry and Chemistry*. Leningrad: LGU.

Lee, C. Y., McCammon, J. A. & Rossky, P. J. (1984). The structure of liquid water at an extended hydrophobic surface. *J. chem. Phys.* **80**, 4448–4455.

Lester, H. (1992). The permeation pathway of neurotransmitter-gated ion channels. *Annu. Rev. Biophys. biomol. Struct.* **21**, 267–292.

Levitt, D. G. (1985). Strong electrolyte continuum theory solution for equilibrium profiles, diffusion limitation, and conductance in charged ion channels. *Biophys. J.* **48**, 19–31.

Levitt, D. G. (1986). Interpretation of biological ion channel flux data – reaction-rate versus continuum theory. *Annu. Rev. Biophys. biophys. Chem.* **15**, 29–57.

Levitt, D. G. (1991). General continuum theory for multi-ion channel. 1. Theory. *Biophys. J.* **59**, 271–277.

Levitt, M., Hirshberg, M., Sharon, R., Laidig, K. E. & Daggett, V. (1977). Calibration and testing of a water model for simulation of the molecular dynamics of proteins and nucleic acids in solution. *J. phys. Chem. (B)* **101**, 5051–5061.

Li, S. C., Hoyles, M., Kuyucak, S. & Chung, S.-H. (1998). Brownian dynamics study of ion transport in the vestibule of membrane channels. *Biophys. J.* **74**, 37–47.

Lim, C., Bashford, D. & Karplus, M. (1991). Absolute pK_a calculations with continuum dielectric methods. *J. phys. Chem.* **95**, 5610–5620.

Lindahl, E. & Edholm, O. (2000). Mesoscopic undulations and thickness fluctuations in lipid bilayers from molecular dynamics simulations. *Biophys. J.* **79**, 426–433.

Liu, H. Y., Mark, A. E. & vanGunsteren, W. F. (1996). Estimating the relative free energy of different molecular states with respect to a single reference state. *J. phys. Chem.* **100**, 9485–9494.

Lonsdale, K. (1958). The structure of ice. *Proc. Roy. Soc. London. (A)* **247**, 424–434.

Loussouarn, G., Amkhina, E. N. & Nichols, C. G. (1999). Structure of the second transmembrane domain of Kir6.2 revealed by the substituted cysteine accessibility method. *Biophys. J.* **76**, A75.

Lu, H., Isralewitz, B., Krammer, A., Vogel, V. & Schulten, K. (1998). Unfolding of titin immunoglobulin domains by steered molecular dynamics simulation. *Biophys. J.* **75**, 662–671.

Lu, J. & Green, M. E. (1997). Simulation of water in a pore with charges: application to the gating mechanism for ion channels. *Progr. Colloid Polym. Sci.* **103**, 121–129.

Luzhkov, V. B. & Åqvist, J. (2000). A computational study of ion binding and protonation states in the KcsA potassium channel. *Biochim. Biophys. Acta* **1481**, 360–370.

Lynden-Bell, R. & Rasaiah, J. C. (1996). Mobility and solvation of ions in channels. *J. chem. Phys.* **105**, 9266–9280.

MacKinnon, R., Cohen, S. L., Kuo, A., Lee, A. & Chait, B. T. (1998). Structural conservation in prokaryotic and eukaryotic potassium channels. *Science* **280**, 106–109.

Mao, Z. G. & Sinnott, S. B. (2000). A computational study of molecular diffusion and dynamic flow through carbon nanotubes. *J. phys. Chem. (B)* **104**, 4618–4624.

Marchesi, M. (1983). Molecular dynamics simulation of liquid water between two walls. *Chem. Phys. Lett.* **97**, 224–230.

Marcus, Y. (1988). Ionic radii in aqueous solutions. *Chem. Rev.* **88**, 1475–1498.

Marcus, Y. (1991). Thermodynamics of solvation of ions. 5. Gibbs free energy of hydration at 298.15 K. *J. Chem. Soc. Faraday Trans.* **87**, 2995–2999.

Marrink, S. J., Berger, O., Tieleman, D. P. & Jahnig, F. (1998). Adhesion forces of lipids in a phospholipid membrane studied by molecular dynamics simulations. *Biophys. J.* **74**, 931–943.

https://doi.org/10.1017/S0033583501003729 Published online by Cambridge University Press

Mashl, R. J., Tang, Y., Schnitzer, J. & Jakobsson, E. (In Press) Hierarchical approach to predicting permeation in ion channels. *Biophys. J.* **81**.

Mathew, M. K. & Balaram, P. (1983). A helix dipole model for alamethicin and related transmembrane channels. *FEBS Lett.* **157**, 1–5.

McCleskey, E. W. (1999). Calcium channel permeation: a field in flux. *J. gen. Physiol.* **113**, 765–772.

McGill, P. & Schumaker, M. F. (1996). Boundary conditions for single ion diffusion. *Biophys. J.* **96**, 1723–1742.

McQuarrie, D. A. (1976). *Statistical Mechanics*. New York: HarperCollins.

Melishchuk, A., Loboda, A. & Armstrong, C. M. (1998). Loss of *Shaker* K channel conductance in 0 K^+ solutions: role of the voltage sensor. *Biophys. J.* **75**, 1828–1835.

Meulenhoff, P. J. (1999). Interfacial action of phospholipase A2. Ph.D. thesis. University of Groningen, Groningen.

Meuser, D., Splitt, H., Wagner, R. & Schrempf, H. (1999). Exploring the open pore of the potassium channel from *Streptomyces lividans*. *FEBS Lett.* **462**, 447–452.

Miller, C. (1999). Ionic hopping defended. *J. gen. Physiol.* **113**, 783–787.

Mitton, P. & Sansom, M. S. P. (1996). Molecular dynamics simulations of ion channels formed by bundles of amphipathic α-helical peptides. *Eur. Biophys. J.* **25**, 139–150.

Miyazawa, A., Fujiyoshi, Y., Stowell, M. & Unwin, N. (1999). Nicotinic acetylcholine receptor at 4.6 angstrom resolution: transverse tunnels in the channel wall. *J. molec. Biol.* **288**, 765–786.

Montal, M. (1995). Design of molecular function: channels of communication. *Annu. Rev. Biophys. biomol. Struct.* **24**, 31–57.

Montal, M., Montal, M. S. & Tomich, J. M. (1990). Synporins – synthetic proteins that emulate the pore structure of biological ionic channels. *Proc. natn. Acad. Sci. USA* **87**, 6929–6933.

Montal, M. O., Iwamoto, T., Tomich, J. M. & Montal, M. (1993). Design, synthesis and functional characterization of a pentameric channel protein that mimics the presumed pore structure of the nicotinic cholinergic receptor. *FEBS Lett.* **320**, 261–266.

Moy, G., Corry, B., Kuyucak, S. & Chung, S. H. (2000). Tests of continuum theories as models of ion channels. I. Poisson–Boltzmann theory versus Brownian dynamics. *Biophys. J.* **78**, 2349–2363.

Murata, K., Mitsuoaka, K., Hirai, T., Walz, T., Agre, P., Heymann, J. B., Engel, A. & Fujiyoshi, Y. (2000). Structural determinants of water permeation through aquaporin-1. *Nature* **407**, 599–605.

Narten, A. H. (1972). Liquid water: atomic pair correlation functions from neutron and X-ray diffraction. *J. chem. Phys.* **56**, 5681–5687.

Nelson, P. H. & Auerbach, S. M. (1999). Self-diffusion in single-file zeolite membranes is Fickian at long times. *J. chem. Phys.* **110**, 9235–9234.

Newns, D. M., Zhong, Q., Moore, P. B., Husslein, T., Pattnaik, P. & Klein, M. L. (2000). Molecular dynamics study of structure and gating of low molecular weight ion channels. *Parallel Comput.* **26**, 965–976.

Nonner, W., Catacuzzeno, L. & Eisenberg, B. (2000). Binding and selectivity in L-type calcium channels: A mean spherical approximation. *Biophys. J.* **79**, 1976–1992.

Nonner, W., Chen, D. P. & Eisenberg, B. (1999). Progress and prospects in permeation. *J. gen. Physiol.* **113**, 773–782.

Nonner, W. & Eisenberg, B. (1998). Ion permeation and glutamate residues linked by Poisson–Nernst–Planck theory in L-type calcium channels. *Biophys. J.* **75**, 1287–1305.

Oiki, S., Danho, W., Madison, V. & Montal, M. (1988). M2δ, a candidate for the structure lining the ionic channel of the nicotinic cholinergic receptor. *Proc. natn. Acad. Sci. USA* **85**, 8703–8707.

Oiki, S., Madison, V. & Montal, M. (1990). Bundles of amphipathic transmembrane α-helices as a structural motif for ion conducting channel proteins: studies on sodium channels and acetylcholine receptors. *Proteins: Struct. Funct. Genet.* **8**, 226–236.

Opella, S. J., Marassi, F. M., Gesell, J. J., Valente, A. P., Kim, Y., Oblatt-Montal, M. & Montal, M. (1999). Structures of the M2 channel-lining segments from nicotinic acetylcholine and NMDA receptors by NMR spectroscopy. *Nature struct. Biol.* **6**, 374–379.

Ortells, M. O., Barrantes, G. E., Wood, C., Lunt, G. G. & Barrantes, F. J. (1996). Molecular modelling of the nicotinic acetylcholine receptor transmembrane region in the open state. *Prot. Engng* **10**, 511–517.

Ortells, M. O. & Lunt, G. G. (1995). Evolutionary history of the ligand gated ion channel superfamily of receptors. *Trends Neurosci.* **18**, 121–127.

Parsegian, A. (1969). Energy of an ion crossing a low dielectric membrane: solution to four relevant electrostatics problems. *Nature* **221**, 844–846.

Partenskii, M. B. & Jordan, P. C. (1992). Theoretical perspectives on ion-channel electrostatics – continuum and microscopic approaches. *Quart. Rev. Biophys.* **25**, 477–510.

Pauling, L. (1927). The theoretical prediction of the physical properties of many-electron atoms and ions. Mole refraction, diamagnetic susceptibility, and extension in space. *Proc. R. Soc. Lond.* (*B*) **114**, 181–211.

Pauling, L. (1960). *Nature of the Chemical Bond and Structure of Molecules and Crystals*. Cornell University Press.

Perozo, E., Cortes, D. M. & Cuello, L. G. (1998).

https://doi.org/10.1017/S0033583501003729 Published online by Cambridge University Press

Three-dimensional architecture and gating mechanism of a K^+ channel studied by EPR spectroscopy. *Nature struct. Biol.* **5**, 459–469.

Perozo, E., Cortes, D. M. & Cuello, L. G. (1999). Structural rearrangements underlying K^+-channel activation gating. *Science* **285**, 73–78.

Perozo, E., Liu, Y. S., Smopornpisut, P., Cortes, D. M. & Cuello, L. G. (2000). A structural perspective of activation gating in K^+ channels. *J. gen. Physiol.* **116**, 5a.

Phale, P. S., Philippsen, A., Widmer, C., Phale, V. P., Rosenbusch, J. P. & Schirmer, T. (2001). Role of charged residues at the OmpF porin channel constriction probed by mutagenesis and simulation. *Biochemistry* **40**, 6319–6325.

Pomes, R. & Roux, B. (1996). Structure and dynamics of a proton wire: a theoretical study of H^+ translocation along the single-file water chain in the gramicidin A channel. *Biophys. J.* **71**, 19–39.

Ranatunga, K. M. (2000). Computational studies of ion channel permeation and selectivity. D.Phil Thesis. Oxford.

Ranatunga, K. M., Shrivastava, I. H., Smith, G. R. & Sansom, M. S. P. (2001). Sidechain ionization states in a potassium channel. *Biophys. J.* **80**, 1210–1219.

Ranatunga, K. M., Smith, G. R., Law, R. J. & Sansom, M. S. P. (In Press). Electrostatics and molecular dynamics of a homology model of the *Shaker* K^+ channel pore. *Eur. Biophys. J.*

Randa, H. S., Forrest, L. R., Voth, G. A. & Sansom, M. S. P. (1999). Molecular dynamics of synthetic leucine-serine ion channels in a phospholipid membrane. *Biophys. J.* **77**, 2400–2410.

Rashin, A. & Honig, B. (1985). Reevaluation of the Born model of ion hydration. *J. phys. Chem.* **89**, 5588.

Reimann, F. & Ashcroft, F. M. (1999). Inwardly rectifying potassium channels. *Curr. Opin. Cell Biol.* **11**, 503–508.

Ren, G., Cheng, A., Reddy, V., Melnyk, P. & Mitra, A. K. (2000). Three-dimensional fold of the human AQP1 water channel determined at 4 angstrom resolution by electron crystallography of two-dimensional crystals embedded in ice. *J. molec. Biol.* **301**, 369–387.

Ren, G., Reddy, V. S., Cheng, A., Melnyk, P. & Mitra, A. K. (2001). Visualization of a water-selective pore by electron crystallography in vitreous ice. *Proc. natn. Acad. Sci. USA* **98**, 1398–1403.

Repunte, V. P., Nakamura, H., Fujita, A., Horio, Y., Findlay, I., Pott, L. & Kurachi, Y. (1999). Extracellular links in Kir subunits control the unitary conductance of SUR/Kir6.0 ion channels. *EMBO J.* **18**, 3317–3324.

Rossiensky, D. R. (1970). Electrode potentials and hydration energies. Theories and correlations. *Chem. Rev.* **65**, 467–490.

Rossky, P. J. & Lee, S. H. (1989). Structure and dynamics of water at interfaces. *Chemica Scripta* **29A**, 93–95.

Rostovtseva, T. K., Aguilella, V. M., Vodyanoy, I., Bezrukov, S. M. & Parsegian, V. A. (1998). Membrane surface-charge titration probed by gramicidin A channel conductance. *Biophys. J.* **78**, 1783–1792.

Roux, B. (1995). Theory of transport in ion channels – from molecular dynamics simulations to experiments. In *Computer Modelling in Molecular Biology* (ed. J. Goodfellow), pp. 113–169. Weinheim: VCH.

Roux, B. (1996). Valence selectivity of the gramicidin channel: a molecular dynamics free energy perturbation study. *Biophys. J.* **71**, 3177–3185.

Roux, B. (1997). Influence of the membrane potential on the free energy of an intrinsic protein. *Biophys. J.* **73**, 2980–2989.

Roux, B. (1999a). Statistical mechanical equilibrium theory of selective ion channels. *Biophys. J.* **77**, 139–153.

Roux, B. (1999b). Theories of ion permeation: a chaser. *J. gen. Physiol.* **114**, 605–608.

Roux, B., Bernèche, S. & Im, W. (2000). Ion channels, permeation and electrostatics: insight into the function of KcsA. *Biochem.* **39**, 13295–13306.

Roux, B. & Karplus, M. (1991a). Ion transport in a gramicidin-like channel: dynamics and mobility. *J. phys. Chem.* **95**, 4856–4868.

Roux, B. & Karplus, M. (1991b). Ion transport in a model gramicidin channel: structure and thermodynamics. *Biophys. J.* **59**, 961–981.

Roux, B. & Karplus, M. (1993). Ion transport in the gramicidin channel: free energy of the solvated right-handed dimer in a model membrane. *J. Am. Chem. Soc.* **115**, 3250–3262.

Roux, B. & Karplus, M. (1994). Molecular dynamics simulations of the gramicidin channel. *Annu. Rev. Biophys. biomol. Struct.* **23**, 731–761.

Roux, B. & MacKinnon, R. (1999). The cavity and pore helices in the KcsA K^+ channel: electrostatic stabilization of monovalent cations. *Science* **285**, 100–102.

Rubi, J. M. & Perez-Madrid, A. (1999). Inertial effects in non-equilibrium thermodynamics. *Physica* (*A*) **264**, 592–602.

Sagui, C. & Darden, T. A. (1999). Molecular dynamics simulations of biomolecules: Long-range electrostatic effects. *Annu. Rev. Biophys. biomol. Struct.* **28**, 155–179.

Salomon, M. (1970). The thermodynamics of ion solvation in water and propylene carbonate. *J. phys. Chem.* **74**, 2519–2524.

Sancho, M., Partenskii, M. B., Dorman, V. & Jordan, P. C. (1995). Extended dipolar chain model

https://doi.org/10.1017/S0033583501003729 Published online by Cambridge University Press

for ion channels: electrostriction effects and the translocational energy barrier. *Biophys. J.* **68**, 427–433.

Sandberg, L. & Edholm, O. (1997). pK_a calculations along a bacteriorhodopsin molecular dynamics trajectory. *Biophys. Chem.* **65**, 189–204.

Sankararamakrishnan, R., Adcock, C. & Sansom, M. S. P. (1996). The pore domain of the nicotinic acetylcholine receptor: molecular modelling and electrostatics. *Biophys. J.* **71**, 1659–1671.

Sansom, M. S. P. (1991). The biophysics of peptide models of ion channels. *Prog. Biophys. molec. Biol.* **55**, 139–236.

Sansom, M. S. P. (1993). Structure and function of channel-forming peptaibols. *Quart. Rev. Biophys.* **26**, 365–421.

Sansom, M. S. P., Adcock, C. & Smith, G. R. (1998a). Modelling and simulation of ion channels: applications to the nicotinic acetylcholine receptor. *J. struct. Biol.* **121**, 246–262.

Sansom, M. S. P., Balaram, P. & Karle, I. (1993). Ion channel formation by zervamicin IIB: a molecular modelling study. *Eur. Biophys. J.* **21**, 369–383.

Sansom, M. S. P., Forrest, L. R. & Bull, R. (1998b). Viral ion channels: molecular modelling and simulation. *BioEssays.* **20**, 992–1000.

Sansom, M. S. P. & Kerr, I. D. (1995). Transbilayer pores formed by β-barrels – molecular modelling of pore structures and properties. *Biophys. J.* **69**, 1334–1343.

Sansom, M. S. P., Kerr, I. D., Breed, J. & Sankararamakrishnan, R. (1996). Water in channel-like cavities: structure and dynamics. *Biophys. J.* **70**, 693–702.

Sansom, M. S. P., Sankararamakrishnan, R. & Kerr, I. D. (1995). Modelling membrane proteins using structural restraints. *Nature struct. Biol.* **2**, 624–631.

Sansom, M. S. P., Smith, G. R., Adcock, C. & Biggin, P. C. (1997). The dielectric properties of water within model transbilayer pores. *Biophys. J.* **73**, 2404–2415.

Sansom, M. S. P. & Weinstein, H. (2000). Hinges, swivels & switches: the role of prolines in signalling via transmembrane α-helices. *Trends Pharm. Sci.* **21**, 445–451.

Sarman, S. S., Evans, D. J. & Cummings, P. T. (1998). Recent developments in non-Newtonian molecular dynamics. *Physics Report* **305**, 1–92.

Schirmer, T. (1998). General and specific porins from bacterial outer membranes. *J. struct. Biol.* **121**, 101–109.

Schirmer, T., Keller, T. A., Wang, Y. F. & Rosenbusch, J. P. (1995). Structural basis for sugar translocation through maltoporin channels at 3.1A resolution. *Science* **267**, 512–514.

Schirmer, T. & Phale, P. S. (1999). Brownian dynamics simulation of ion flow through porin channels. *J. molec. Biol.* **294**, 1159–1167.

Schmid, R., Miah, A. M. & Sapunov, V. N. (2000). A new table of the thermodynamic quantities of ionic hydration: values and some applications (enthalpy-entropy compensation and Born radii). *Phys. Chem. chem. Phys.* **2**, 97–102.

Schmitt, P., Beer, P. D., Drew, M. G. B. & Sheen, P. D. (1997). Calix[4]tube: a tubular receptor with remarkable potassium ion selectivity. *Angew. Chem. Int. Edit.* **36**, 1840–1842.

Schmitt, U. W. & Voth, G. A. (1998). Multistate empirical valence bond model for proton transport in water. *J. phys. Chem. (B)* **102**, 5547–5551.

Schrempf, H., Schmidt, O., Kummerlein, R., Hinnah, S., Muller, D., Betzler, M., Steinkamp, T. & Wagner, R. (1995). A prokaryotic potassium-ion channel with 2 predicted transmembrane segments from *Streptomyces lividans*. *EMBO J.* **14**, 5170–5178.

Schulz, G. E. (2000). β-Barrel membrane proteins. *Curr. Opin. struct. Biol.* **10**, 443–447.

Schweighofer, K. J. & Pohorille, A. (2000). Computer simulation of ion channel gating: the M-2 channel of influenza A virus in a lipid bilayer. *Biophys. J.* **78**, 150–163.

Senapati, S. & Chandra, A. (1999). Molecular dynamics simulations of simple dipolar liquids in spherical cavity: Effects of confinement on structural, dielectric, and dynamical properties. *J. chem. Phys.* **111**, 1223–1230.

Shannon, R. D. & Prewitt, C. T. (1969). Effective ionic radii in oxides and fluorides. *Acta Crystallogr. (B)* **25**, 925–946.

Shrivastava, I. H., Biggin, P. C., Tieleman, D. P. & Sansom, M. S. P. (In Press). Simulations of a bacterial K channel: ion selectivity and the flexibility of the filter? *Biophys. J.*

Shrivastava, I. H., Capener, C., Forrest, L. R. & Sansom, M. S. P. (2000). Structure and dynamics of K^+ channel pore-lining helices: a comparative simulation study. *Biophys. J.* **78**, 79–92.

Shrivastava, I. H. & Sansom, M. S. P. (2000). Simulations of ion permeation through a potassium channel: molecular dynamics of KcsA in a phospholipid bilayer. *Biophys. J.* **78**, 557–570.

Shrivastava, I. H. & Sansom, M. S. P. (In Press). Molecular dynamics simulations and KcsA channel gating. *Eur. Biophys. J.*

Smart, O. (1994). A new method to calculate reaction paths for conformational transitions of large molecules. *Chem. Phys. Lett.* **222**, 503–551.

Smart, O. S., Breed, J., Smith, G. R. & Sansom, M. S. P. (1997). A novel method for structure-based prediction of ion channel conductance properties. *Biophys. J.* **72**, 1109–1126.

Smart, O. S., Coates, G. M. P., Sansom, M. S. P., Alder, G. M. & Bashford, C. L. (1998). Structure-based prediction of the conductance properties of ion channels. *Faraday Discuss.* **111**, 185–199.

https://doi.org/10.1017/S0033583501003729 Published online by Cambridge University Press

Smart, O. S. & Goodfellow, J. M. (1995). On the simulation of conformational transitions: smoothing path energy minimization results. *Molec. Simul.* **14**, 291–302.

Smart, O. S., Goodfellow, J. M. & Wallace, B. A. (1993). The pore dimensions of gramicidin A. *Biophys. J.* **65**, 2455–2460.

Smith, G. R. & Sansom, M. S. P. (1997). Molecular dynamics study of water and Na^+ ions in models of the pore region of the nicotinic acetylcholine receptor. *Biophys. J.* **73**, 1364–1381.

Smith, G. R. & Sansom, M. S. P. (1998). Dynamic properties of Na^+ ions in models of ion channels – a molecular dynamics study. *Biophys. J.* **75**, 2767–2782.

Smith, G. R. & Sansom, M. S. P. (1999). Effective diffusion coefficients of K^+ and Cl^- ions in ion channel models. *Biophys. Chem.* **79**, 129–151.

Smith, G. R. & Sansom, M. S. P. (In Press). Free energy of a potassium ion in a model of the channel formed by an amphipathic leucine-serine peptide. *Eur. Biophys. J.*

Song, Z., Kovacs, F. A., Wang, J., Denny, J. K., Shekar, S. C., Quine, J. R. & Cross, T. A. (2000). Transmembrane domain of M2 protein from influenza A virus studied by solid-state ^{15}N polarization inversion spin exchange at magic angle NMR. *Biophys. J.* **79**, 767–775.

Starostin, A. V., Butan, R., Borisenko, V., James, D. A., Wenschuh, H., Sansom, M. S. P. & Woolley, A. G. (1999). An anion-selective analogue of the channel-forming peptide alamethicin. *Biochem.* **38**, 6144–6150.

Straatsma, T. P. & Berendsen, H. J. C. (1988). Free-energy of ionic hydration – analysis of a thermodynamic integration technique to evaluate free-energy differences by molecular-dynamics simulation. *J. chem. Phys.* **89**, 5876–5886.

Straatsma, T. P. & McCammon, J. A. (1992). Computational alchemy. *Annu. Rev. phys. Chem.* **43**, 407–435.

Syganow, A. & von Kitzing, E. (1999a). The drift approximation solves the Poisson–Nernst–Planck, and continuum equations in the limit of large external voltages. *Eur. Biophys. J.* **28**, 393–414.

Syganow, A. & von Kitzing, E. (1999b). (In)validity of the constant field and constant currents assumptions in theories of ion transport. *Biophys. J.* **76**, 768–781.

Thompson, G. A., Leyland, M. L., Ashmole, I., Sutcliffe, M. J. & Stanfield, P. R. (2000). Residues beyond the selectivity filter of the K^+ channel Kir2.1 regulate permeation and block by external Rb^+ and Cs^+. *J. Physiol.* **526**, 231–240.

Tieleman, D. P. & Berendsen, H. J. C. (1998). A molecular dynamics study of the pores formed by *Escherichia coli* OmpF porin in a fully hydrated palmitoyloleoylphosphatidylcholine bilayer. *Biophys. J.* **74**, 2786–2801.

Tieleman, D. P., Berendsen, H. J. C. & Sansom, M. S. P. (1999). An alamethicin channel in a lipid-bilayer: molecular dynamics simulations. *Biophys. J.* **76**, 1757–1769.

Tieleman, D. P., Breed, J., Berendsen, H. J. C. & Sansom, M. S. P. (1998). Alamethicin channels in a membrane: molecular dynamics simulations. *Faraday Disc.* **111**, 209–223.

Tieleman, D. P., Marrink, S. J. & Berendsen, H. J. C. (1997). A computer perspective of membranes: molecular dynamics studies of lipid bilayer systems. *Biochim. Biophys. Acta* **1331**, 235–270.

Tieleman, D. P., Shrivastava, I. H., Ulmschneider, M. B. & Sansom, M. S. P. (2001). Proline-induced hinges in transmembrane helices: possible roles in ion channel gating. *Proteins: Struct. Funct. Genet.* **44**, 63–72.

Tikhonov, D. B. & Zhorov, B. S. (1998). Kinked-helices model of the nicotinic acetylcholine receptor ion channel and its complexes with blockers: simulation by the Monte Carlo minimization method. *Biophys. J.* **74**, 242–255.

Tobias, D. J., Tu, K. C. & Klein, M. L. (1997). Atomic-scale molecular dynamics simulations of lipid membranes. *Curr. Opin. Coll. Interface Sci.* **2**, 15–26.

Tucker, S. J., Gribble, F. M., Zhao, C., Trapp, S. & Ashcroft, F. M. (1997). Truncation of Kir6.2 produces ATP-sensitive K^+ channels in the absence of the sulphonylurea receptor. *Nature* **387**, 179–183.

Unwin, N. (1993). Nicotinic acetylcholine receptor at 9 Å resolution. *J. molec. Biol.* **229**, 1101–1124.

Unwin, N. (1995). Acetylcholine receptor channel imaged in the open state. *Nature*. **373**, 37–43.

Vlachy, V. (1999). Ionic effects beyond Poisson-Boltzmann theory. *Annu. Rev. Phys. Chem.* **50**, 145–165.

von Heijne, G. (1992). Membrane protein structure prediction. Hydrophobicity analysis and the positive inside rule. *J. molec. Biol.* **225**, 487–494.

von Kitzing, E. & Soumpasis, D. M. (1996). Electrostatics of a simple membrane model using Green's function formalism. *Biophys. J.* **71**, 795–810.

Waber, J. T. & Cromer, D. T. (1965). Orbital radii of atoms and ions. *J. chem. Phys.* **42**, 4116–4123.

Wallace, B. A. (1992). Crystallographic studies of a transmembrane ion channel, gramicidin A. *Prog. Biophys. molec. Biol.* **57**, 59–69.

Wallace, B. A. (1999a). Gramicidin and related ion channel-forming peptides. In *Novartis Foundation Symposium*. Chichester: Wiley.

Wallace, B. A. (1999b). X-ray crystallographic structures of gramicidin and their relation to the *Streptomyces lividans* potassium channel structure. *Novartis Foundation Symp.* **225**, 23–37.

Wallace, B. A. (2000). Common structural features in gramicidin and other ion channels. *BioEssays* **22**, 227–234.

https://doi.org/10.1017/S0033583501003729 Published online by Cambridge University Press

Wang, C., Lamb, R. A. & Pinto, L. H. (1995). Activation of the M2 ion channel of influenza virus: a role for the transmembrane domain histidine residue. *Biophys. J.* **69**, 1363–1371.

Warshel, A. & Åqvist, J. (1991). Electrostatic energy and macromolecular function. *Annu. Rev. Biophys. biophys. Chem.* **20**, 267–298.

Warshel, A. & Papazyan, A. (1998). Electrostatic effects in macromolecules: fundamental concepts and practical modeling. *Curr. Opin. struct. Biol.* **8**, 211–217.

Weber, W., Hunenberger, P. H. & McCammon, J. A. (2000). Molecular dynamics simulations of a polyalanine octapeptide under Ewald boundary conditions: influence of artificial periodicity on peptide conformation. *J. phys. Chem (B)* **104**, 3668–3675.

Weetman, P., Goldman, S. & Gray, C. G. (1997). Use of the Poisson-Boltzmann equation to estimate the electrostatic free energy barrier for dielectric models of biological ion channels. *J. phys. Chem.* **101**, 6073–6078.

Woolf, T. B. (1997). Molecular dynamics of individual α-helices of bacteriorhodopsin in dimyristoyl phosphatidylcholine. I. Structure and dynamics. *Biophys. J.* **73**, 2376–2392.

Woolley, G. A., Biggin, P. C., Schultz, A., Lien, L., Jaikaran, D. C. J., Breed, J., Crowhurst, K. & Sansom, M. S. P. (1997). Intrinsic rectification of ion flux in alamethicin channels: studies with an alamethicin dimer. *Biophys. J.* **73**, 770–778.

Woolley, G. A. & Wallace, B. A. (1992). Model ion channels: gramicidin and alamethicin. *J. Membr. Biol.* **129**, 109–136.

Yeh, I. C. & Berkowitz, M. L. (2000). Effects of the polarizability and water density constraint on the structure of water near charged surfaces. Molecular dynamics simulations. *J. chem. Phys.* **112**, 10491–10495.

You, S., Peng, S., Lien, L., Breed, J., Sansom, M. S. P. & Woolley, G. A. (1996). Engineering stabilized ion channels: covalent dimers of alamethicin. *Biochem.* **35**, 6225–6232.

Zhang, L., Davis, H. T., Kroll, D. M. & White, H. S. (1995). Molecular dynamics simulations of water in a spherical cavity. *J. phys. Chem.* **99**, 2878–2884.

Zhong, Q., Husslein, T., Moore, P. B., Newns, D. M., Pattnaik, P. & Klein, M. L. (1998a). The M2 channel of influenza A virus: a molecular dynamics study. *FEBS Lett.* **434**, 265–271.

Zhong, Q., Jiang, Q., Moore, P. B., Newns, D. M. & Klein, M. L. (1998b). Molecular dynamics simulation of an ion channel. *Biophys. J.* **74**, 3–10.

Zhong, Q., Moore, P. B., Newns, D. M. & Klein, M. L. (1998c). Molecular dynamics study of the LS3 voltage-gated ion channel. *FEBS Lett.* **427**, 267–270.

https://doi.org/10.1017/S0033583501003729 Published online by Cambridge University Press